2009

The allometry of bird flight performance

Brandon Edward Jackson
The University of Montana

THE ALLOMETRY OF BIRD FLIGHT PERFORMANCE

By

BRANDON EDWARD JACKSON
B. A. Colgate University, Hamilton, NY, 1999
M. S. The University of Montana, Missoula, MT 2003

Dissertation

presented in partial fulfillment of the requirements
for the degree of

Doctor of Philosophy
in Organsimal Biology and Ecology

The University of Montana
Missoula, MT

December 2009

Approved by:

Perry Brown, Associate Provost for Graduate Education
Graduate School

Kenneth P. Dial, Chair
Division of Biological Sciences

Thomas Martin
Division of Biological Sciences

Erick Greene
Division of Biological Sciences

James Jacobs
Department of Physics and Astronomy

Robert Dudley
Department of Integrative Biology
The University of California, Berkeley, CA

Jackson, Brandon, Ph.D., December 2009 Organismal Biology and Ecology

The allometry of bird flight performance

Chairperson: Kenneth P. Dial

Avian flight performance decreases with body size in birds, but previous work has been unable to define the underlying mechanism. Wingbeat frequency is hypothesized to ultimately constrain flight performance *via* muscular mechanical power output because frequency decreases with body size. I measured maximal burst take-off and vertical accelerating flight in 32 species of songbirds (Passeriformes), including the entire range of body mass in this clade (5-900 g). Jump forces against the ground were recorded with a forceplate. High-speed digital video captured the movement of morphological landmarks in order to estimate aerodynamic power requirements and dynamic morphology in flight. Surgically implanted gauges recorded the components of muscle power (muscle length change, force production, frequency) in the four largest species (Common raven, American crow, Black-billed magpie, and Gray jay). Flight performance and total aerodynamic power scaled with negative allometry, but were significantly influenced by foraging ecology. Species that forage on the ground had relatively lower jump impulses, shorter wings, higher wingbeat frequencies, and higher power output than species that forage on elevated substrates. I also found two unexpected internal scaling patterns. Both proportional muscle length change (muscle strain) and average cross-sectional area specific force (muscle stress) increased with size. Longer wingbeat cycles may permit more complete muscle activation in larger birds, thereby partially compensating for the constraint imposed by wingbeat frequency. These data offer the strongest support and the only direct evidence for power-limited scaling of flight performance to date.

PREFACE

> You can drop a mouse down a thousand-yard mineshaft; and, on arriving at the bottom, it gets a slight shock and walks away, provided that the ground is fairly soft. A rat is killed, a man is broken, a horse splashes.
>
> - J.B.S. Haldane 1928
>
> 'On being the right size'

Body size is likely the single most influential phenotypic element for virtually all other aspects of an organism's biology. Schmidt-Nielsen (1984) argued that over 95% of any organism's phenotype could be predicted knowing only its phylogenetic placement and its body mass. It was this idea that first piqued my interest in the study of allometry. As any scientist, or any inquisitive five-year old, would follow such a statement, I wondered "Why?" Despite the countless life-history, physiological, and morphological traits that vary with body-size (e.g. Hill 1950; Greenewalt 1962; Schmidt-Nielsen 1984; Calder 1996), the underlying mechanisms behind these correlations tend to be subjects of much debate. Additionally, size has been suggested as both a target of selection, particularly sexual selection (e.g. Andersson & Iwasa 1996), and as influencing evolutionary patterns (e.g. diversification rates within clades, Dial & Marzluff 1989). Given the importance of body size to evolutionary biology and ecology a number of significant questions remain unanswered. Why are animals a given size? Why does a clade have specific minimum and maximum sizes? How does natural or sexual selection act on size?

Birds in particular demonstrate interesting patterns in size. They are the most speciose clade among tetrapod vertebrates, a factor that is typically attributed to their ability to fly and exploit novel niches unavailable to most ground based organisms. Yet

the largest of the extant flying species, within several divergent avian orders, are all ~13-15 kg (Kori bustard, Mute swan, Wild turkey). Among volant bird species it has been suggested anecdotally, but minimally quantified, that flight ability varies inversely with body size. Very large birds appear to have difficulty taking off, and have restricted aerial behavior. Restrictions on flight performance increase with size until ~15 kg, when they become too great to allow even steady flight. Similar locomotor restrictions likely influence the upper size limit within other clades, but flight is so costly that body-size induced limitations should be much more observable in birds.

At least two hypotheses attempt to explain the scaling of flight performance ability, but neither has been fully tested. The first (and generally accepted) hypothesis suggests that relative muscle power decreases with size since wing-beat frequency also decreases (Pennycuick 1975). At some size, large birds with large (long) wings cannot produce enough muscle power to overcome the effects of drag and gravity, and flight is thus impossible. The second hypothesis suggests that relative muscle power is invariable with size, but the ability to produce actual lift from a given amount of power decreases with size (Marden 1994). Under this hypothesis, birds (and any flying organism) would not be restricted at 15 kg if a large enough proportion of their body mass was composed of flight muscle. Not only has the pattern of scaling of flight performance remained un-quantified, neither hypothesis attempting to explain it has previously been tested in a large and ecologically diverse sample of species.

This collection of work sets out as an initial examination of the influence of body size on avian burst locomotor abilities. It approaches three main questions: Does flight performance ability vary with body size among bird species? What morphological and

physiological mechanisms explain such variation? And what are the ecological and evolutionary consequences of variation of flight performance with size in birds?

Herein I present three chapters written for various journals, each with a unique focus on one or more of the aforementioned questions. Chapter 1 reports on the actual performance abilities of a survey of passerines, spanning from 5 g Ruby-crowned kinglets to an 898 g Common raven, which represent the entire extant body-mass range of the most speciose avian order (Passeriformes). While I demonstrate that flight performance scales negatively, in passerines size is not the entire story. Elements of ecology and morphological allometry confound the size-performance relationship. Chapter 2 discusses the mechanics of burst takeoff and vertical flight (hindlimb contribution, forelimb and body kinematics, estimates of total muscle power output). Surprisingly, despite large variation in ecology, size, phylogeny, and performance, most of the species used relatively similar and invariant kinematics. Having established that there is some size-performance relationship and that variation in kinematics and hindlimb contributions can not explain it, Chapter 3 goes to the heart of the matter by examining *in vivo* muscle function in four species of corvids during burst vertical flight. The two outstanding hypotheses make divergent predictions about the scaling of mass-specific power output from the muscles, and the *in vivo* techniques in Chapter 3 are the only available ways of assessing actual muscle power.

References

Andersson, M. & Iwasa, Y. 1996 Sexual selection. *Trends in Ecology & Evolution* **11**, 53-58. (doi:10.1016/0169-5347(96)81042-1).

Calder, W.A. 1996 *Size, Function, and Life History*, Dover Publications.

Dial, K.P. & Marzluff, J.M. 1989 Nonrandom Diversification within Taxonomic Assemblages. *Systematic Zoology* **38**, 26-37.

Greenewalt, C.H. 1962 *Dimensional relationships for flying animals*, Smithsonian Institution.

Haldane, J.B.S. 1928 On being the right size. *A treasury of science*, 321–325.

Hill, A.V. 1950 The dimensions of animals and their muscular dynamics. *Sci. Prog* **38**, 209-230.

Marden, J.H. 1994 From damselflies to pterosaurs: how burst and sustainable flight performance scale with size. *Am J Physiol Regul Integr Comp Physiol* **266**, R1077-1084.

Pennycuick, C.J. 1975 Mechanics of flight. *Avian biology* **5**, 1–75.

Schmidt-Nielsen, K. 1984 *Scaling: Why is Size so Important*, New York: Cambridge University Press, New York.

Table of Contents **Page**

CORRELATIONS OF BODY SIZE AND ECOLOGY WITH SCALING OF BURST FLIGHT PERFORMANCE AMONG PASSERIFORMES

Abstract

Body size correlates with limits on avian flight performance (i.e., maneuverability, acceleration, climb rate), thereby possibly influencing behavior and explaining the upper size limit for flight capable species. Previous tests for a correlation between size and burst flight capacity have been limited in scope (at most 4-5 species) or used artificial load-lifting to elicit maximal performance, and the conclusions from these studies have been ambiguous. In order to offer a robust examination of this important aspect of avian biology, I tested burst take-off and vertical escape flight in 32 species of wild, and therefore naïve, Passeriformes, covering the full body mass range (5-900 g) of the most speciose clade (>5000 species) of birds. Maximal flight performance was measured in a vertical flight chamber ('The Tower of Power'). Performance estimates were quantified from high-speed three-dimensional kinematics. Flight performance, measured as either the net change in velocity or the net acceleration with each wingbeat, scaled negatively with body mass ($M_b^{-1.04}$); wherein the two largest species slowed with each wingbeat subsequent to take-off. The mass-specific rate-change in potential and kinetic energies among wingbeats (climb power, P_{cl}) scaled negatively with body mass ($M_b^{-.27}$), and in proportion to wingbeat frequency ($f^{.85}$). The ecological relevance of these data suggest a correlation with foraging location (ground vs. elevated, open vs. cover). For example, open-ground foragers generated greater mass-specific power output with higher wingbeat frequencies and possessed relatively shorter wings. These data

combined with two additional avian clades (Columbiformes and Galliformes) supports the hypothesis that flight performance scales negatively with vast majority of birds (5 g to over 5 kg).

Introduction

Differences in body size have been shown to influence patterns morphological design (Biewener 1989), physiological rates (Schmidt-Nielsen 1984), and life history strategies (Calder 1996), yet we have a minimal understanding as to how body size affects animal behavior (Dial et al. 2008). Arnold (1983) posited that morphological traits, such as body size, may constrain the performance capacity of an activity required for a specific behavior, thereby size may indirectly constrain behavioral variation. For example, diet may depend on maximum bite force whereas bite force may be constrained by jaw size, which itself correlates with body size (e.g. Verwaijen et al. 2002). Predator escape, prey apprehension, courtship display, and territory defense behaviors depend on maximal burst (i.e. accelerative) ability. However, our empirical knowledge of the relationship between size and maximal locomotor performance is limited and conclusions have been ambiguous (e.g. Domenici & Blake 1997; Chai & Millard 1997; Tobalske & Dial 2000; Irschick et al. 2003).

Aerodynamic and physiological scaling theory predict that burst flight capacity in birds should be negatively related to body mass (hereafter the 'power-limiting hypothesis'; Hill 1950; Pennycuick 1972). Burst ability is a result of the marginal power, defined as the power the muscles can produce in excess of the minimal power required for level flight. In geometrically similar birds, mass-specific muscle power is expected to

vary with wing-beat frequency, which scales as body-mass $M_b^{-0.33}$ (Greenewalt 1962). Mass-specific power requirements of level flight are predicted to be roughly invariant with size (M_b^0 to $M_b^{0.16}$, Pennycuick 1975, Ellington 1991). Therefore marginal power (the difference between power output and required power) is predicted to scale as $M_b^{-0.33 \text{ to } -0.17}$. This is also true for flight ability during behaviors that require marginal power (e.g. flying slowly or quickly, accelerating, taking off, maneuvering). Such negative scaling of burst flight ability is supported anecdotally in the field when observing flight repertoires of the smallest bird species (e.g. hummingbirds, 2-5 g) compared to the stilted flight capacity of the largest species (e.g. large Galliformes and Anseriformes, >10 kg). However, mass-performance relationships in birds have been empirically described as negative (Tobalske & Dial 2000; Altshuler et al. in press), positive (Marden 1994), and neutral (Chai & Millard 1997; Askew et al. 2001), thus the true relationship between size and maximum flight ability in birds remains in question.

Defining maximum flight performance is notoriously difficult, as illustrated by the variety of previously used techniques in studies of inter-specific scaling (vertical escape flight, climb power: Tobalske and Dial 2000, Askew et al. 2001; sequentially loaded flights, maximum load lifted: Marden 1987; asymptotic load lifting, maximum load lifted: Chai & Millard 1997, Altshuler et al. in press). Thus, a primary focus of this study was to elicit maximal performance in an ecologically relevant behavior. Birds are most likely to maximally perform in perceived life and death situations. Take-off and accelerating flight are used by many passerine (i.e., songbird) species to avoid predation (Lima 1993), and require more aerodynamic power than other types of flight (Norberg 1990). However, body mass is not likely the only determinant of escape flight

performance. Variation in wing shape, relative wing size, or wing movement will influence the minimal power requirements (Norberg 1990), and variation in relative muscle size or fiber type will influence the maximal power output. Since extant bird species vary in each factor (e.g. from high-speed to high aspect-ratio to elliptical wings) depending on ecological strategies (e.g. foraging niche, migratory behavior), variation in burst ability likely reflects ecological and morphological variation in addition to scaling patterns.

The primary objective of this research is to empirically demonstrate the relationship between size and maximal flight performance among bird species. I examined burst take-off and vertical flight across the full range of body mass (~5 g to ~ 1 kg) in the most speciose clade of living birds (Order Passeriformes, aka. songbirds, with >5000 species). More that half of extant avian species are included in Passeriformes, making the pattern of scaling in this order critical to our understanding of scaling in birds in general. Additionally, using a single order minimizes the confounding effects of variation in morphology on flight performance. Nevertheless, the ecological, morphological, and phylogenetic variation that is present within Passeriformes offers the opportunity to explore the interplay between these factors and body size in relation to maximal performance.

Methods

Wild birds were captured by mist-net using male song recordings as an attractant, between May 1 and July 31, over three years. Following capture birds were immediately transported to the Field Research Station at Fort Missoula (FRS) in Missoula, MT. All

birds were released within three hours near their capture site. Corvids were caught using carrion bait in either a remote-controlled bow trap or rocket-net within 200 miles of Missoula. Upon arrival at FRS, they were housed in large outdoor aviaries and provided food (canned dog food, raw eggs, meal worms, bird seed mix) and water *ad libitem*. All procedures were approved by The University of Montana IACUC (No. 044-07KDDBS-122007).

The testing protocol initially consisted of both vertical and horizontal escape flights. For both tests, the birds were placed within a spring-loaded plexi-glass pyramid that opened outwardly when triggered (Fig. 1). The four walls of the pyramid were painted black except for the top 4 cm (vertical test) or one side (horizontal test). The pyramid served several functions: (1) safely contained and constrained the bird on the forceplate, (2) visually oriented the bird in the direction of desired escape, and (3) when opened startled the bird to escape but imposed no restriction to wing movement.

The vertical flight tests were conducted in a specially constructed vertical flight chamber (the 'Tower of Power'; two versions: 2 x 2 x 3.7 m, and 2 x 2 x 7.6 m, hereafter the tower) indoors at FRS (Fig. 1). Depending on the size of the test subject the width of the Tower was adjusted to between 0.5 and 2 m by repositioning two of the netted side-panels. Upon opening the pyramid, all naive birds immediately ascended, often accelerating into the ceiling, and flew into the recapture cage at the top of the tower. Only the maximal flights of each individual were included in further analyses.

For horizontal tests the pyramid/force plate was placed at one end of a netted horizontal flight tunnel (2 x 2 x 8 m) that had an exit through an open garage door to the outdoors. The 'front' and side walls of the pyramid were opened in an attempt to induce

the birds to fly down the tunnel to escape. In addition to the pyramid, birds were also presented a taxidermy Saw-whet owl mounted to look like it was attacking from above the forceplate, and offered branches, bushes, and dark corners at the far end of the tunnel as additional attractants. Only two species satisfactorily performed in the horizontal test (see results section), so further methodological description is limited to the vertical test.

Filming and kinematic analysis

All flights were filmed with four high-speed (250 frames per second cameras; Fig. 1). Lenses and exact camera positions depended on the size of the bird. The calibrated filmed volume ranged from 0.5 x 0.5 x 1 m (birds less than 20 g) to 2 x 2 x 2.5 m (birds greater than 300 g). Ten landmarks (head, shoulder, wrist, wingtip, middle primary, first secondary, longest tertial, rump, middle retrix, left retrix) were marked by small (1-4 mm) pieces of reflective tape (3M part no. 8850) and digitized to determine three-dimensional coordinates (DLT; Ariel Performance Analysis Software, San Diego, CA, or DLTdv3.m, Hedrick 2008, in MATLAB, The Mathworks). All further analyses were performed in IGOR Pro (v 6.0, Wavemetrics, Inc.). Positional coordinates were smoothed with a cubic spline, and all velocities were calculated from the first derivative of smoothed positional coordinates. Error in positional coordinates was estimated at <1% (Chapter 2).

Downstroke initiation was defined as the transition from dorsal to ventral wrist movement. Wing area and length, and tail area were calculated dynamically from triangular planes formed by the wing markers, and are presented as mean values measured over downstroke. The angle of travel, body velocity, and kinetic and potential

energies for each wingbeat cycle were based on the average of the shoulder and rump markers.

Performance calculations

Locomotor performance in flight is described using three measurements of linear movement: net change in velocity per wingbeat (dv), acceleration per wingbeat (v'), and mass-specific climb power (P_{cl}). The latter incorporates changes in both velocity and altitude by summing the rate change in mass-specific kinetic and potential energies (P_{KE}, P_{PE} respectively):

$$(1)\quad P_{cl} = P_{KE} + P_{PE}$$

$$(2)\quad P_{KE} = \tfrac{1}{2}\left(v_{n+1}^2 - v_n^2\right) * f_n$$

$$(3)\quad P_{PE} = g(h_{n+1} - h_n) * f_n$$

where v is the body velocity at the start of wingstroke n, h is the z-value (height) of the body at the start of wingstroke n, and f is the frequency of that wingstroke calculated as the inverse of the wingstroke duration.

Phylogenetic and statistical analysis

Since the first downstroke of most flights started before toe-off, and since the first wingbeat is recognized as being unique (Simpson 1983, Earls 2000), this analysis includes only wingbeats subsequent to the first. Individuals' flight performance measurements were not significantly different within species. Thus, wingbeat values were pooled across all individuals for a given species to calculate mean and s.e.m.

To test for the possibility that scaling trends resulted from shared evolutionary histories I performed all scaling analyses using phylogenetic methods. I constructed a phylogenetic tree in Mesquite (PDAP module, Midford et al. 2003; Mesquite v. 2.71 build 514, Maddison & Maddison 2009) for the study species using recently published maximum likelihood molecular trees (Cicero & Johnson 2001; Lovette & Bermingham 2002; Carson & Spicer 2003; Spicer & Dunipace 2004; Treplin et al. 2008). Given the diverse sources and techniques used to assemble the source trees, branch lengths were arbitrarily set using Pagel's (1992) method. A 'tip' file and a variance-covariance matrix file (.dsc) were exported to the Regressionv2.m program (Lavin et al. 2008) in Matlab (). Each regression model included individually, and in combination, effects of foraging level (ground vs. elevated), foraging cover (open vs. cover), and migratory behavior (resident vs. migrant). Habitat and migration variables for each species were determined using personal observations of each species prior to capture, and supplemented by species accounts in Poole (2005). Using the best-fit model (based on Akaike information criteria, AIC) from ordinary least squares regression (OLS, assuming star phylogeny) two phylogenetic controlled analyses were performed: generalized least squares (pGLS) analysis, which assumes the given branch lengths; and the Ornstein-Uhlenbeck transformation (RegOU), which estimates intermediate levels of phylogenetic signal. Bootstrapping (n=2000 repetitions) was used to create 95% confidence intervals around coefficient estimates.

Ordinary linear regression tends to underestimate the slope of the best-fit line and is inappropriate for allometric correlations (Warton et al. 2006). However, to estimate the best-fit line describing the relationship between two variables (as in studies of

allometry), standardized major axis regression (SMA, also known as reduced major axis regression, RMA) is more appropriate (Warton et al. 2006). SMA was performed in the (S)MATR package (Warton & Weber 2002; Warton et al. 2006) in R (R Development Core Team 2009) on each of the OLS best-fit models, since no phylogenetic model improved the fit over OLS. All other statistics were also performed in R. All slopes presented in the text are common or guild (e.g. ground foragers) slopes from SMA regression.

Results

A total of 32 species (Table 1) were captured and performed the maximal effort vertical flight test. Only two individuals (house sparrow and cliff swallow) flew >1 m in the horizontal flight test. Every other bird flew immediately to the top of the tunnel to perch on the netting. Thus, results herein are from only the vertical tests. The 32 species represent 14 families of passerines, and include the smallest (*Regulus*, Ruby-crowned Kinglet, 5.4 g), and largest genera (*Corvus*, Common Raven, 898.4 g) of passeriformes. Phylogenetic models (pGLS and RegOU) never improved fit over OLS models, suggesting very low phylogenetic signal.

Performance and Power

All three measurements of flight performance (*dv*, *v'*, and P_{cl}) negatively correlated with body mass (Table 2). Most species were able to accelerate with each wingbeat after take-off. However, the largest species (American Crow, Common Raven) reached peak velocity at toe-off and lost velocity with each wingbeat thereafter (Crow *dv* = -0.12 m s^{-1}, Raven *dv* = -0.41 m s^{-1}; Fig. 2A). Per-wingbeat change in velocity (*dv*) and

the resulting acceleration (v') scaled with similar negative allometry (mean dv: $M_b^{-1.04}$; mean v': $M_b^{-1.04}$, Table 2; Fig. 2A), even after removing the negative values of performance in order to log-transform the data for correlation analysis. Mean and maximum P_{cl} scaled with significant negative allometry as $M_b^{-.26}$ and $M_b^{-.32}$, respectively (Fig. 2B, Table 2). For all measurements of performance the best-fit model included an interaction between foraging elevation and foraging cover, such that open-ground foragers performed better after accounting for body mass (Table 3).

Wingbeat frequency (f) scaled as $M_b^{-.31}$, with a significant effect of foraging elevation and cover such that open-ground foragers had higher wingbeat frequencies (Fig. 2C, Table 2). Mass-specific climb power scaled as $f^{0.85}$, which was not significantly different than the prediction from the power-limiting hypothesis, f^1 (p=0.34, Table 3).

Morphometrics

Wing and tail dimensions scaled with significant positive allometry. Wing length, measured dynamically during mid downstroke, increased as $M_b^{.42}$ (Fig. 3A, Table 3, Appendix I), which was significantly greater than isometry ($M_b^{.33}$, p=0.002). Wing length in ground foragers was significantly shorter than in elevated foragers (p=.015, Table 3). Muscle masses were only available from the corvids, which were euthanized for a concurrent study, and the single individual (a Ruby-crowned Kinglet not included in the performance analyses) that died during this study. Flight-muscle mass (combined pectoralis m. and supracoracoideus m.) scaled isometrically, averaging 15-16 % of M_b in all five species.

Discussion

This study is the largest quantitative investigation to date into the maximal locomotor flight performance of unloaded birds, and clearly demonstrates negative scaling of burst flight ability with support for the power-limiting hypothesis. With increasing size birds were less able to accelerate vertically, hence produced lower P_{cl}. Additionally, I found a subtle and unpredicted correlation between morphology (wing-length), kinematics (wingbeat frequency), flight performance (dv, v', and P_{cl}), and ecological niche (open-ground foragers). Not only do these data offer evidence for the scaling of flight performance, they also offer insight to the factors that drive variation in flight performance at a given size.

The power-limiting hypothesis describes the upper limit on performance imposed by the scaling of wingbeat frequency for otherwise geometrically and dynamically similar birds (Pennycuick 1975). Rather than describing the mean trend, therefore, the hypothesis describes a ceiling (Fig. 2B) for a given body plan. Morphological and physiological traits specific to burst flight (e.g. large flight muscles, fast-twitch muscle fibers, short broad wings) may conflict with traits for other important behaviors (e.g. migration), or may be costly to use or maintain. Such trade-offs could lead to deviations from the design optimized for burst flight, and relatively lower flight performance. I therefore hypothesize that species that depend on elevated cover to provide alternative predator evasion strategies (i.e. hiding, Lima 1993) and are less susceptible to predation (Gotmark & Post 1996) have been released from the selective pressures on burst flight ability. As a result, such species have longer wings that provide for more efficient

cruising flight. While beyond the scope of this study, this hypothesis would predict that relative muscle size and muscle fiber type should also vary as a function of ecological niche. Nevertheless, the passerine species herein were relatively geometrically and dynamically similar when compared to the variation among avian orders. It follows that studies of inter-order scaling of performance may be hampered by the greater levels of morphological variation.

Unladen maximal burst flight has been studied in two other avian orders (five species of columbiformes: Seveyka 1999; four species of Galliformes: Tobalske & Dial 2000; one Galliformes species, Blue Quail: Askew et al. 2001). With all available data from these three orders, body mass specific P_{cl} scales with significant allometry as $M_b^{-.25}$ ($p<0.001$; Fig. 4A), and is directly proportional to wingbeat frequency ($f^{1.0}$; $p=0.84$; Fig. 4B). Columbiformes perform better at a given mass, or at a given wingbeat frequency, than either the Galliformes or Passeriformes ($p<0.001$). The most likely explanation for this discrepancy is relative muscle size; Columbids have relatively larger flight muscles (pectoralis and supracoracoideus 24-30% body mass; Hartman 1961; Seveyka 1999) than passerines or gallinaceous species (15-20%; this study; Hartman 1961; Tobalske & Dial 2000). Additionally, columbids use a wingtip-reversal upstroke. Wingtip-reversal has been suggested as a sign of an active upstroke, but empirical evidence for its efficacy is unavailable. If the upstroke muscles (supracoracoideus m.) produced aerodynamically useful power, this could also contribute to P_{cl}. Lastly, Altshuler et al. (in press) have demonstrated similar scaling of flight power output in an impressive study of load-lifting capacities in 62 species of hummingbirds. Thus, among four orders and over three orders

of magnitude of body mass, the negative effects of size on maximal avian flight performance are abundantly clear.

The size-performance relationship likely has significant behavioral and ecological implications (Dial et al. 2008) beyond the relationship with habitat use previously discussed. Selection for any behavior dependent on burst flight may lead to selection for small size. For example, shorebird species that use aerial displays as a form of courtship exhibit relatively small average body size and reverse sexual size dimorphism (i.e. males smaller than females; Székely et al. 2004), a possible outcome of power-limitation on aerial performance. However, size has its benefits, especially absolute strength. Shorebirds that use male-male combat on the ground tend to be larger overall and exhibit typical sexual size dimorphism (Székely et al. 2004). Additionally, size alone may act as a signal of performance to inform predators and prey of each other's flight abilities, resulting in possible size-based patterns in alert calls (Templeton et al. 2005), mobbing behavior, and prey selection. Therefore, the effects of body size on relevant measures of locomotor performance should be considered when examining intra- and inter-specific behavioral patterns.

References

Arnold, S.J. 1983 Morphology, Performance and Fitness. *American Zoologist* **23**, 347-361.

Askew, G.N., Marsh, R.L. & Ellington, C.P. 2001 The mechanical power output of the flight muscles of blue-breasted quail (Coturnix chinensis) during take-off. *J Exp Biol* **204**, 3601-3619.

Biewener, A.A. 1989 Scaling Body Support in Mammals: Limb Posture and Muscle Mechanics. *Science* **245**, 45-48.

Calder, W.A. 1996 *Size, Function, and Life History*, Dover Publications.

Carson, R.J. & Spicer, G.S. 2003 A phylogenetic analysis of the emberizid sparrows based on three mitochondrial genes. *Molecular Phylogenetics and Evolution* **29**, 43–57.

Chai, P. & Millard, D. 1997 Flight and size constraints: hovering performance of large hummingbirds under maximal loading. *J Exp Biol* **200**, 2757-2763.

Cicero, C. & Johnson, N.K. 2001 Higher-level phylogeny of new world vireos (Aves: Vireonidae) based on sequences of multiple mitochondrial DNA genes. *Molecular Phylogenetics and Evolution* **20**, 27–40.

Dial, K.P., Greene, E. & Irschick, D.J. 2008 Allometry of behavior. *Trends in Ecology & Evolution* **23**, 394-401. (doi:10.1016/j.tree.2008.03.005).

Domenici, P. & Blake, R. 1997 The kinematics and performance of fish fast-start swimming. *J Exp Biol* **200**, 1165-1178.

Ellington, C.P. 1991 Limitations on Animal Flight Performance. *J Exp Biol* **160**, 71-91.

Gotmark, F. & Post, P. 1996 Prey Selection by Sparrowhawks, Accipiter nisus: Relative Predation Risk for Breeding Passerine Birds in Relation to their Size, Ecology and Behaviour. *Philosophical Transactions: Biological Sciences* **351**, 1559-1577.

Greenewalt, C.H. 1962 *Dimensional relationships for flying animals*, Smithsonian Institution.

Hartman, F.A. 1961 Locomotor mechanisms of birds. *Smithson. Misc. Coll.* **143**, 1-91.

Hedrick, T.L. 2008 Software techniques for two- and three-dimensional kinematic measurements of biological and biomimetic systems. *Bioinspiration & Biomimetics* **3**, 034001.

Hill, A.V. 1950 The dimensions of animals and their muscular dynamics. *Sci. Prog* **38**, 209-230.

Irschick, D.J., Vanhooydonck, B., Herrel, A. & Andronescu, A. 2003 Effects of loading and size on maximum power output and gait characteristics in geckos. *J Exp Biol* **206**, 3923-3934. (doi:10.1242/jeb.00617).

Lavin, S.R., Karasov, W.H., Ives, A.R., Middleton, K.M. & Garland Jr., T. 2008 Morphometrics of the avian small intestine compared with that of nonflying mammals: a phylogenetic approach. *Physiological and Biochemical Zoology* **81**, 526-550. (doi:10.1086/590395).

Lima, S.L. 1993 Ecological and Evolutionary Perspectives on Escape from Predatory Attack: A Survey of North American Birds. *The Wilson Bulletin* **105**, 1-47.

Lovette, I.J. & Bermingham, E. 2002 What is a wood-warbler? Molecular characterization of a monophyletic Parulidae. *The Auk* **119**, 695–714.

Maddison, W.P. & Maddison, D.R. 2009 Mesquite: a modular system for evolutionary

analysis. Version 2.71.

Marden, J.H. 1994 From damselflies to pterosaurs: how burst and sustainable flight performance scale with size. *Am J Physiol Regul Integr Comp Physiol* **266**, R1077-1084.

Marden, J.H. 1987 Maximum Lift Production During Takeoff in Flying Animals. *J Exp Biol* **130**, 235-258.

Midford, P.E., Garland Jr, T. & Maddison, W.P. 2003 PDAP Package, Version 1.14.

Norberg, U.M. 1990 *Vertebrate Flight: Mechanics, Physiology, Morphology, Ecology and Evolution (Zoophysiology, Vol. 27)*, Berlin: Springer Verlag.

Pagel, M.D. 1992 A method for the analysis of comparative data. *Journal of Theoretical Biology* **156**, 431–442.

Pennycuick, C.J. 1972 *Animal flight*, Hodder Arnold.

Pennycuick, C.J. 1975 Mechanics of flight. *Avian biology* **5**, 1–75.

Poole, A. ed. 2005 *The Birds of North America Online: http://bna.birds.cornell.edu/BNA/*, Ithaca, NY: Cornell Laboratory of Ornithology.

R Development Core Team 2009 *R: a language and environment for statistical computing*, Vienna, Austria: R Foundation for Statistical Computing.

Schmidt-Nielsen, K. 1984 *Scaling: Why is Size so Important*, New York: Cambridge University Press, New York.

Seveyka, J. 1999 *The effects of body size and morphology on the flight behavior and escape flight performance of birds*. M.S. The University of Montana.

Spicer, G.S. & Dunipace, L. 2004 Molecular phylogeny of songbirds (Passeriformes) inferred from mitochondrial 16S ribosomal RNA gene sequences. *Molecular Phylogenetics and Evolution* **30**, 325–335.

Székely, T., Freckleton, R.P. & Reynolds, J.D. 2004 Sexual selection explains Rensch's rule of size dimorphism in shorebirds. *Proceedings of the National Academy of Sciences of the United States of America* **101**, 12224-12227. (doi:10.1073/pnas.0404503101).

Templeton, C.N., Greene, E. & Davis, K. 2005 Allometry of Alarm Calls: Black-Capped Chickadees Encode Information About Predator Size. *Science* **308**, 1934-1937. (doi:10.1126/science.1108841).

Tobalske, B. & Dial, K. 2000 Effects of body size on take-off flight performance in the Phasianidae (Aves). *J Exp Biol* **203**, 3319-3332.

Treplin, S., Siegert, R., Bleidorn, C., Thompson, H.S., Fotso, R. & Tiedemann, R. 2008 Molecular phylogeny of songbirds (Aves: Passeriformes) and the relative utility of common nuclear marker loci. *Cladistics* **24**, 328–349.

Verwaijen, D., Damme, R.V. & Herrel, A. 2002 Relationships between Head Size, Bite Force, Prey Handling Efficiency and Diet in Two Sympatric Lacertid Lizards. *Functional Ecology* **16**, 842-850.

Warton, D.I. & Weber, N.C. 2002 Common Slope Tests for Bivariate Errors-in-Variables Models. *Biometrical Journal* **44**, 161-174.

Warton, D.I., Wright, I.J., Falster, D.S. & Westoby, M. 2006 Bivariate Line-Fitting Methods for Allometry. *Biological Reviews* **81**, 259-291. (doi:10.1017/S1464793106007007).

Figure Legends

Figure 1. Birds were filmed in a vertical flight chamber, taking off from a forceplate. Flights were induced by the sudden opening of a plexi-glass pyramid, which also contained the bird on the forceplate and directed their sight through a clear window to the white cotton sheet at the top of the tower. The width of the tower was adjusted from .5 to 2 m depending on the size of species being tested.

Figure 2. Flight performance measured as (A) maximum change in velocity per wingstroke, or (B) body mass specific climb power scaled negatively with body mass, but were higher in open-ground foragers (see table 2 for scaling coefficients). (C) Wingbeat frequency also varied significantly with foraging habitat such that open-ground foragers had higher wingbeat frequencies at a given mass.

Figure 3. Mean wing-length measured dynamically during the downstroke from 3-D kinematics scaled with positive allometry. Open-ground foragers had significantly shorter wings for their mass than other species.

Figure 4. (A) Flight performance measured as body-mass specific climb power across three avian orders scales as $M_b^{-.25}$, with variable but negative scaling within each order. (B) Across the three orders flight performance scales as wingbeat frequency $f^{1.0}$, supporting the power-limiting hypothesis. Columbiformes (doves) have significantly higher power output at a given mass or at a given wingbeat frequency. Columbiformes data from Seveyka (1999). Galliformes data from Tobalske and Dial (2000) and Askew et al. (2001).

Table 1. Phylogenetic relationship and ecological categories of the 32 species of Passeriformes included in this study. Mass is given as the mean (s.d.) of the number of individuals (n) of each species. See text for phylogenetic sources.

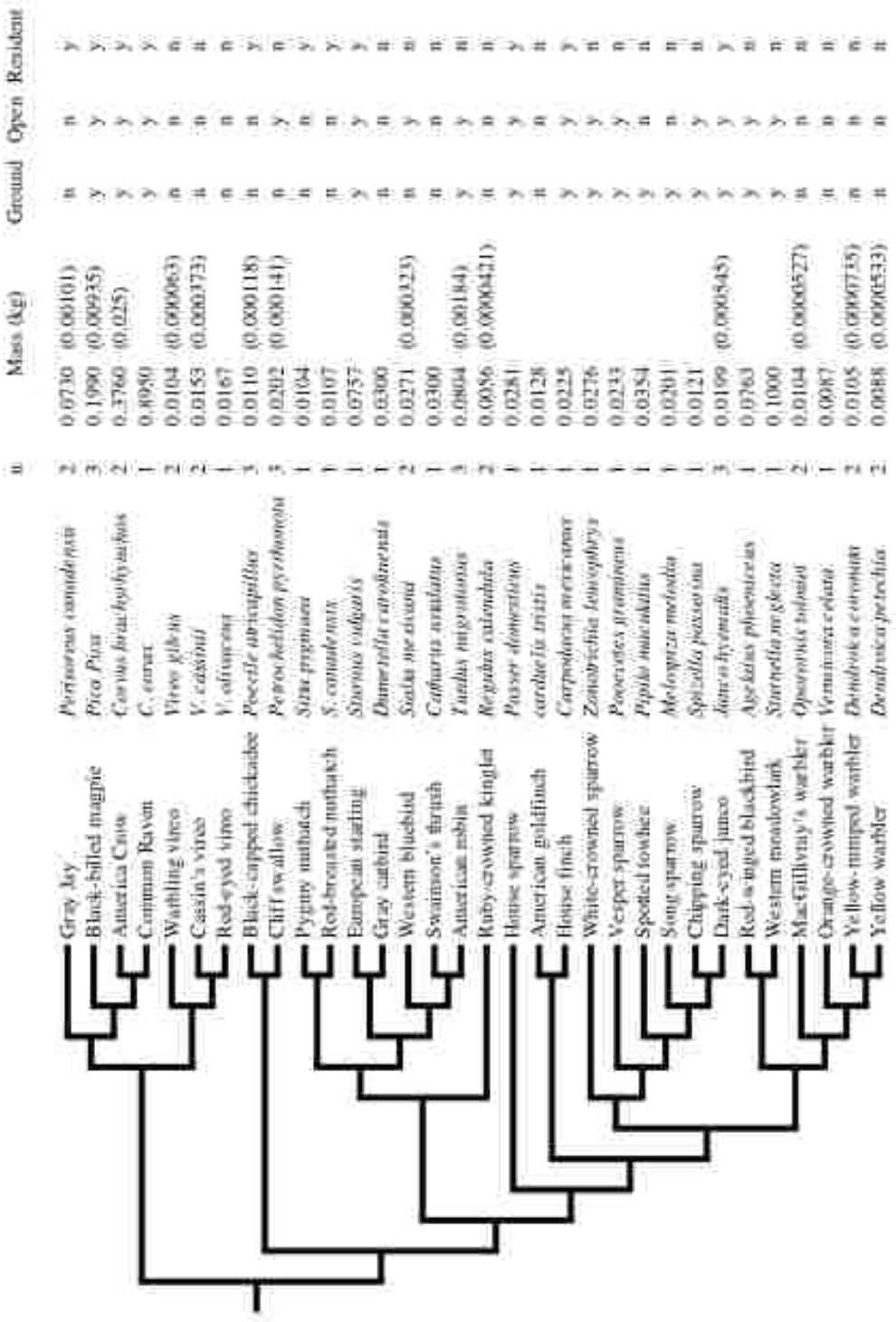

Table 2. Mass-specific power scaling coefficients from ordinary least squares (OLS) and standarised major axis (SMA) regression against body mass (M) and covariates, based on log base 10 transformed variables. All best fit models were from nonphylogenetic (OLS) analysis; phylogenetic transformed (RegOU) analyses provided similar fit and coefficients, but tranformation values (REML d) were always <0.001 indicative of very low phylogenetic signal. P-values for SMA are for tests of difference of slope and elevation (intercept) unless stated otherwise. *dv*: change in velocity per wingstroke; *v'*: wingstroke acceleration; P_{cl}: climb power; *f*: wingbeat frequency.

	OLS					SMA		
Performance measure	Independent vars.	model F	p	Coef. (-95% ,+95%)	AIC	Independent vars.	slope (-95% ,+95%)	intercept
dv	M only	1.9	0.18	-.27 (-.67, .13)	31.3	M	-1.04 (-.72, -1.5)	-2.5
	M	1.2	0.15	-.36 (-.86, .13)	32.9	open-ground	-1.2 (-.65, -2.4)	-2.6
	elevation*cover		0.52	-.01 (-.05, .02)		other	-1.3 (-.79, -2.14)	-3.2
							p=0.90	p=0.02
v'	M only	6.6	0.016	-.46 (-.83, -.10)	26.9	M	-1.04 (-.73, -1.5)	-1.2
	M	4.4	0.007	-.64 (-1.1, -.19)	26.7	open-ground	-1.2 (-.66, -2.2)	-1.3
	elevation*cover		0.17	-.02 (-.05, .01)		other	-1.3 (-.83, -2.1)	-1.8
							p=0.80	p=0.02
P_a	M only	0.9	0.35	-.04 (-.14, .05)	-34	M	-.26 (-.38, -.18)	1.1
	M	5.6	0.01	-.15 (-.25, -.04)	-42	open-ground	-.28 (-.45, -.17)	1
	elevation*cover		0.004	-.02 (-.03, -.01)		other	-.43 (-.73, -.25)	0.8
							p=0.23	p<0.0001
Max. P_a	M only	4.5	0.04	-.11 (-.22, -.01)	-26.1	M	-.32 (-.45, -.23)	1.1
	M	8	0.001	-.23 (-.35, -.10)	-33.0	open-ground	-.35 (-.56, -.22)	1.06
	elevation*cover		0.005	-.02 (0.03, -.01)		other	-.50 (-.84, -.30)	0.8
							p=0.30	p=0.0003
f	M only	111.1	<0.001	-.27 (-.33, -.22)	-72.6	M	-.31 (-.26, -.37)	0.8
	M	100.7	<0.001	-.55 (-.39, -.29)	-87.3	open-ground	-.39 (-.32, -.46)	0.75
	elevation*cover		<0.001	-.01 (-.02, -.01)		other	-.32 (-.24, -.43)	0.85
							p=0.25	p<0.0001
Max. P_a	*f*	12.9	0.001	.56 (.24, .88)	-33.1	*f*	.85 (.61, 1.19)	0.35
							p=0.34 if different from 1	

Table 3: Morphologcial coefficients from best-fit ordinary least squares (OLS) and standarised major axis (SMA) regression against body mass, based on log base 10 transformed variables. All best fit models were from nonphylogenetic (OLS) analysis; phylogenetic transformed (RegOU) analyses provided similar fit and coefficients, but tranformation values (REML d) were always <0.001 indicative of very low phylogenetic signal. P-values for SMA are for tests of difference of slope and elevation (intercept) unless stated otherwise.

	OLS					SMA		
Morph	Independent vars	F	p	Coef. (-95%,+95%)	AIC	Independent vars	slope (-95%,+95%)	intercept
Wing length	M	448.6	0.000	0.41 (0.37, 0.45)	-105	common	.42 (.38, .46)	-0.34
	ground	8.4	0.007	0.06		ground	.43 (.38, .48)	-0.32
						elevated	.40 (.32, .49)	-0.25
							p=.48	p=.0015
Wing area	M	552.8	0.000	0.79 (0.72, 0.86)	-69	common	.81 (.74, .89)	-.76 (-.86, -.67)
	ground	6.6	0.016	0.09		ground	.82 (.73, .91)	-0.73
						elevated	.79 (.67, .94)	-0.63
							p=.76	p=.005
Tail area	M	119.2	0.000	0.74 (0.60, 0.88)	-12	common	.92 (.77, 1.12)	-1.41 (-1.63, -1.19)
						ground	.89 (.70, 1.12)	-1.35
						elevated	1.03 (.72, 1.48)	-1.17
							p=.46	p=.037
Aspect ratio	no significant scaling or covariates							

Figure 1

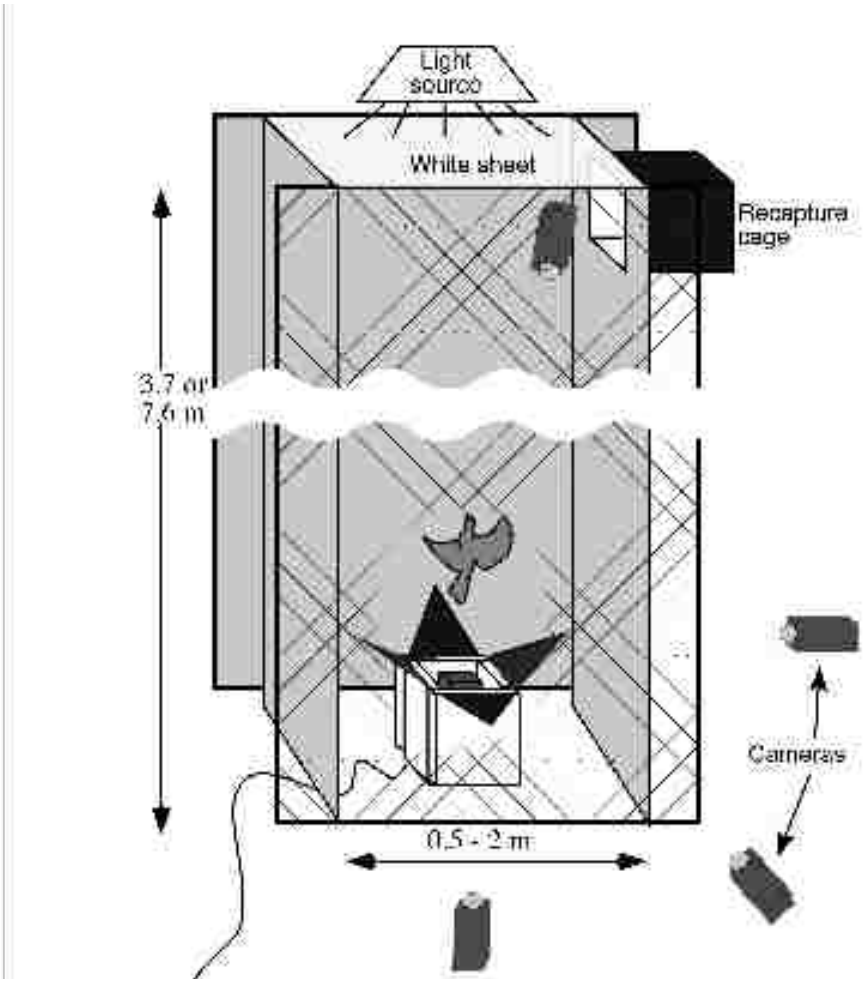
Light source
White sheet
Recapture cage
3.7 or 7.6 m
Cameras
0.5 - 2 m

Figure 2

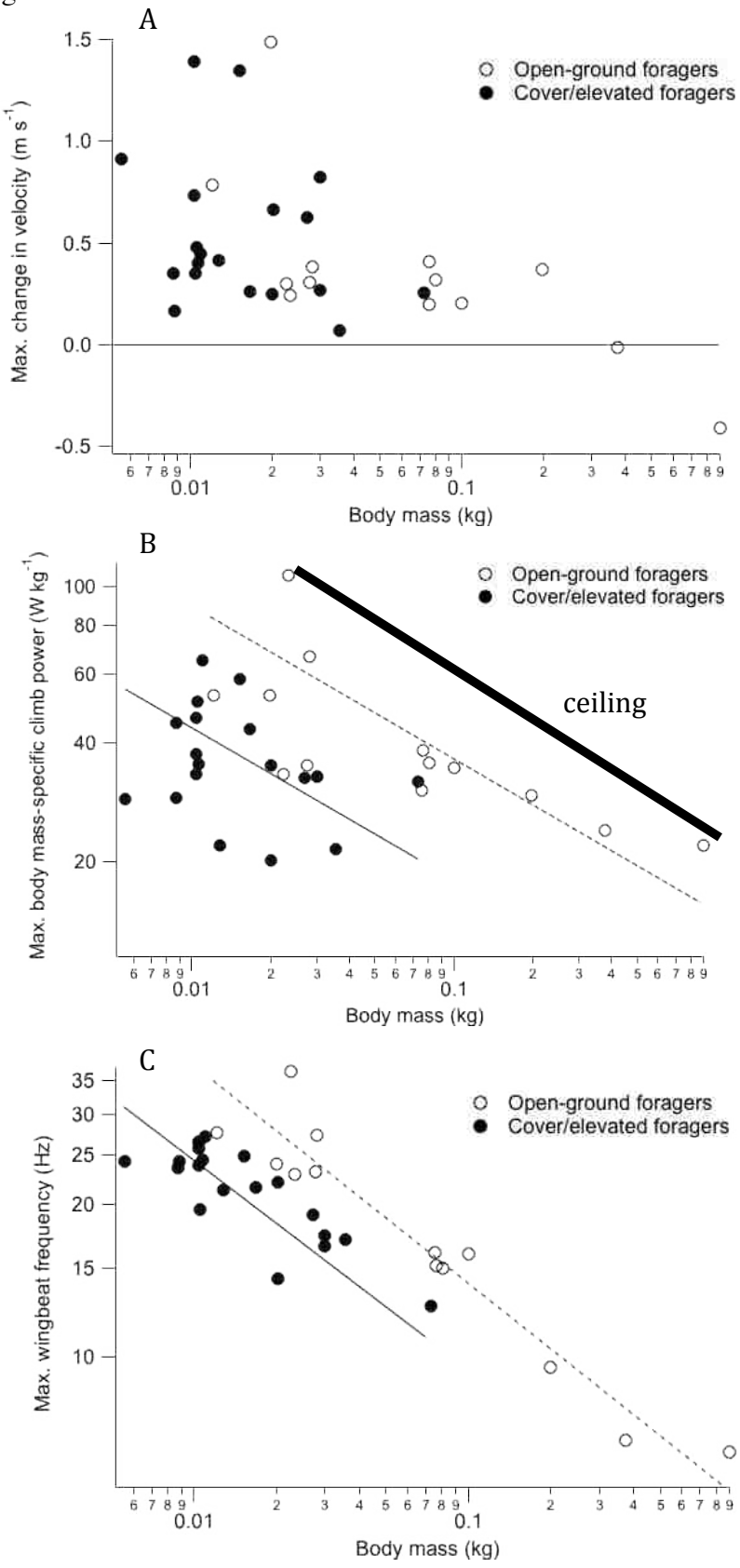
A
Open-ground foragers
Cover/elevated foragers
Max. change in velocity (m s-1)
1.5
1.0
0.5
0.0
-0.5
0.01
0.1
Body mass (kg)
B
Open-ground foragers
Cover/elevated foragers
ceiling
Max. body mass-specific climb power (W kg-1)
100
80
60
40
20
0.01
0.1
Body mass (kg)
C
Open-ground foragers
Cover/elevated foragers
Max. wingbeat frequency (Hz)
35
30
25
20
15
10
0.01
0.1
Body mass (kg)

Figure 3

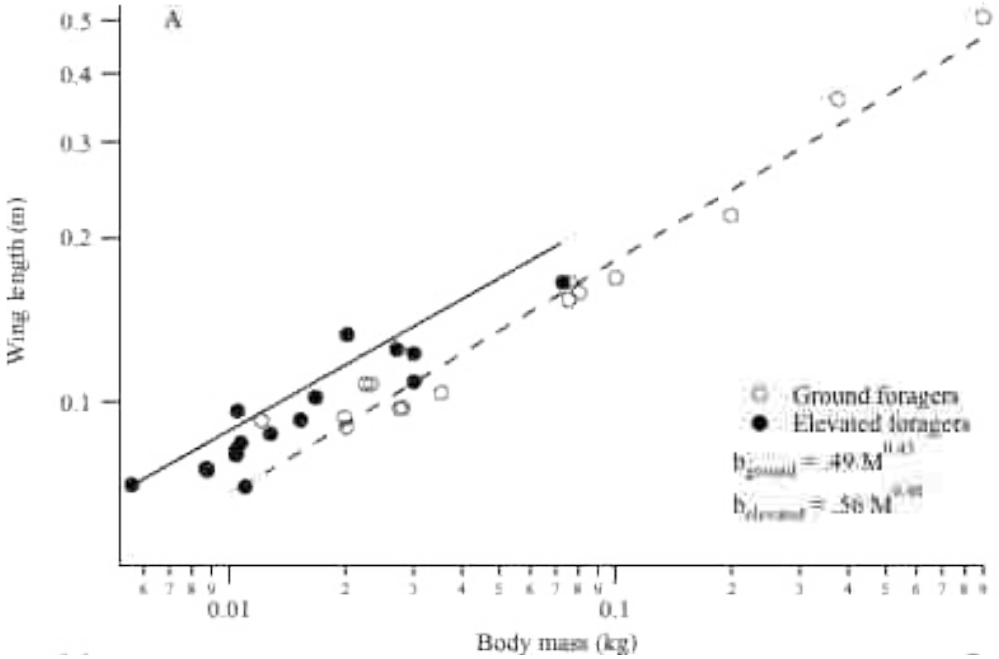
A
0.5
0.4
0.3
0.2
0.1
Wing length (m)
0.01
0.1
Body mass (kg)
Ground foragers
Elevated foragers

Figure 4

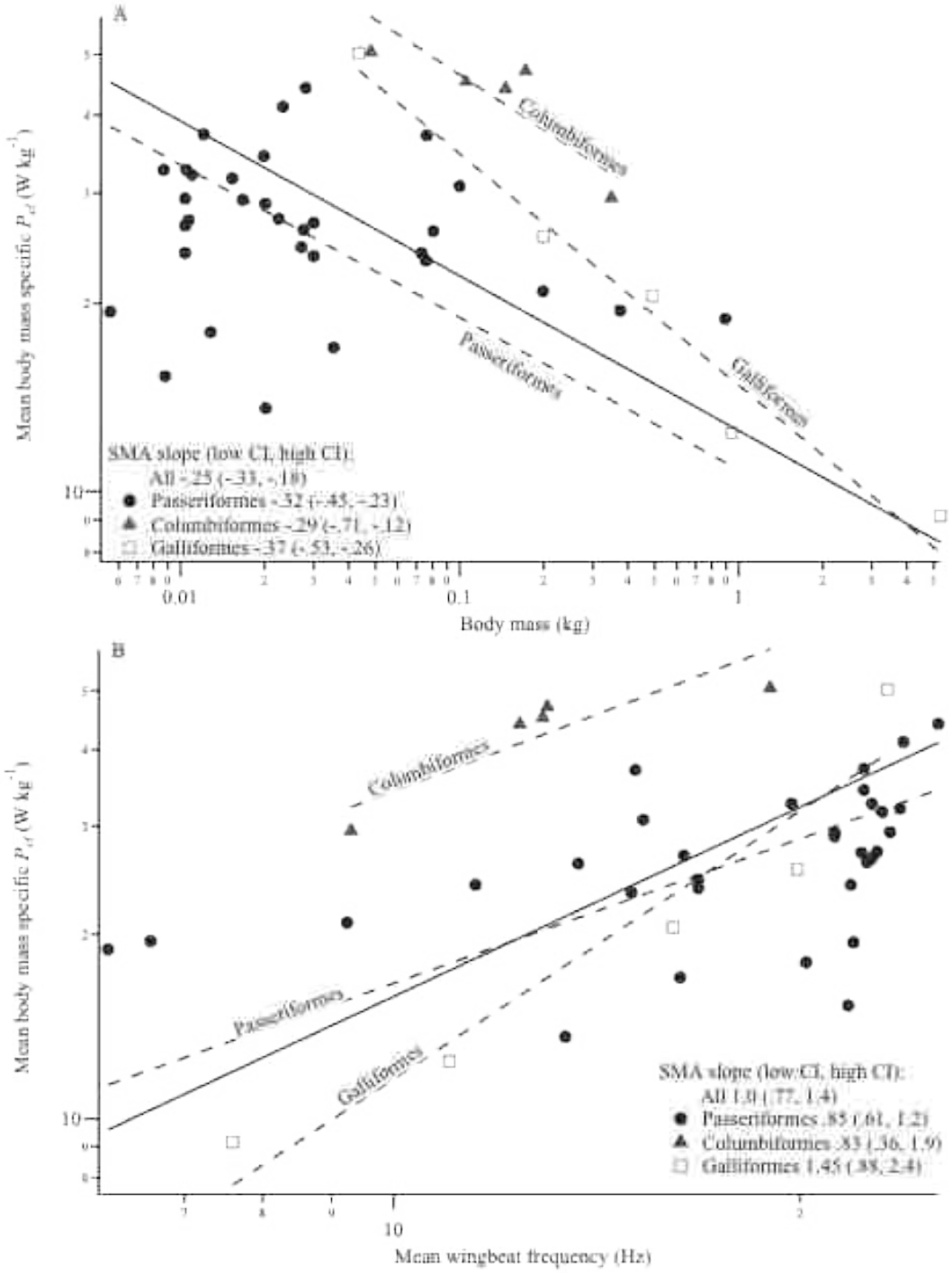
A
Mean body mass specific P_{cf} (W kg^{-1})
Columbiformes
Passeriformes
Galliformes
SMA slope (low CI, high CI):
All -.25 (-.33, -.18)
Passeriformes -.32 (-.45, -.23)
Columbiformes -.29 (-.71, -.12)
Galliformes -.37 (-.53, -.26)
0.01
0.1
1
Body mass (kg)
B
Mean body mass specific P_{cf} (W kg^{-1})
Columbiformes
Passeriformes
Galliformes
SMA slope (low CI, high CI):
All 1.0 (.77, 1.4)
Passeriformes .85 (.61, 1.2)
Columbiformes .83 (.36, 1.9)
Galliformes 1.45 (.88, 2.4)
10
Mean wingbeat frequency (Hz)

MECHANICS OF STANDING TAKE-OFF AND VERTICAL ACCELERATING FLIGHT AMONG PASSERIFORMES

Abstract

Burst locomotor performance is crucial for survivorship because of its role in predator escape and prey capture. Escape flight ability in birds has been shown to be negatively correlated with body mass (M_b), but the underlying mechanism is unknown. Traditionally, the scaling of burst flight performance has been explained as a result of negative scaling of mass-specific mechanical (muscle) power output, but empirical evidence for the hypothesis is limited. Escape take-off involves a transition from hind- to fore-limb dependent locomotion, and is fundamentally different from the most commonly studied flight behavior (i.e. level cruising flight). Herein, I present the first survey of the mechanics (ground-reaction forces, three-dimensional kinematic measurements, and aerodynamic power estimates) of burst take-off and vertical flight in a broad range of Passeriformes (32 species, 5-900 g body mass). Maximal flights were all preceded by a single counter-movement crouch and jump that produced a peak force on average 5 times body weight. The first downstroke consistently began just prior to toe-off. The body-mass specific impulse applied to the ground scaled positively ($M_b^{-0.18}$), thus hindlimbs in larger birds give them an early speed advantage over smaller birds. Wingbeat kinematics during the subsequent flights did not scale significantly, but the estimate of total mass-specific power scaled as $M_b^{-0.32}$. Wingbeat kinematics during burst vertical flight were unexpectedly similar to published values of other low-speed flight behaviors (e.g. slow level flight, hovering, ascending and descending flight). Additionally, the kinematics suggest that drag forces on the wings contributed as much or more than lift to

aerodynamic weight-support, supporting a fundamental rethinking of the role of drag in the economy of flight. When considered with *in vivo* measurements of muscle power from a concurrent study the results herein provide the most robust support to date for the negative scaling of muscle power and the role of body-size in constraining locomotor performance.

Introduction

Animals of various clades use a stereotypic style of burst locomotion for escaping predators or capturing prey (e.g. fish C-starts: for review see Domenici & Blake 1997; running/jumping in lizards: Irschick et al. 2003, Vanhooydonck et al. 2006; take-off and accelerating flight in birds: Lima 1993, Jackson in prep). Slight variation in burst locomotor performance could result in the life or death outcome for predator and prey. Thus, the morphological and physiological mechanisms underlying variation in performance should be under strong selective pressures. For example, it has been hypothesized that increased leg length in Anolis lizards is selected for under strong predation pressure because longer legs positively correlate with running speed (Losos & Sinervo 1989). In birds, however, little is known of the mechanics and constraints of take-off and burst flight because the prarameters are complex and often difficult to metric.

Burst flight performance in birds has been shown to be negatively correlated with body mass (Tobalske & Dial 2000; Altshuler et al. in press; Chapter 1). Typically, this correlation has been hypothesized to be a result of adverse scaling of mass-specific muscle power (hereafter the power-limiting hypothesis; Pennycuick 1975). That is, the

ratio of power produced by the muscles relative to the body mass of the bird decreases as body mass increases. In the only direct test of the power-limiting hypothesis, Jackson & Dial (Chapter 3) measured *in vivo* muscle mechanical power in four species of corvids and found that mass-specific muscle power scaled as body mass $M_b^{-0.18}$. However, the surgical techniques used in Jackson & Dial (Chapter 3) were limited to relatively large birds (>60 g), and measure the power from a single flight muscle (pectoralis), thereby ignoring possible contributions from the hindlimbs during take-off and other muscles during flight. Therefore, the current study aims to measure the hindlimb contribution to flight performance, as well as estimate total muscle power during subsequent flight in a large range of body masses (5 g to 1 kg), in order to gain insight to various factors that might influence burst flight performance.

Bird take-off involves a complex interplay of relatively independent hind- and fore-limb locomotor modules (Gatesy & Dial 1996), and a transition from terrestrial to fluid locomotion. Hindlimbs contribute most of the initial velocity at take-off (~50% in Rufous hummingbirds, ~90% in European starlings *Sturnus vulgaris* and Common quail *Coturnix coturnix,* Earls 2000; Tobalske et al. 2004) in order to reduce the aerodynamic costs associated with producing lift (i.e. induced power) at low velocities (Norberg 1985). Flight performance subsequent to toe-off may therefore be strongly influenced by the ability of the hindlimbs to provide initial velocity; a low take-off velocity requires high induced power costs *per se* (*sensu* Askew et al. 2001), and thus less of the limited muscle power would be available for accelerating the center of mass of the bird.

Following the transition to flight, locomotor performance is determined by the high amplitude, high angle of attack downstrokes characteristic of vertical flight

(Tobalske & Dial 2000; Askew et al. 2001; Berg & Biewener 2008). Each wingbeat cycle is a result of the activity of a number of muscles (although dominated by the massive paired *m. pectoralis* Biewener et al. 1992) that provide power to overcome drag on the body and wings and produce aerodynamic forces to accelerate the bird. The total power (P_{tot}) output from all muscles can be estimated using aerodynamic models based on three dimensional (3-D) kinematic measurements (Wakeling & Ellington 1997a; Askew et al. 2001; Berg & Biewener 2008; Altshuler et al. in press). Only Altshuler et al. (in press) have estimated the scaling of maximum P_{tot} in wild birds (62 species of hummingbirds, 2.0-5 g body mass), and found that P_{tot} scaled as $M_b^{-0.3}$. However, they used an artificial load-lifting assay. There are no known published data on the escape flight mechanics or power output of maximal unladen flight in wild untrained birds.

This study partitions the hindlimb module performance from the forelimb module performance during burst (escape) take-off in order to (1) test the power-limiting hypothesis and (2) describe the mechanics of each module over a range of body sizes. Burst flight performance in 32 species of passerines scales negatively with body mass ($M_b^{-.21}$; Chapter 1). Herein I obtain ground reaction forces (using a forceplate) and evaluate 3-D kinematic measurements to quantify the mechanics and scaling of escape take-off and vertical accelerating flight in these species.

Methods

A total of 32 species of Passeriformes were captured in the field ranging in mass from 5 g (Ruby-crowned Kinglet) to 900 g (Common Raven). Capture and testing

protocols will be briefly described here (for a detailed explanation see Chapter 1) and were approved by The University of Montana IACUC (No. 044-07KDDBS-122007).

Birds were placed on a force plate (Bertec, A6810) within plexi-glass pyramid consisting of spring-loaded bottom-hinged walls that opened outwardly to startle the bird. To insure stability of the apparatus, the forceplate was mounted to a concrete block isolated from the pyramid. The pyramid was housed at the bottom of a specially constructed netted vertical flight chamber (the 'Tower of Power' 2 x 2 x 7.6 m, width adjustable to 0.5 m; hereafter the tower; Fig. 1). Upon takeoff, all birds immediately ascended toward a false-escape window, often accelerating into the illuminated fabric ceiling, and then flew into an entrance-only recapture cage,. Birds performed the test between one and three times, with at least five minutes rest in the cage between runs. Only maximal flights are included in the analyses.

Forceplate analysis

At take-off, birds pushed on a forceplate that measures force on three axes: vertical (normal), and two orthogonal horizontal (lateral and fore-aft) axes. Ground reaction forces were recorded at 2000 Hz in Axoscope (v. 10.1 Molecular Devices, Toronto, Canada, Digitata 1322A analog-digital converter), and filtered with a 100 Hz low pass Butterworth filter in IGOR Pro to remove noise from the vibration of the top plate surface (172 Hz resonance). The forceplate signals were synchronized with the video via simultaneously recording the trigger signal that stopped the video recording. I present two measurements from the forceplate recordings, peak ground reaction force (GRF) and impulse. Peak GRF is the maximum value of the net force applied to the

forceplate. The impulse was calculated as the integral of the net GRF, starting when the normal force (F_z) exceeded 105% body weight ($M_b\,g$), and ending when F_z dropped below 5% body weight (toe-off). Both measures are presented as multiples of body weight.

Filming and kinematic analysis

Flights were filmed with four synchronized cameras (combinations of 2 Redlake PCI 500 480x480 resolution, 2 Fastec Troubleshooter HR 1280 x 1024, 2 Photron 1024 PCI, 1 Photron SA3 1024 x 1024) filming at 250 frames per second. Lenses and exact camera positions depended on the size of the bird. The filmed volume ranged from 0.5 x 0.5 x 1 m (birds less than 20 g) to 2 x 2 x 2.5 m (birds greater than 300 g). This volume was calibrated for direct-linear transformation analysis by hanging six strings at known coordinates from the tower ceiling, so that the strings filled the corners and middle of the filmed volume. Each string held reflective beads (5 mm diam.) at 15 cm height increments. Thirty beads were visible to all cameras in the smallest volume, and 56 in the largest volume.

Ten reference points (Fig. 2) on the left wing and body of each bird were marked by small (1-4 mm) pieces of reflective tape (3M part no. 8850). For small birds (<20 g) markers were not used on the primary and secondary feather tips, since the added mass caused significant inertial distortion of the feathers during wing turnaround. The markers were manually digitized, and three dimensional (3D) coordinates calculated by direct linear transformation (DLT; Ariel Performance Analysis Software, San Diego, CA, or DLTdv3.m, Hedrick 2008, in MATLAB, The Mathworks). All further analyses were

performed in IGOR Pro (v 6.0, Wavemetrics, Inc.). Coordinates were imported and filtered with the smoothing spline function (smoothing factor = 0.01, similar to cubic spline) for three reasons: 1) to interpolate missing points (not visible in at least two camera views), 2) to reduce digitizing error, and 3) to fit points between the 250 Hz samples, effectively increasing sampling to 2000 Hz to aid finding specific levels (e.g. upstroke-downstroke transitions). All velocities were calculated from the first derivative of positional coordinates.

Digitizing and analysis error was estimated as follows. Three mock wings representing birds of 10 g, 100 g, and 1000 g, with known dimensions were filmed at various angles, using the appropriate camera set up. Relative positional error of points averaged 1 mm, 3 mm, and 4 mm on each wing, respectively, which mirrors the approximate radii of each marker. A free-falling golf ball was also filmed in each camera set-up. Pooling all recordings, mean (± standard deviation) vertical acceleration was measured as 9.809 ± .003 ms^{-2}.

Coordinates were transformed and rotated for three frames of reference: global, gravitational, and vertebral (Dial et al. 2008, Jackson et al. 2009). The origin and orientation of the coordinate axes are fixed in the global, the orientation only is fixed while the origin tracks the bird's shoulder in the gravitational, and the orientation and origin track the bird's movements in the vertebral. Each kinematic variable was then calculated using the appropriate frame of reference.

Downstroke initiation was defined as the transition from dorsal to ventral wrist movement, calculated from vertebral coordinates. Wing area and length, and tail area were calculated dynamically from triangular planes formed by the appropriate markers

(Fig. 2), and are presented as mean values measured over downstroke. The center of mass (COM) was estimated as the average of the shoulder and rump markers to calculate angle of travel, body velocity, and kinetic and potential energies for each wingbeat cycle.

Several kinematic variables were calculated from the movement of the leading edge of the wing (shoulder marker to tip marker) between sample points during downstroke (Fig. 3). The movement of the leading edge can be visualized as a solid rod anchored at the shoulder traveling through small angles between sample times (t_n). The leading edge at each sample time was described the as a vector (le_t). The dot product was used find the angle between *le* at t_n and *le* at t_{n+1}, and the vector cross product was used to define the orientation and area of the plane defined by the two vectors. The stroke amplitude is defined as the sum of the dot-product angles throughout a downstroke, and is the total angle swept by the leading edge. The actuator disc area (S_{disc}) is the sum of the areas swept during downstroke (doubled to account for the right wing, assuming left-right symmetry). Stroke plane angle (SPA) is the area-weighted average of the orientation of the planes during a downstroke projected on the x-z plane, describing the elevation of the wing-stroke above horizontal (Fig. 3). SPA was calculated for both the vertebral and global frames of reference, since each measurement describes different functions. The vertebral SPA describes the wing movement relative to the body-axis (Fig. 4) and may be related to morphological constraints, while the global SPA (Fig. 3) estimates the location and orientation of the vortex ring shed by the wing tips. Angle of attack is defined as the angle between the wing plane in global coordinates and the wing velocity. The angle of attack for any moment in time was calculated separately for each of the four triangular wing planes, which were averaged using each plane's area and velocity squared for

weighting to describe the angle of attack for the entire wing. The aerodynamic angle of attack should be calculated using estimates of induced velocity (Tobalske et al. 2007). I chose to present the geometric angle of attack instead, to avoid introducing additional error from kinematic estimates of the induced velocity (see Discussion).

Power calculations

The mass-specific mechanical power produced by the muscles during flight can be partitioned into mass-specific parasite power (Ppar), profile power (Ppro), induced power *per se* (Pind), and climb power (P_{cl}; except as noted calculated as in Berg & Biewener 2008, modified from the models of Wakeling & Ellington 1997b, 1997a). Each power was calculated on a per-wingbeat basis.

$$P_{tot} = P_{par} + P_{pro} + P_{ind} + P_{cl} \quad (1)$$

Muscle power must also be used to accelerate and decelerate the wings (inertial power, P_{inert}). However, most of the power required to accelerate the wings during the first half of downstroke is recaptured as aerodynamic power during the second half of downstroke as the wings passively decelerate (Askew et al. 2001). Therefore, I assume that P_{inert} is represented in the estimates of aerodynamic power.

The aerodynamic model is based on the net resultant aerodynamic force (F_R) for each wingbeat, calculated as body mass times the vector sum of gravitational acceleration, center of mass (COM) acceleration, and the parasite drag force (D_{par}). However, since D_{par} is partially dependent on the induced velocity (w), which is in turn dependent on F_R (calculations below, Wakeling & Ellington 1997a), I calculated F_R

iteratively. The COM velocity alone was used to calculate an initial D_{par} and F_R. The resulting initial induced velocity vector was added to the COM velocity to calculate a new D_{par}, F_R, and *w*; this calculation loop was repeated for 10 cycles. In all runs, after two cycles the estimate of w converged to within 0.001 m s^{-1}, thus I present the results after the second cycle.

Induced velocity (*w*) at each iteration was calculated as

$$w^4 - 2Vw^3 \sin\alpha' + V^2 w^2 - \left(\frac{F_R}{2\rho S_{disc,F_R}} \right)^2 = 0 \qquad (2)$$

where *V* is the body velocity, *a'* is the angle between *V* and $S_{disc,FR}$, which is the projection of S_{disc} onto the plane orthogonal to F_R (Fig. 3). Induced power was calculated as the product of F_R and the velocity of air through the actuator disc, minus the rates change of kinetic and potential energy usually included in P_{ind}:

$$P_{ind} = F_R k_{ind} w - M_b g V_h \sin\alpha_{disc} \qquad (3)$$

where k_{ind} is a correction factor (taken as 1.2 after Pennycuick 1975), V_h is the horizontal velocity of the COM, and a_{disc} is the angle between $S_{disc,FR}$ and the horizontal. Since D_{par} was used in the calculation of F_R, P_{par} is included in P_{ind} (Wakeling and Ellington 1997a).

The estimate of profile power (P_{pro}) differed from previous work. The equation was the same:

$$P_{pro} = 2\sum 0.5\rho C_{D,pro}\left[(\omega r_i)^3 S_i \right] \qquad (4)$$

where $C_{D,pro}$ was taken as 0.02, ω is the angular velocity of a wing section a distance of r_i from the shoulder with surface area S_i. Rather than defining wing sections as strips as in Askew et al (2001) and Berg and Biewener (2008), properties of the dynamic triangular wing planes (Fig. 2) were used in equation 4.

Lift and drag coefficients at mid-downstroke ($C_{L,mds}$, $C_{D,mds}$) were estimated from modified thin aerofoil model (Norberg 1990) as:

$$C_{L,mds} = \frac{F_R \sin\beta_{mds}}{0.5\rho S_{wing}(v_{wt,mds})^2} \quad (5)$$

and

$$C_{D,mds} = \frac{F_R \cos\beta_{mds}}{0.5\rho S_{wing}(v_{wt,mds})^2} \quad (6)$$

where β_{mds} is the angle between the wingtip path and FR at mid-downstroke, ρ is the density of air taken to be 1.075 kg m^{-3} based on 975 m elevation and ambient conditions in the lab, S_{wing} is the surface area of both wings, and $v_{wt,mds}$ is the global velocity of the wingtip at mid-downstroke.

Phylogenetic and statistical analysis

Every flight was preliminary digitized (shoulder and rump markers only) to calculate P_{cl}. Only the run with the highest P_{cl} for each individual was fully digitized (i.e.

all points). Each kinematic and performance variable was calculated for each wingbeat. Since the first downstroke of most flights started before toe-off, and since the first wingbeat is recognized as being unique (Simpson 1983, Earls 2000), it was analyzed separately. Individual means of power and forceplate measurements were not significantly different within species. Thus, wingbeat values were pooled across all individuals for a given species to calculate mean and s.e.m.

All results were analyzed controlling for phylogeny as in Jackson (in prep). Regression models were analyzed in the Regressionv2.m program (Lavin et al. 2008). Since flight performance was significantly related to foraging habitat (open-ground vs. elevated and/or covered habitats; Jackson in prep) each regression model included foraging habitat as a factor. Phylogenetic models never improved model fit over ordinary least squares models (OLS) based on Akaike information criteria (AIC). However, since OLS tends to underestimate the slope of the best-fit line standardized major axis regression (SMA) is considered more appropriate in allometric studies (Warton et al. 2006). SMA was performed in the (S)MATR package (Warton & Weber 2002; Warton et al. 2006) in R (R Development Core Team 2009) on each of the best-fit models based on OLS. All slopes presented in the text are from SMA regression.

Results

Take-off: hindlimb forces and the first wingbeat

Every bird except for the Black-billed Magpies initiated the first downstroke prior to toe-off (Fig. 5). Individuals of various species (Dark-eyed Junco, House Sparrow, Yellow warbler) and all Cliff Swallows took one or two steps or hops rather than leaping

when startled by the opening pyramid. However, those flights did not demonstrate maximal Pcl for those individuals, and are therefore not included in the maximum performance analyses. Cliff Swallows stepped or hopped during every take-off, therefore they are not included in forceplate analyses. Black-billed Magpies held their wings folded against their body until after toe-off, and did not initiate the first downstroke until 1-2 body lengths above the forceplate. Maximal flights for all species were always preceded by a jump that included a countermovement (i.e. the crouching common in most animals before a jump).

Hind-limb output varied with mass and foraging ecology. Weight specific impulse (average jump force x jump duration x $M_b \boldsymbol{g}^{-1}$) scaled positively ($M_b^{.18}$, Fig. 6A, Table 1) due to positive scaling of jump duration ($M_b^{.26}$; Fig. 6A, Table 1). Peak GRF did not scale significantly (mean 4.7 times body weight). Maximum observed peak GRF was 7.4 times body weight produced by the House Finch (Fig. 6B, Appendix II). Calculations of the proportion of the toe-off velocity due to hind-limb contribution varied from 71% to 115%, and did not correlate with ecological covariates or body mass. The combinations of hind- and fore-limb use during take-off generated >80% of the peak velocity observed during the subsequent vertical flight; the largest species (CORA, AMCR) were unable to maintain take-off velocity once airborne.

Previous treatments of bird take-off have ignored the first wingbeat by starting analysis at the beginning of the downstroke following toe-off. Given the temporal variation that defines the take-off patterns described above, the first downstroke of each flight was analyzed separately. In every case, the first downstroke was an abbreviated

version of subsequent downstrokes (described below), exhibiting slightly lower stroke amplitudes (~10° less) but otherwise similar.

Kinematics and Power Estimates

Wingbeat kinematics were similar among all species (Fig. 4 Appendix III). Geometric angle of attack averaged 36° across all species, with maximum of 54° averaged through a wingbeat in a Ruby-crowned kinglet (Appendix III). Vertebral stroke plane angle averaged 121°, and global SPA averaged 148°. Maximum stroke amplitude averaged 160°, and several species had maximal values over 180° (Appendix III).

Mass-specific total power (P_{tot}) scaled as $M_b^{-0.32}$ overall, and was significantly higher in open-ground foragers (Table 1; Fig. 7A). P_{pro} scaled positively with SMA analyses, but the OLS slope was non-significant and it contributed no more than 4% of the power estimates. P_{ind} scaled strongly negatively ($M_b^{-0.60}$) and did not vary significantly with foraging guild. From Jackson (Chapter 1), P_{cl} scaled negatively ($M_b^{-0.27}$). Combined, P_{cl} and P_{ind} contributed to 95-99% of P_{tot}, but the contributions varied with mass. In the smallest birds P_{cl} represented approximately 20%, and P_{ind} approximately 80%, of P_{tot}, while the inverse was observed in the largest birds.

The 3-D kinematic analyses permit estimates of the relative contributions of 'lift' (the component of F_R orthogonal to the stroke-plane) and 'drag' (the component of F_R parallel to the stroke-plane) to F_R. The lift to drag ratio for most species was less than 0.6 (Fig. 8) and was independent of M_b.

Discussion

Total mass-specific power (P_{tot}) scaled negatively ($M_b^{-0.32}$) and in nearly parallel to flight performance (P_{cl}; $M_b^{-0.27}$). The American Goldfinch produced the highest average body-mass specific P_{tot} at 116 W kg^{-1}. Flight performance scaled negatively despite the take-off velocity advantage offered by the hindlimbs of larger species (impulse). In a related study mass-specific *in vivo* muscle power in the four species of corvid included here scaled as $M_b^{-0.18}$ (Chapter 3). Combined, these data lend the strongest support to date for the power-limiting hypothesis in passerines: body size constrains burst flight performance by limiting mass-specific muscle power output.

Maximal take-off performance is a critical component to avian ecology because of its role during predator escape, prey apprehension, courtship display, and territory defense behaviors. Yet, our previous understanding of the mechanics of take-off has been limited to four species (Rock pigeons, European starling, Common quail, Rufous hummingbirds; Heppner & Anderson 1985; Bonser & Rayner 1996; Earls 2000; Tobalske et al. 2004). In this study hindlimbs generally contributed 90 to 105% of take-off velocity, which is similar to previous results from non-hummingbird species. Based solely on the scaling of impulse ($M_b^{.18}$), velocity at toe-off scales positively with size. Impulse was independent of foraging habitat, in contrast to most flight variables and flight performance. Therefore, while the contribution of the hindlimbs is important during take-off instantaneous flight performance appears independent of hindlimb contribution. The Cliff swallows were the notable exception to this conclusion. They produced the lowest impulse and peak ground reaction forces, the and very low P_{tot} P_{cl}. Given that the species is an aerial specialist, their poor performance taking off from the ground is not surprising.

Wingbeat kinematics during vertical flight were very similar to kinematics during a wide range of flight behaviors. The first wingbeat was typically a relatively low-amplitude version of subsequent wingbeats, and did not vary systematically among species or foraging ecology. Stroke amplitude (mean 148°) and the geometric angle of attack (mean 38°) in passerine vertical flight are comparable to values from low speed wind tunnel flight (cockatiels, Hedrick et al. 2002), hovering hummingbirds (Tobalske et al. 2007), and pigeons in ascending flight (60° ascents, Berg & Biewener 2008). The only difference in kinematics among behaviors is the stroke plane angle (SPA, global mean 148°). Pigeons employed a ~165° SPA during 60° ascending and descending flight (Berg & Biewener 2008), whereas during wing-assisted incline running and slow level flight in Chukar SPA is steeper (~120-130° Dial et al. 2008; Jackson et al. 2009). Nevertheless, stroke plane angle shows amazing similarity (~35° range) among species as distant as chukars, passerines, and pigeons performing behaviors as varied as vertical escape and descending flight.

In conventional Rankin-Froude aerodynamic theory, lift represents the useful aerodynamic force whereas drag represents a cost normally considered to be minimized for efficiency (e.g. Norberg 1990). The resultant aerodynamic force (F_R) is dominated by lift, which is oriented orthogonally to the stroke plane. Under this logic, SPA would be predicted to be horizontal (180°) during vertical accelerating flight where the resultant aerodynamic force (F_R) is oriented approximately vertically. Instead, SPA was elevated from the horizontal by ~30°. Rather than being orthogonal to the global stroke plane, the resultant aerodynamic force (F_R) of each downstroke was oriented approximately 50° posterior to the orthogonal (represented in Fig. 3 by δ, the angle between the kinematic

actuator disc and the F_R disc). As a result, the component of F_R parallel to the stroke plane ('drag') was of similar or greater magnitude as the perpendicular component ('lift'). In other words, drag provided the very useful function of weight-support and acceleration. These results support recent arguments that drag and lift forces (and coefficients) may be similar during low-speed flight, when animals use high stroke amplitudes and high angles of attack with low translational velocities (Usherwood & Ellington 2002; Tobalske 2007; Jackson et al. 2009; Usherwood 2009; Warrick et al. 2009). As such, we need to reconsider our perceptions of lift and drag for behaviors such as vertical accelerating flight, when efficacy is probably more important than efficiency since predation should be avoided at all costs.

References

Askew, G.N., Marsh, R.L. & Ellington, C.P. 2001 The mechanical power output of the flight muscles of blue-breasted quail (Coturnix chinensis) during take-off. *J Exp Biol* **204**, 3601-3619.

Berg, A.M. & Biewener, A.A. 2008 Kinematics and power requirements of ascending and descending flight in the pigeon (Columba livia). *J Exp Biol* **211**, 1120-1130. (doi:10.1242/jeb.010413).

Biewener, A.A., Dial, K.P. & Goslow, G.E. 1992 Pectoralis muscle force and power output during flight in the starling. *J Exp Biol* **164**, 1-18.

Bonser, R. & Rayner, J. 1996 Measuring leg thrust forces in the common starling. *J Exp Biol* **199**, 435-439.

Dial, K.P., Jackson, B.E. & Segre, P. 2008 A fundamental avian wing-stroke provides a new perspective on the evolution of flight. *Nature* **451**, 985-989. (doi:10.1038/nature06517).

Domenici, P. & Blake, R. 1997 The kinematics and performance of fish fast-start swimming. *J Exp Biol* **200**, 1165-1178.

Earls, K. 2000 Kinematics and mechanics of ground take-off in the starling Sturnis vulgaris and the quail Coturnix coturnix. *J Exp Biol* **203**, 725-739.

Gatesy, S.M. & Dial, K.P. 1996 Locomotor Modules and the Evolution of Avian Flight. *Evolution* **50**, 331-340.

Hedrick, T.L. 2008 Software techniques for two- and three-dimensional kinematic measurements of biological and biomimetic systems. *Bioinspiration & Biomimetics* **3**, 034001.

Hedrick, T.L., Tobalske, B.W. & Biewener, A.A. 2002 Estimates of circulation and gait change based on a three-dimensional kinematic analysis of flight in cockatiels (Nymphicus hollandicus) and ringed turtle-doves (Streptopelia risoria). *J Exp Biol* **205**, 1389-1409.

Heppner, F.H. & Anderson, J.G.T. 1985 Leg Thrust Important in Flight Take-Off in the Pigeon. *J Exp Biol* **114**, 285-288.

Irschick, D.J., Vanhooydonck, B., Herrel, A. & Andronescu, A. 2003 Effects of loading and size on maximum power output and gait characteristics in geckos. *J Exp Biol* **206**, 3923-3934. (doi:10.1242/jeb.00617).

Jackson, B.E., Segre, P. & Dial, K.P. 2009 Precocial development of locomotor performance in a ground-dwelling bird (Alectoris chukar): negotiating a three-dimensional terrestrial environment. *Proceedings of the Royal Society B: Biological Sciences* **276**, 3457-3466. (doi:10.1098/rspb.2009.0794).

Lavin, S.R., Karasov, W.H., Ives, A.R., Middleton, K.M. & Garland Jr., T. 2008 Morphometrics of the avian small intestine compared with that of nonflying mammals: a phylogenetic approach. *Physiological and Biochemical Zoology* **81**, 526-550. (doi:10.1086/590395).

Lima, S.L. 1993 Ecological and Evolutionary Perspectives on Escape from Predatory Attack: A Survey of North American Birds. *The Wilson Bulletin* **105**, 1-47.

Losos, J.B. & Sinervo, B. 1989 The Effects of Morphology and Perch Diameter on Sprint Performance of Anolis Lizards. *J Exp Biol* **145**, 23-30.

Norberg, U.M. 1990 *Vertebrate Flight: Mechanics, Physiology, Morphology, Ecology and Evolution (Zoophysiology, Vol. 27)*, Berlin: Springer Verlag.

Norberg, U.M. 1985 Evolution of Vertebrate Flight: An Aerodynamic Model for the Transition from Gliding to Active Flight. *The American Naturalist* **126**, 303-327.

Pennycuick, C.J. 1975 Mechanics of flight. *Avian biology* **5**, 1–75.

R Development Core Team 2009 *R: a language and environment for statistical computing*, Vienna, Austria: R Foundation for Statistical Computing.

Tobalske, B.W. 2007 Biomechanics of bird flight. *J Exp Biol* **210**, 3135-3146. (doi:10.1242/jeb.000273).

Tobalske, B.W., Altshuler, D.L. & Powers, D.R. 2004 Take-off mechanics in hummingbirds (Trochilidae). *J Exp Biol* **207**, 1345-1352. (doi:10.1242/jeb.00889).

Tobalske, B.W., Warrick, D.R., Clark, C.J., Powers, D.R., Hedrick, T.L., Hyder, G.A. & Biewener, A.A. 2007 Three-dimensional kinematics of hummingbird flight. *J Exp Biol* **210**, 2368-2382. (doi:10.1242/jeb.005686).

Tobalske, B. & Dial, K. 2000 Effects of body size on take-off flight performance in the Phasianidae (Aves). *J Exp Biol* **203**, 3319-3332.

Usherwood, J. 2009 The aerodynamic forces and pressure distribution of a revolving pigeon wing. *Experiments in Fluids* **46**, 991-1003. (doi:10.1007/s00348-008-0596-z).

Usherwood, J.R. & Ellington, C.P. 2002 The aerodynamics of revolving wings II. Propeller force coefficients from mayfly to quail. *J Exp Biol* **205**, 1565-1576.

Vanhooydonck, B., Herrel, A., Van Damme, R. & Irschick, D.J. 2006 The quick and the fast: the evolution of acceleration capacity in anolis lizards. *Evol* **60**, 2137. (doi:10.1554/06-413.1).

Wakeling, J.M. & Ellington, C.P. 1997a Dragonfly flight. III. Lift and power requirements. *J Exp Biol* **200**, 583-600.

Wakeling, J.M. & Ellington, C.P. 1997b Dragonfly flight. II. Velocities, accelerations and kinematics of flapping flight. *J Exp Biol* **200**, 557-582.

Warrick, D.R., Tobalske, B.W. & Powers, D.R. 2009 Lift production in the hovering hummingbird. *Proceedings of the Royal Society B: Biological Sciences*. (doi:10.1098/rspb.2009.1003) [Accessed August 6, 2009].

Warton, D.I. & Weber, N.C. 2002 Common Slope Tests for Bivariate Errors-in-Variables Models. *Biometrical Journal* **44**, 161-174.

Warton, D.I., Wright, I.J., Falster, D.S. & Westoby, M. 2006 Bivariate Line-Fitting Methods for Allometry. *Biological Reviews* **81**, 259-291. (doi:10.1017/S1464793106007007).

Table 1. Kinematic scaling coefficients from ordinary least squares (OLS) and standarised major axis (SMA) regression against body mass (M) and covariates, based on log base 10 transformed variables. All best fit models were from nonphylogenetic (OLS) analysis; phylogenetic transformed (RegOU) analyses provided similar fit and coefficients, but tranformation values (REML d) were always <0.001 indicative of very low phylogenetic signal. P-values for SMA are for tests of difference of slope and elevation (intercept) unless stated otherwise.

	OLS					SMA			
Morph	Independent vars.	F	p	Coef. (-95%,+95%)	AIC	Independent vars.	slope (-95%,+95%)	intercept
Weight specific impulse	M	4.6	0.041	0.09 (0.01, 0.17)	-56	common	.29 (.20, .40)	.73 (.60, .87)
	ground	5.9	0.022	-0.13 (-0.23, -0.02)		open	.23 (.14, .38)	0.74
	open	5.7	0.024	0.12 (0.02, 0.22)		cover	.35 (.22, .57)	0.88
							p=.20	p=.007
Mean wingbeat frequency	M	4.4	0.043	-0.26 (-0.51, -0.01)	27	common	-.36 (-.42, -.32)	.79 (.73, .85)
						ground	-.37 (-.43, -.32)	0.74
						elevated	-.33 (-.44, -.25)	0.62
							p=.47	p<.0001
Max. wingbeat frequency	M	231.4	0.000	-0.36 (-0.41, -0.31)	-92	common	-.38 (-.43, -.33)	0.79
	ground	17.9	0.000	-0.10 (-0.15, -0.05)		ground	-.38 (-.44, -.33)	0.75
						elevated	-.37 (-.49, -.25)	0.64
							p=.85	p<.0001
Travel angle	ground	5.8	0.023	-0.08 (-0.14, -0.01)	-60	–	–	–
Mass-specific work (mean)	M	52.0	0.000	0.23 (0.17, 0.30)	-59		.29 (.23, .36) p<0.001 that slope is greater than 0	.62 (.52 .73)
Disc area	M	445.2	0.000	0.78 (0.71, 0.86)	-64	common	.84 (.76, .93)	-.28 (-.38, -.18)
	ground	13.4	0.001	0.17 (0.08, 0.26)		ground	.85 (.76, .94)	-0.24
	open	8.7	0.006	-0.13 (-0.22, -0.04)		elevated	.81 (.64, 1.02)	-0.14
							p=.72	p=.011
Stroke amplitude	open	7.7	0.009	-0.03 (-0.05, -0.01)	-137	–	–	–
Aspect ratio	open	4.3	0.046	-0.05 (-0.09, -0.00)	-82	–	–	–
	resident	2.7	0.108	0.04 (-0.01, 0.09)				
Tail area	M	119.2	0.000	0.74 (0.60, 0.88)	-12	common	.92 (.77, 1.12)	-1.41 (-1.63, -1.19)
						ground	.89 (.70, 1.12)	-1.35
						elevated	1.03 (.72, 1.48)	-1.17
							p=.46	p=.037

Figure Legends

Figure 1. Birds were filmed in a vertical flight chamber, taking off from a forceplate. Flights were induced by the sudden opening of a plexi-glass pyramid, which also contained the bird on the forceplate and directed their sight through a clear window to the white cotton sheet at the top of the tower. The width of the tower was adjusted from .5 to 2 m depending on the size of species being tested.

Figure 2. Digitizing landmarks were marked on each bird using reflective tape. The tip, mid-primary, and first secondary markers were omitted on species less than 30 g since the added mass caused significant inertial feather bending during wing acceleration at the start of downstroke. Triangles between markers define planes used to calculate wing area and angle of attack. The leading edge of the wing, used in calculations of stroke amplitude and stroke plane angles, was defined as the vector between the shoulder and tip markers.

Figure 3. The wingtip path (dotted ellipse) defined the actuator disc area (S_{disc}), and the inclination of the disc from the horizontal defined the global stroke plane angle (*SPA*). The net resultant aerodynamic force (F_R) for a wingbeat cycle was calculated from the change in velocity of the estimated center of mass (midway between shoulder and rump markers) and gravitational acceleration. The aerodynamic actuator disc (dark grey ellipse, $S_{disc,FR}$) was defined as the projection of S_{disc} onto the plane orthogonal to F_R, for use in the aerodynamic estimates. The angle between the kinematic S_{disc} and $S_{disc,\ FR}$ is defined as *d*. All angles drawn based on the average for the Black-billed magpie (pictured), which was not significantly different than other species.

Figure 4. Three-dimensional wing plane representations for the smallest and largest elevated foragers (Ruby-crowned kinglet RCKI, and Gray jay GRJA), and the smallest and largest ground foragers (Vespers sparrow VESP, and Common raven CORA) are drawn in lateral and anterior (cranial) perspectives. No significant differences in wingbeat kinematics were detected with body size. Each wing plane represents ~15% of the duration of a given downstroke such that timings between species are unrelated. Dimensional scale for all views of each species given by 5 cm scale bars.

Figure 5. Representative force plate recordings for the smallest and largest elevated foragers (Ruby-crowned kinglet RCKI, and Gray jay GRJA), and the smallest and largest ground foragers (Vespers sparrow VESP, and Common raven CORA), all scaled as -2 to 6 times weight-specific force over 0.5 s. Arrows indicate start of kinematic downstroke and upstroke; 'X' indicates toe-off.

Figure 6. Scaling of ground reaction force measurements. Body weight specific impulse (A) scaled positively, due to the duration of the jump rather than average or peak force magnitude (B). Cliff Swallows hopped during takeoff (see text for details) and are not included in the allometric models for hindlimb variables.

Figure 7. Total mass-specific power output estimated from aerodynamic models scaled as $M_b^{-0.32}$, and was significantly higher in open-ground foragers (open symbols) than other species.

Figure 8. Estimated mid-downstroke lift and drag coeffecients. The line indicates C_L to C_D ratio of one. Nearly all values fall below the line suggesting the importance of wing drag to producing useful aerodynamic forces.

Figure 1

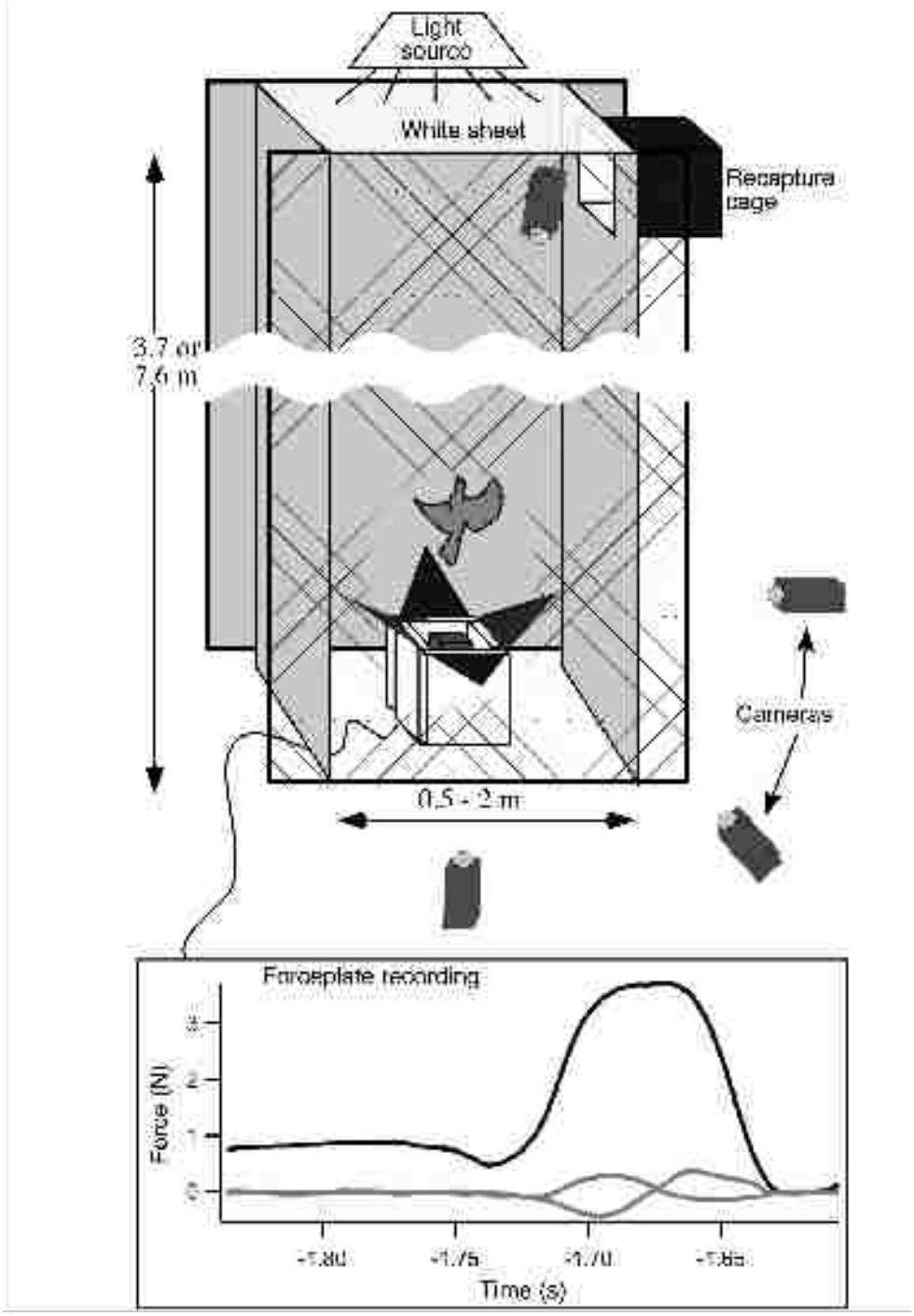
Light source
White sheet
Recapture cage
3.7 or 7.6 m
Cameras
0.5 - 2 m
Forceplate recording
Force (N)
Time (s)

Figure 2

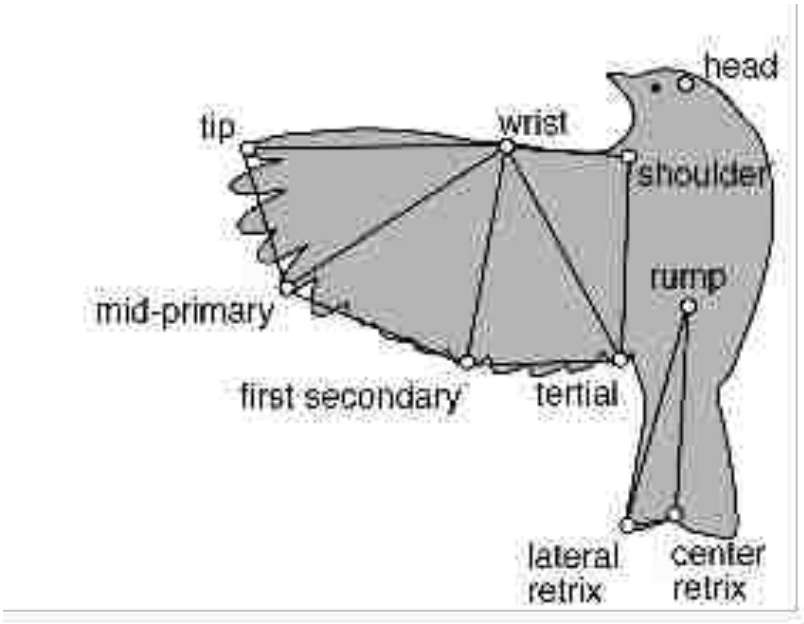
head
tip
wrist
shoulder
rump
mid-primary
first secondary
tertial
lateral retrix
center retrix

Figure 3

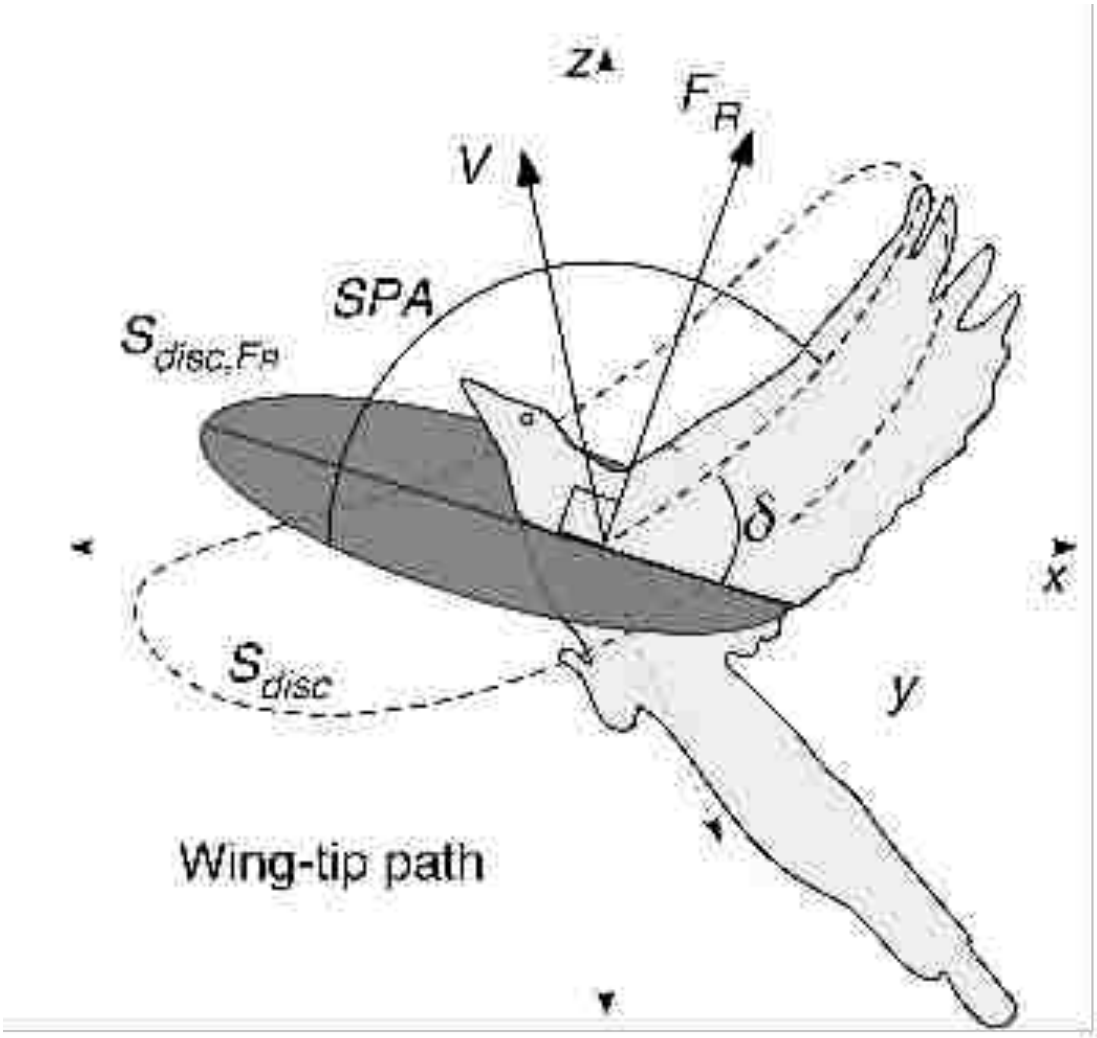

Figure 4

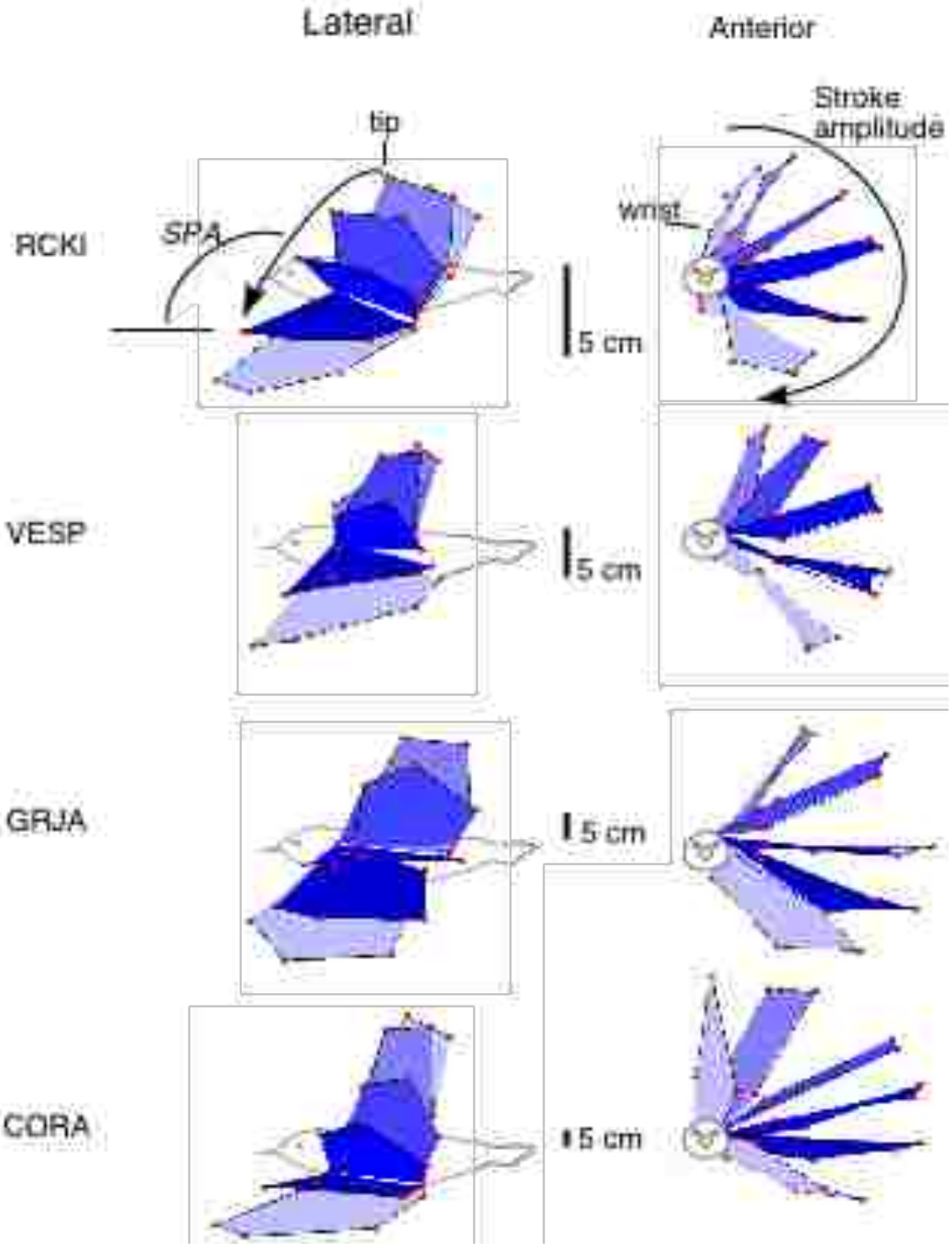
Lateral
Anterior
tip
Stroke amplitude
wrist
SPA
RCKI
5 cm
VESP
5 cm
GRJA
5 cm
CORA
5 cm

Figure 5

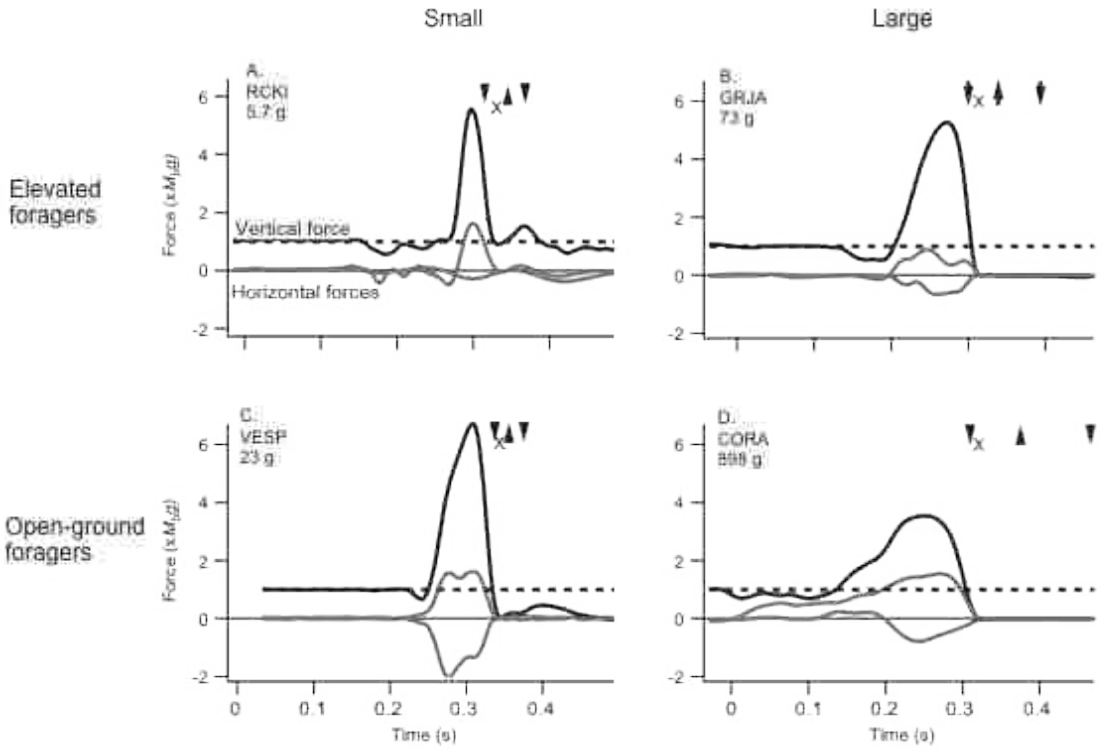
Small
Large
Elevated foragers
Open-ground foragers
A.
RCKI
5.7 g
B.
GRJA
7.3 g
C.
VESP
23 g
D.
CORA
888 g
Vertical force
Horizontal forces
Force (xM_g)
Time (s)

Figure 6

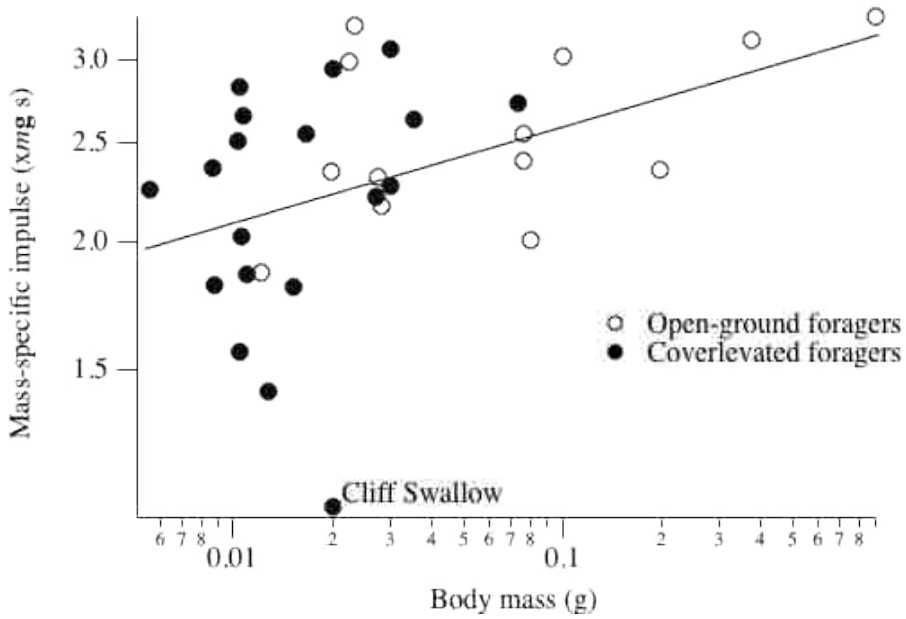
Mass-specific impulse (xmg s)
3.0
2.5
2.0
1.5
Open-ground foragers
Coverlevated foragers
Cliff Swallow
0.01
0.1
Body mass (g)

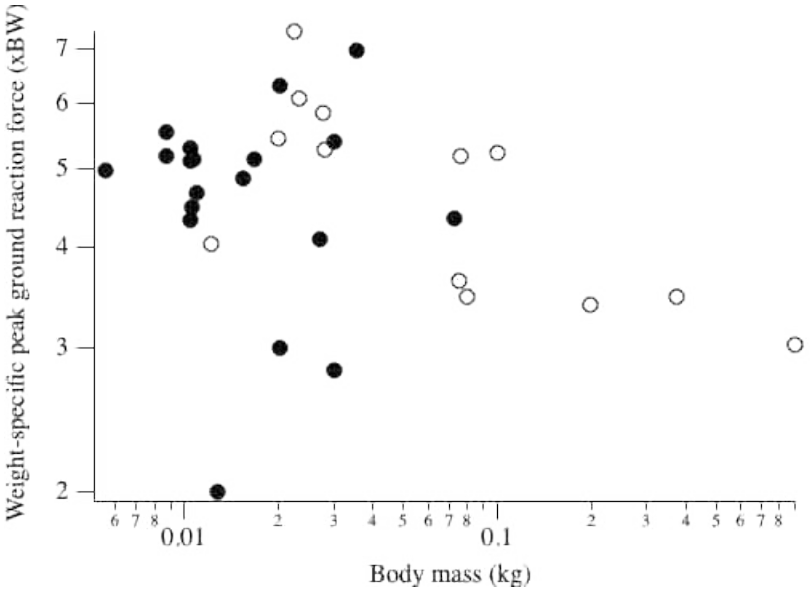
Weight-specific peak ground reaction force (xBW)
7
6
5
4
3
2
0.01
0.1
Body mass (kg)

Figure 7

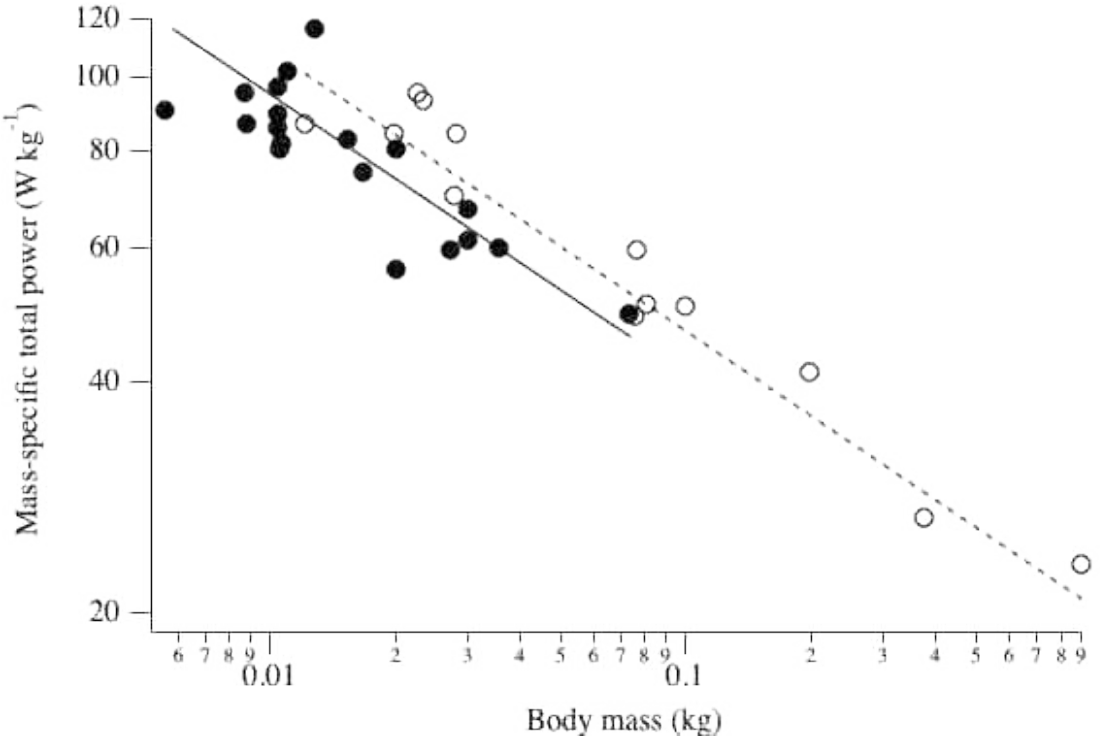
120
100
80
60
40
20
Mass-specific total power (W kg^{-1})
6 7 8 9
0.01
2 3 4 5 6 7 8 9
0.1
2 3 4 5 6 7 8 9
Body mass (kg)

Figure 8

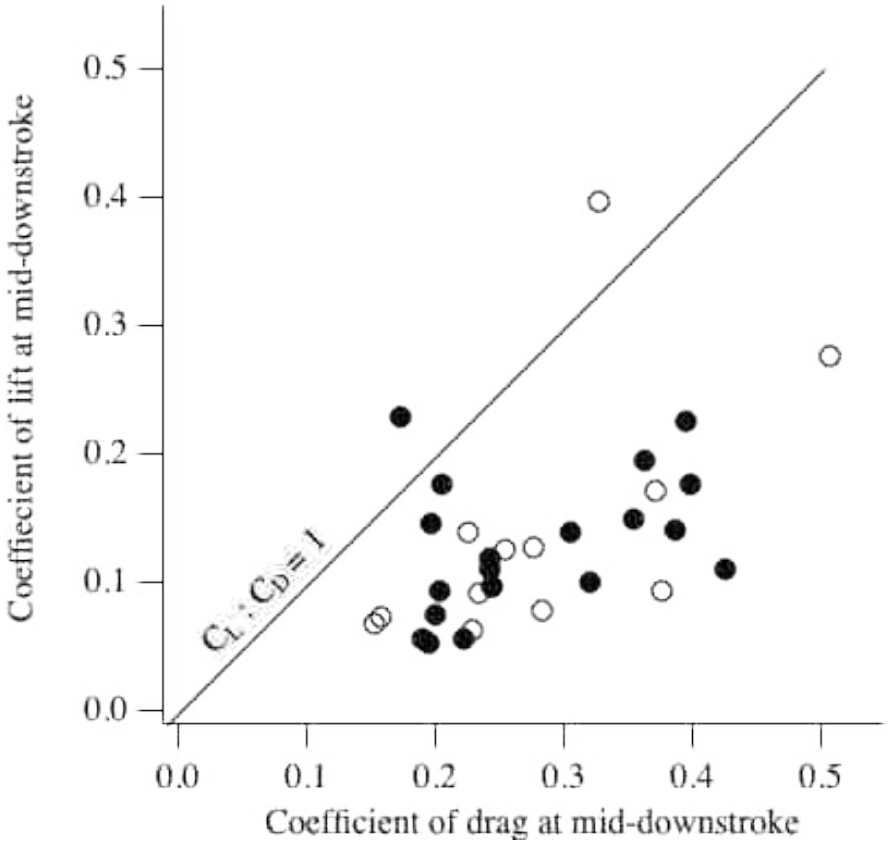
Coefficient of lift at mid-downstroke
0.5
0.4
0.3
0.2
0.1
0.0
$C_L : C_D = 1$
0.0
0.1
0.2
0.3
0.4
0.5
Coefficient of drag at mid-downstroke

SCALING OF MECHANICAL POWER OUTPUT DURING BURST ESCAPE FLIGHT IN FOUR SPECIES OF CORVIDS

Summary

Organismal size enforces physical constraints on many phenotypic characters. Avian locomotor burst performance (e.g. acceleration, maneuverability) in particular decreases with size and has significant implications for survivorship, ecology, and the evolution of birds. However, the underlying mechanism of this scaling relationship has been elusive. The most cited hypothesis addressing the scaling of flight performance posits that muscular power output is limited by wingbeat frequency alone and, as such, constrains aerodynamic performance. A concurrent study demonstrated negative scaling of flight performance in Passeriformes (songbirds), thus we ask, does scaling of muscle function explain the observed scaling of flight performance? To this end, we recorded *in vivo* muscular mechanical power from work loop mechanics by surgically implanted sonomicrometry (measuring muscle length change) and strain gauges (measuring muscle force) in four species of corvidae performing burst take-off and vertical escape flight. This study marks the first time that *in vivo* muscle force was successfully measured during burst flight in a comparative context. Maximum muscle-mass specific power scaled negatively with pectoralis mass ($M_m^{-.22}$) and maximum body mass specific power scaled negatively with body mass ($M_b^{-.18}$), but slightly less than the scaling of wingbeat frequency ($M_b^{-.30}$). Mean muscle strain (percent length change) scaled positively ($M_b^{.12}$), which is consistent with other results from ground birds (Order Galliformes). Mechanical force output patterns during downstroke also changed with size, such that

peak muscle stress (force per cross-sectional muscle area) scaled negatively ($M_b^{-.12}$) whereas average stress scaled positively ($M_b^{.11}$). Consequently 'shape factor' (i.e. the proportion of possible work performed given total muscle strain and peak stress in a wingbeat) scaled with positive allometry ($M_b^{.10}$). We hypothesize that the longer duration of downstroke in larger species may permit a more complete activation of the pectoralis, leading to the observed positive scaling of total strain and average stress. These allometries may function as compensatory mechanisms for large birds to produce relatively greater muscle power than suggested by wing beat frequency, but are insufficient to completely overcome scaling constraints.

Introduction

Variation in body size imposes fundamental constraints on the evolution of morphological and physiological traits (e.g. Schmidt-Nielsen 1984). However, the role of size in determining limits to behavior is largely unknown (for review see Dial et al. 2008). Body size may influence behavioral patterns by constraining relevant locomotor performance abilities (Arnold 1983) through morphological and physiological scaling. Generally, burst (i.e., accelerative) performance is thought to decrease with body size, implying that size is important for critical behaviors (e.g. predator-prey interactions); yet empirical evidence is limited to several species within each class of animals (e.g. Emerson 1978; Huey & Hertz 1984; Carrier 1995; Domenici & Blake 1997; Tobalske & Dial 2000; Askew et al. 2001; Toro et al. 2003; Vanhooydonck et al. 2006).

Much of the effort to describe the scaling of locomotor performance has focused on bird flight. Maximum burst flight performance scales negatively within avian orders, approximately in proportion to body mass (M_b) to the -0.3 power (Columbiformes: Seveyka 1999; Galliformes: Tobalske & Dial 2000; Apodiformes: Altshuler et al. in press; Passeriformes: Jackson in prep; but see Marden 1987, 1994; Askew et al. 2001). Traditionally, the scaling of flight performance has been argued to be a result of negative scaling of mass-specific muscle power (hereafter the *power-limiting hypothesis*, Pennycuick 1975). The power-limiting hypothesis is founded on fundamental morphological and physiological scaling predictions for vertebrates (Hill 1950), and would therefore offer insight to scaling effects in many taxa, but maximum muscle power has never been measured directly across a range of sizes in birds. Alternatively, Marden (1987; 1994) argued that mass-specific power is independent of body mass, thus performance should be limited by the ability to produce aerodynamic force (hereafter the *force-limiting hypothesis*; also see Ellington 1991). Birds produce as much as 95% of the power used in flight from a single, paired muscle (*m. pectoralis*, Biewener et al. 1992) that inserts on a bony cantilever (delto-pectoral crest, DPC) conducive to biomechanical instrumentation and calibration. As such, we can reliably measure *in vivo* mechanical power output (e.g. Tobalske et al. 2003). Thus avian burst flight offers an excellent model to examine the relationship between body size, muscle power, and locomotor performance.

The power-limiting hypothesis poses that maximum flight performance is limited by the amount of power the flight muscles can produce in excess of that required for minimal flight (Pennycuick 1975). Muscle-mass specific power output (P_{Mm}) is a

function of wingbeat frequency (f), muscle stress (σ, force per unit cross sectional area), strain (ε, percent length change), and muscle density (ρ; $P_{Mm}=\sigma\,\varepsilon\,f\,\rho^{-1}$). The power-limiting hypothesis assumes that σ, ε, and ρ do not change with size since the micro-anatomy of vertebrate striated muscle is generally size-invariant (Hill 1950). Wingbeat frequency scales as roughly $M_b^{-.33}$ among extant birds (Greenewalt 1962), leading to the prediction that P_{Mm} also scales as $M_b^{-.33}$. Since minimal mass-specific power requirements of flight vary little with size ($M_b^{0 \text{ to } 1/6}$; Pennycuick 1975; Ellington 1991), the amount of excess or marginal power the muscles are capable of producing decreases with size, as does performance of flight behaviors (e.g. accelerating, maneuvering) that depend on marginal power.

A concurrent study of 32 species of passerines demonstrated that maximum P_{cl} scales as $M_b^{-.32}$ (Jackson, in prep). To determine how muscle power output scales with body mass in those species, we surgically implanted sonomicrometry crystals and strain gauges to measure muscle strain and stress, respectively, thus directly measuring *in vivo* two critical components of muscle power (Josephson 1985). Because the surgical techniques are difficult on smaller birds, and to control for phylogenetic effects, we chose members of the largest-bodied passerine family, *Corvidae*: Gray jay *Perisoreus canadensis*, Black-billed magpie *Pica hudsonia*, American crow *Corvus brachyrhynchos*, and Common raven *C. corax.* Performing repeatable calibrations of the strain gauges has been an Achilles heel for the technique previously (see discussion in Tobalske & Biewener 2008), but the new technique used herein offers greater repeatability and congruence with alternative measurement techniques for level flight (Bundle et al. in prep.).

Methods

Birds were trapped using remote-triggered bow nets and rocket nets baited with carrion. Birds were transported to The University of Montana's Field Research Station (FRS) at Fort Missoula, Montana, USA, housed in large outdoor aviaries (4 x 4 x 15 m), and provided food (e.g. raw eggs, canned dog food, wild bird seed mixes) and water *ad libitum*. Birds were housed for as few as 2 days and as long as 30 days prior to flight tests. All procedures were approved by The University of Montana IACUC (No. 044-07KDDBS-122007).

Burst take off and vertical flight were measured in our adjustable-width experimental vertical flight chamber ('Tower of Power'; 2 x 2 x 7.6 m; Fig. 1). Flight performance (climb power, P_{cl}) and estimated total power output (P_{tot}) data are from Jackson (Chapter 2). Both the surgery and the added mass of cables and implants may influence flight behavior or reduce flight performance. As such whole body performance and aerodynamic power data are presented from a single pre-surgery flight (data from Chapter 2), except for the Common raven (CORA). In the CORA the greatest concern was that this notoriously intelligent species would habituate to the testing protocol. Therefore, since the total added surgical mass was less than 3% of M_b, flight performance data are presented from post-surgical flights. Within 24 hours of the initial flight *in vivo* recording gauges were surgically implanted, and flights recorded 12-24 hours after surgery. Immediately following successful recording sessions, the birds were anesthetized with inhaled isoflourane (5%) and euthanized with an overdose of sodium pentobarbital (100 mg kg^{-1}).

Surgical procedures

Implant construction and surgical procedures generally followed Tobalske and Biewener (2008) and Bundle et al. (in prep, detailed methods described in Appendix V). Briefly, all implanted gauges were soldered to a plug made of two miniature connectors (GF-6 Microtech Inc., Boothwyn, USA) embedded in an epoxy platform. The gauges on each plug consisted of two single-element strain gauges (FLA-1-11, Tokyo Sokki Kenkyujo, Ltd, Japan, 0.5-2 mm), one pair of sonomicrometry crystals (1 or 2 mm, 38 or 36 AUG, Sonometrics Corp. Canada), an indwelling EMG electrode (California Fine Wire Co., pair of twisted 100 μm diameter 99.9% silver wire, 1 mm inter-tip distance with 0.5 mm insulation removed), and a ground wire (3 cm 28 gauge insulated copper).

Birds were anesthetized using inhaled isofluorane (HME109, Highland medical Equipment, CA, 5% to induce, 2-3% to maintain). Feathers were removed at each incision site (the midline between scapulae, over each deltopectoral crest (DPC), and over the left pectoralis). A small (1-2 cm) incision was made in the skin at each location immediately prior to implantation at that site. Implants were passed subcutaneously from the midline incision to respective implant sites (Fig. 2). Each sonomicrometry crystal was inserted 0.5 cm deep, approximately 1.5 cm apart, into openings made along a single pectoralis fascicle near the central tendon. Each opening was closed and the crystal secured by suturing (0-6 polypropylene monofilament, Surgilene; Davis & Geck, Division of American Cyanamid Co., Danbury, CT) the fascia across the hole and around the emerging wire. The EMG electrode was implanted immediately caudal to the

sonomicrometry crystals. All leads were sutured to the superficial fascia with slack to control tension on the implants.

The strain gauges were implanted bilaterally on the delto-pectoral crest (DPC) of the humerus (Fig. 2). The implant site was cleared of muscle fibers, periosteum, and fatty deposits using a bone scraper, scalpel blade, and solvent (xylene or methyl-ethyl-ketone). The gauge was attached with self-catalyzing cyanoacrylate, oriented perpendicular to the long-axis of the humerus, and positioned mid-distally on the DPC at the cranial edge.

The bare end of the ground wire was sutured (0-3 silk) to the intervertebral ligament at the cranial end of the synsacrum. The epoxy base of the back-plug was sutured (0-0 silk) to the intervertebral ligaments cranial to the ground wire. The skin was pulled over the epoxy base, leaving the plug exposed, sutured closed, and covered with elastic surgical tape. Post-surgical birds recovered in small heated cages supplied with food and water for 12-24 hours prior to flight tests.

Acquisition and signal processing

The back plug was attached to two shielded cables with six leads each (Cooner Wire, CA, 4 m total length, 17 g m^{-1} with a matching male microconnector, GM-6). The sonomicrometry signals were sent to a Tritron System 6 sonomicrometry amplifier (Triton Technology Inc., San Diego, CA), strain signals to a Measurements Group Vishay 2120A strain-gauge signal conditioner (Raleigh, NC), and the EMG signals to a Grass CP511 EMG amplifier (West Warwick, USA, gain 1000x, 100-3000 Hz bandpass filter). Each amplifier's output signal was recorded at 2 kHz in Axoscope (v 10.1, Molecular

Devices, Sunnyvale, CA) *via* an Axon instruments Digitata 1322 16-bit A/D converter (Union City, CA).

Signal processing and analysis follows Hedrick et al (2003) and Tobalske and Biewener (2008). Briefly, EMG signals were filtered with a 250 Hz Butterworth high-pass filter to removed low frequency movement artifacts and rectified. EMG activity was defined as continuous peaks greater than two times mean baseline noise in the rectified signal. Sonomicrometry and strain gauge signals were filtered with a 50 Hz digital Butterworth low-pass filter, and corrected as in Tobalske and Dial (2000) and Tobalske and Biewener (2008). Resting length (L_{rest}) was recorded immediately prior to each flight while the bird was enclosed on the force plate with wings folded. Muscle strain (ε), was calculated as $\Delta L\ L_{rest}^{-1}$, where ΔL is the difference between instantaneous fascicle length and L_{rest}.

Muscle force calibration

A new technique was developed to improve the repeatability of calibrating the strain gauge recordings from the bone to muscle force (Bundle et al, in prep). Following euthanasia, the left pectoralis was exposed to verify placement of sonomicrometry crystals and EMG implantations. The wing was held in positions approximating start, middle, and end of downstroke, as observed in the high-speed video. At each position, the orientation (both proximo-distal and cranio-caudal) of the pectoral fascicles as they inserted on the ventral side of the DPC were measured using a protractor. The muscle was then dissected from the DPC, and the bone removed with the strain gauge and back-plug intact. This process was then repeated for the right pectoralis and humerus.

The articular surfaces of each end of each humerus were embedded in epoxy. A steel cable (1/64 in. dia. X 19 strand brass plated, Nelson Hobby Specialties, Keller, TX) was adhered (Loctite epoxy putty, Henkel Corp. Dusseldorf, Germany) to the ventral side of the DPC, immediately adjacent to the scar of the central tendon of the pectoralis. The epoxy ends were mounted in 3-D articular vices on a steel platform. The steel cable was attached to the pulley of a computer-controlled servo (CP-GV6, Gemini I/O module, Parker Compumotor, Rohnert Park, CA) with a calibrated torque output on the same steel platform. The bone was positioned such that the cable had the same insertion orientation at each of the three wingstroke positions, and the motor was used to repeatedly pull with *in vivo* wingbeat frequency and force while simultaneously recording motor torque and bone strain *via* the original strain gauge. An average calibration coefficient was determined for each wing position after repositioning the bone to each orientation three times. In all cases, the calibration factor declined significantly (>20%) between start and end of downstroke positions. Given the sensitivity of calibration to the pull orientation (also see Biewener et al. 1992) we used the position-dependent calibration factors to calculate dynamic calibrations throughout the downstroke dependent on instantaneous muscle strain. The calibration factors of the three wing positions (start, middle, and end of downstroke) were associated with a muscle strain level (maximum, resting, and minimum strain), and intermediate factors were determined by linear regression of calibration factor against strain level. Thus, a dynamic calibration factor, dependent on instantaneous *in vivo* muscle strain recordings, could be used to calibrate bone strain to muscle force accounting for changes in orientation of fiber insertion through a downstroke.

Work and power calculations

Each pectoralis muscle was carefully removed from the sternum. We determined average fascicle length by taking 15 length measurements of varying regions each of the superficial and deep surfaces of the muscle. Mass of each pectoralis and each supracoracoideus was determined to 0.1 g with an electronic balance.

Muscle work (W_{mus}) for each wingbeat was determined using the work-loop technique (Josephson 1985; Biewener et al. 1998). The start and end of each downstroke were defined by pectoralis shortening and lengthening, respectively, as measured by sonomicrometry. The wingbeat period (T_{wb}) was defined as the duration of a downstroke and subsequent upstroke. The integral of muscle force against muscle length represents the positive work performed for the duration of a downstroke (i.e. during shortening). Only positive work is considered here. Muscle power (P_{mus}) was calculated as $W_{mus} T_{wb}^{-1}$. We also determined peak and average force/stress through the downstroke, fractional lengthening (muscle strain above L_{rest}), fractional shortening (muscle shortening below L_{rest}), and shape factor (the ratio of W_{mus} to the area of a rectangle with dimensions of peak stress and total strain; Hedrick et al. 2003).

Statistical analyses

In order to control for possible effects of evolutionary relationships all data were analyzed as raw data and with models that included phylogenetic controls. We constructed a phylogeny of the four species using maximum likelihood trees based on mitochondrial genes (Bonaccorso & Peterson 2007) in Mesquite (v 2.71, Maddison & Maddison 2009; including the PDAP module, Midford et al. 2003) using Pagel's (1992)

arbitrary branch lengths. A '.tip' file and variance-covariance matrix ('.dsc' file) were imported to Regressionv2.m for analyses (Lavin et al. 2008). We used three of the models available in Regressionv2.m: ordinary least squares regression (OLS, assumes star phylogeny), phylogenetic generalized least squares (pGLS, assumes given branch lengths), and an Ornstein-Uhlenbeck transformation (RegOU) to transforms the node positions and output a transformation parameter (d) between zero (star phylogeny) and one (given branch lengths). Based on Akaike information criteria (AIC), OLS always produced the best-fit models indicating little or no phylogenetic signal (Lavin et al. 2008). However, OLS tends to underestimate fitted slopes, and is generally inappropriate in correlative and allometric analyses (Warton & Weber 2002; Warton et al. 2006). Therefore we also estimated model coefficients using standardized major axis regression (i.e. reduced major axis regression, SMATR module Warton & Weber 2002; Warton et al. 2006; R statistics program, R Development Core Team 2009). Measured values are presented as the mean ± s.e.m. of all wingbeats from likely maximal flights. Scaling coefficients are presented as values with 95% confidence intervals (CI) from SMA regression, unless otherwise noted.

Results

Maximal performance flights with quality implant signals were obtained from one Gray Jay (GRJA), two Black-billed Magpies (BBMA), three American Crows (AMCR), and one Common Raven (CORA) (Table 1). Representative implant recordings for each species are presented in Fig. 3.

Take-off styles of BBMA differed from the other species. Magpies started their first downstroke only after their feet left the forceplate, whereas the other species completed a partial downstroke before toe-off (Fig. 4). All four species used a pre-lift-off counter-movement, visible in the force-plate traces as a drop in force prior to the main peak (Fig. 4). Peak body-weight specific ground reaction force decreased as $M_b^{-.14}$ (-.31 to -.06; OLS: slope=-.13, F_2=21.4, p=.044). Body-weight specific impulse did not scale significantly ($M_b^{.10}$, .03 to .36; OLS: slope=.09, F_2=5.3, p=.15). The duration and muscle strain of the first wingbeat were similar to subsequent wingbeats. However, average and peak stresses were typically 50-70% of the mean of subsequent wingbeats, resulting in a similarly reduced mass-specific power output during the initial wingbeat (Figs. 5, 6). Since the first wingbeat was unique it is not included in further analyses.

Muscle stress, strain, and EMG timings followed similar patterns in all species (Figs. 3, 7). EMG activity and stress development started shortly before the start of muscle shortening. There were typically two stress peaks per downstroke; the first peak was larger in BBMA and AMCR, and the second peak was larger in GRJA and CORA. EMG activity continued in all species until the second stress peak (Figs. 3, 6).

Flight performance decreased with body mass after take-off. The two smaller species (GRJA, BBMA) generally accelerated with every wingbeat (gaining 0.03 and 0.16 m s^{-1} per wingbeat, respectively), but AMCR (-0.11 m s^{-1}) and CORA (-0.25 m s^{-1}) lost velocity with every wingbeat after toe-off. Body mass specific climb power (P_{cl}) decreased as $M_b^{-.17}$ (-.08 to -.34; OLS: slope = -.16, F_2=27.2, p=.034). Body mass specific total power output (P_{tot}), estimated from aerodynamic models and including P_{cl}, scaled as $M_b^{-.67}$ (-.48 to -.93; OLS: slope = -.66, F_2=160, p=.006).

In vivo measurements of muscle function diverged from predictions based on isometry. Wingbeat frequency scaled as $M_b^{-.30}$ (Fig. 8B) but mean muscle mass (M_m) specific work scaled positively as $M_m^{.18}$ (Fig. 8C). As a result mean muscle mass specific *in vivo* power output ($P_{mus, Mm}$) scaled as $M_m^{-.20}$ (Fig. 8A). Pectoralis muscle mass scaled isometrically ($M_b^{1.05}$, .97 to 1.15, p=.12) averaging 14.7% of M_b (Table 1). The GRJA produced the maximum muscle mass specific power produced in a single wingbeat at 471 W kg^{-1}.

The general shape and pattern of the work loops changed with size (Fig. 6). The two smaller species produced high peak stresses (Fig. 9A) as single peaks either late (GRJA) or early in downstroke (BBMA, Fig. 6). The two larger species produced lower peak stresses, but a more consistent stress through the duration of downstroke. As a result peak stress decreased slightly with body mass ($M_b^{-.12}$) but average stress ($M_b^{.11}$) and shape factor ($M_b^{.10}$) increased (Fig. 9B,C). Total muscle strain also scaled allometrically. Total shortening strain scaled as $M_b^{.12}$, from 0.32 in GRJA to 0.43 in CORA (Fig. 10A). This scaling occurred equally as fractional shortening ($M_b^{.22}$) and lengthening ($M_b^{.22}$) (Fig. 10B). Shortening rate scaled as $M_b^{.24}$ (Fig. 10C).

Discussion

In vivo muscle-mass specific power output scaled with negative allometry ($M_m^{-.20}$) providing the first direct empirical support to the power-limiting hypothesis for maximal flight ability in birds. However, the scaling of muscle power was not determined solely by wingbeat frequency because both muscle strain and average stress increased with M_b

(as $M_b^{.12}$ and $M_b^{.11}$, respectively), contrary to theory and the hypothesis (Hill 1950; Pennycuick 1975). Nevertheless, the scaling of the *in vivo* measurements of P_{mus} is similar to the scaling of flight performance in these four species, as measured by P_{cl} ($M_b^{-.17}$).

The force-limiting hypothesis, in contrast to the power-limiting hypothesis, predicts that relative muscle power is independent of size (Marden 1994). Therefore, muscle stress and/or strain would have to scale positively enough to compensate for the known negative scaling of wingbeat frequency. Only one other study has examined allometric trends of *in vivo* muscle strain in burst flight (Tobalske and Dial 2000); they also identified positive scaling of muscle strain in Galliformes ($M_b^{.19}$), but were unable to measure muscle stress. Since this is the first time that *in vivo* muscle stress has been measured during maximal burst flight for any group of species, it is also the first time that concurrent scaling of stress production patterns (i.e. shape factor) has been observed. Nevertheless, the scaling of stress and strain did not fully compensate for the power-limiting effects of wingbeat frequency. Thus, frequency-limited power appears to constrain performance, despite the inaccuracy of the underlying assumptions of the power-limiting hypothesis.

Previous scaling studies have struggled with two distinct challenges that were addressed in the current study: eliciting maximal performance from the animals under investigation and quantifying muscle power directly. Various authors have employed artificial load-lifting by flying insects and birds to challenge the subjects to perform maximally (Marden 1987, 1994, Chai & Millard 1997, Altshuler et al in press). This technique is suitable for hummingbirds because of their innate hovering abilities and

apparent comfort with the added mass (Chai et al. 1997, Altshuler et al in press). However, many species of birds (including the species in the current study, pers. obs.) simply refuse to fly carrying artificial loads unless thoroughly trained. Alternatively, marginal power has been estimated from body-mass specific climb power (P_{cl} ; rate change in kinetic and potential energies) during constrained vertical flight in un-weighted birds (Seveyka 1999; Tobalske & Dial 2000; Askew et al. 2001; Chapter 1), or by estimating muscle power from aerodynamic models (Askew et al. 2001, Chapter 2). Only Tobalske and Dial (2000) attempted to measure *in vivo* muscle power using surgically implanted gauges, but were stymied in recording muscle force due to the inappropriate shape of the Galliforme delto-pectoral crest as a force transducer. Additionally, Tobalske & Dial (2000) and Askew et al (2001) used captive-bred birds, some of which had been trained or habituated to the flight tests prior to measurements; using trained birds potentially compromises the assumption of maximal performance. Thus no previous has successfully recorded *in vivo* muscle power during burst flights across a range of body masses.

What physiological or anatomical allometry could explain the scaling patterns of stress and strain described herein? First, avian pectoralis muscles are generally composed of two to three types of fast-twitch fibers that may vary in optimal contractile velocities (Rosser & George 1986). Size-related variation of fiber composition could explain the allometry of stress and/or strain. Tobalske (1996) found such variation with body size in woodpeckers, yet the scaling of fiber composition in passerine flight muscle is unknown. Alternatively, in small species the shorter downstroke durations may constrain the ability of the flight muscle to produce maximal stress. Birds must

deactivate their pectoralis during the downstroke to avoid lingering pectoralis force during the upstroke (Askew and Marsh 2001). Longer downstroke durations permit more complete activation and less residual pectoralis force during upstroke; the downstroke duration can be extended with an asymmetrical sawtooth cycle (i.e. >50% of cycle period spent shortening; Askew and Marsh 2001). Our data suggest that large species may gain equivalent benefits as a result of having lower wingbeat frequencies and hence longer absolute shortening durations compared to smaller species. More fully activated muscles may be able to develop greater stress as well as undergo greater total shortening.

The values of strain reported herein are similar to those from other species, while the values of stress are generally higher. Askew and Marsh (2001) measured *in vivo* strain and *in vitro* stress in blue quail pectoralis muscle. Quail strain (23.4%) was similar to other small phasianids (19.1-22.2% Tobalske & Dial 2000), but much shorter than either Wild turkey (35.2%; Tobalske & Dial 2000) or corvids (33-44%). Such high total strains have been observed in trained pigeons performing ascending flight (42%; Tobalske & Biewener 2008), and in cockatiels flying at very low (1 m s^{-1}, 41%) and very fast speeds (13 m s^{-1}, 44%; minimum strain was 34% at 5 m s^{-1}; Hedrick et al. 2003). Measurements of stress presented herein (mean peak stress in GRJA = 157 kPa, max stress =220 kPa) are slightly higher than most published values for birds (Blue quail *in vitro,* 131 kPa, Askew & Marsh 2001; trained ascending pigeons, 58 kPa, Tobalske and Biewener 2008; European starlings,122 kPa peak isometric, Biewener et al. 1992), as would be expected in wild compared to trained birds.

As a result of our relatively high stress and strain data the muscle power values we found are also among the highest ever measured in birds and the first *in vivo*

measurements to agree with aerodynamic models. The maximum muscle-mass specific power recorded was 471 W kg^{-1} in GRJA (mean 350 W kg^{-1}). While the mean value is similar to the maximum previously reported value (*in vitro* blue quail pectoralis, 349 W kg^{-1}, Askew and Marsh 2001), the GRJA was roughly 50% more massive and therefore may be expected to produce lower P_{mus}. However, Askew and Marsh (2001) had difficulty with the *in vitro* preparation and suggested that their measurement is an underestimate. Muscle power is used to induce airflow and overcome drag on the body, quantities estimated as total aerodynamic power (P_{aero}) from kinematic measurements. In ascending flight previous *in vivo* measurements of P_{mus} have at best accounted for 60% of P_{aero} (Tobalske & Biewener 2008). We report, using the new strain gauge calibration technique, the closest agreement to date between P_{mus} and P_{aero} (CORA, 89 %). However, P_{mus} in the GRJA, BBMA, and AMCR were significantly lower than aerodynamic estimates (at 59%, 53% and 79%, respectively). Several factors may explain the discrepancy between the two measures of power. First, P_{aero} is an estimate for the total power output of all muscles involved in producing aerodynamically functional movements, and power from other muscles may be involved in the downstroke (e.g. sternocoracoideus, coracobrachialis, Dial et al. 1991) but not measured by the implants. Second, except for the CORA, we measured P_{tot} and P_{mus} during different flights to avoid complications caused by the surgically implanted equipment on whole-body performance; the recording cable noticeably affected the flight behavior of the GRJA, and therefore may have resulted in lower overall effort. Third, the implants themselves may additionally adversely affect muscle performance or motivational level particularly in the smaller species, possibly explaining the apparent size-based

discrepancy between *in vivo* and kinematic power estimates. If P_{mus} was negatively affected by the implants, the values herein for the smallest species are likely conservative estimates, implying that P_{mus} may scale more negatively than presented. Given the inherent difficulties with both *in vivo* measurements and kinematic estimates (Jackson in prep.) of total power output, a third independent technique (e.g. particle image velocimetry, PIV) may be required to further elucidate the relationship between body mass and power output.

References

Arnold, S.J. 1983 Morphology, Performance and Fitness. *American Zoologist* **23**, 347-361.

Askew, G. & Marsh, R. 1997 The effects of length trajectory on the mechanical power output of mouse skeletal muscles. *J Exp Biol* **200**, 3119-3131.

Askew, G.N. & Marsh, R.L. 2001 The mechanical power output of the pectoralis muscle of blue-breasted quail (Coturnix chinensis): the in vivo length cycle and its implications for muscle performance. *J Exp Biol* **204**, 3587-3600.

Askew, G.N., Marsh, R.L. & Ellington, C.P. 2001 The mechanical power output of the flight muscles of blue-breasted quail (Coturnix chinensis) during take-off. *J Exp Biol* **204**, 3601-3619.

Biewener, A., Corning, W. & Tobalske, B. 1998 In vivo pectoralis muscle force-length behavior during level flight in pigeons (Columba livia). *J Exp Biol* **201**, 3293-3307.

Biewener, A.A., Dial, K.P. & Goslow, G.E. 1992 Pectoralis muscle force and power output during flight in the starling. *J Exp Biol* **164**, 1-18.

Bonaccorso, E. & Peterson, A.T. 2007 A multilocus phylogeny of New World jay genera. *Molecular Phylogenetics and Evolution* **42**, 467-476. (doi:10.1016/j.ympev.2006.06.025).

Bundle, M.W., Dial, K.P. & Jackson, B.E. Efficiency of avian flight muscle. *in prep.*

Carrier, D.R. 1995 Ontogeny of jumping performance in the black tailed jack rabbit (Lepus californicus). *Zoology* **98**, 309-313.

Chai, P., Chen, J. & Dudley, R. 1997 Transient hovering performance of hummingbirds

under conditions of maximal loading. *J Exp Biol* **200**, 921-929.

Chai, P. & Millard, D. 1997 Flight and size constraints: hovering performance of large hummingbirds under maximal loading. *J Exp Biol* **200**, 2757-2763.

Dial, K.P., Goslow Jr., G.E. & Jenkins Jr., F. 1991 The functional anatomy of the shoulder in the European starling (Sturnus vulgaris). *Journal of Morphology* **207**.

Dial, K.P., Biewener, A.A., Tobalske, B.W. & Warrick, D.R. 1997 Mechanical power output of bird flight. *Nature(London)* **390**, 67-70.

Dial, K.P., Greene, E. & Irschick, D.J. 2008 Allometry of behavior. *Trends in Ecology & Evolution* **23**, 394-401. (doi:10.1016/j.tree.2008.03.005).

Domenici, P. & Blake, R. 1997 The kinematics and performance of fish fast-start swimming. *J Exp Biol* **200**, 1165-1178.

Ellington, C.P. 1991 Limitations on Animal Flight Performance. *J Exp Biol* **160**, 71-91.

Emerson, S.B. 1978 Allometry and jumping in frogs: helping the twain to meet. *Evolution* **32**, 551-564.

Greenewalt, C.H. 1962 *Dimensional relationships for flying animals*, Smithsonian Institution.

Hedrick, T.L., Tobalske, B.W. & Biewener, A.A. 2003 How cockatiels (Nymphicus hollandicus) modulate pectoralis power output across flight speeds. *J Exp Biol* **206**, 1363-1378. (doi:10.1242/jeb.00272).

Hill, A.V. 1950 The dimensions of animals and their muscular dynamics. *Sci. Prog* **38**, 209-230.

Huey, R.B. & Hertz, P.E. 1984 Effects of Body Size and Slope on Acceleration of a Lizard (Stellio Stellio). *J Exp Biol* **110**, 113-123.

Josephson, R.K. 1985 Mechanical power output from striated muscle during cyclic contraction. *Journal of Experimental Biology* **114**, 493-512.

Lavin, S.R., Karasov, W.H., Ives, A.R., Middleton, K.M. & Garland Jr., T. 2008 Morphometrics of the avian small intestine compared with that of nonflying mammals: a phylogenetic approach. *Physiological and Biochemical Zoology* **81**, 526-550. (doi:10.1086/590395).

Maddison, W.P. & Maddison, D.R. 2009 Mesquite: a modular system for evolutionary analysis. Version 2.71.

Marden, J.H. 1994 From damselflies to pterosaurs: how burst and sustainable flight performance scale with size. *Am J Physiol Regul Integr Comp Physiol* **266**, R1077-1084.

Marden, J.H. 1987 Maximum Lift Production During Takeoff in Flying Animals. *J Exp Biol* **130**, 235-258.

Midford, P.E., Garland Jr, T. & Maddison, W.P. 2003 PDAP Package, Version 1.14.

Norberg, U.M. 1990 *Vertebrate Flight: Mechanics, Physiology, Morphology, Ecology and Evolution (Zoophysiology, Vol. 27)*, Berlin: Springer Verlag.

Pagel, M.D. 1992 A method for the analysis of comparative data. *Journal of Theoretical Biology* **156**, 431–442.

Pennycuick, C.J. 1975 Mechanics of flight. *Avian biology* **5**, 1–75.

R Development Core Team 2009 *R: a language and environment for statistical computing*, Vienna, Austria: R Foundation for Statistical Computing.

Rosser, B.W. & George, J.C. 1986 The avian pectoralis: histochemical characterization and distribution of muscle fiber types. *Can. J. Zool.* **64**, 1174-1185. (doi:10.1139/z86-176).

Schmidt-Nielsen, K. 1984 *Scaling: Why is Size so Important*, New York: Cambridge University Press, New York.

Seveyka, J. 1999 *The effects of body size and morphology on the flight behavior and escape flight performance of birds*. M.S. The University of Montana.

Tobalske, B.W., Hedrick, T.L., Dial, K.P. & Biewener, A.A. 2003 Comparative power curves in bird flight. *Nature* **421**, 363-366. (doi:10.1038/nature01284).

Tobalske, B.W. 2007 Biomechanics of bird flight. *J Exp Biol* **210**, 3135-3146. (doi:10.1242/jeb.000273).

Tobalske, B.W. 1996 Scaling of Muscle Composition, Wing Morphology, and Intermittent Flight Behavior in Woodpeckers. *The Auk* **113**, 151-177.

Tobalske, B.W. & Biewener, A.A. 2008 Contractile properties of the pigeon supracoracoideus during different modes of flight. *J Exp Biol* **211**, 170-179. (doi:10.1242/jeb.007476).

Tobalske, B. & Dial, K. 2000 Effects of body size on take-off flight performance in the Phasianidae (Aves). *J Exp Biol* **203**, 3319-3332.

Toro, E., Herrel, A., Vanhooydonck, B. & Irschick, D.J. 2003 A biomechanical analysis of intra- and interspecific scaling of jumping and morphology in Caribbean Anolis lizards. *J Exp Biol* **206**, 2641-2652. (doi:10.1242/jeb.00473).

Vanhooydonck, B., Herrel, A., Van Damme, R. & Irschick, D.J. 2006 The quick and the fast: the evolution of acceleration capacity in anolis lizards. *Evol* **60**, 2137. (doi:10.1554/06-413.1).

Warton, D.I. & Weber, N.C. 2002 Common Slope Tests for Bivariate Errors-in-Variables Models. *Biometrical Journal* **44**, 161-174.

Warton, D.I., Wright, I.J., Falster, D.S. & Westoby, M. 2006 Bivariate Line-Fitting Methods for Allometry. *Biological Reviews* **81**, 259-291. (doi:10.1017/S1464793106007007).

Figure Legend

Figure 1. Birds were filmed in our vertical flight chamber, taking off from a forceplate. Flights were induced by the sudden opening of a plexi-glass pyramid, which also contained the bird on the forceplate and directed their sight through a clear window to the white cotton sheet at the top of the tower. The width of the tower was adjusted from .5 to 2 m depending on the size of species being tested. Each flight was filmed with three or four high-speed cameras synchronized to the forceplate and *in vivo* instrument recordings.

Figure 2. Implantation sites for *in vivo* instruments. Modified from Dial et al. 1997.

Figure 3. Representative filtered and calibrated traces from all four species (see text for species abbreviations). Bone strain, as measured by the strain gauge on the humeral delto pectoral crest (DPC) is drawn in gray to illustrate the effect of applying a dynamic calibration coefficient dependent on muscle strain. Gray columns and arrows delineate downstroke as defined by muscle fascicle shortening.

Figure 4. Representative body-weight specific ground reaction force traces. Arrows indicate start of down- and upstroke. 'X' indicates time of toe-off.

Figure 5. Representative work loops showing the first complete wing stroke after initiation of lift-off. For GRJA, AMCR, and CORA the first downstroke started before toe-off. Hashed areas are below zero muscle stress and not included in calculation of work or power. Thick gray trace delineates the period of EMG activity.

Figure 6. Representative work loops showing the third wing stroke after initiation of lift-off. Hashed areas are below zero muscle stress and not included in calculation of work or power. Thick gray trace delineates the period of EMG activity.

Figure 7. Timing of EMG activity, pectoralis force production and peak force timing, and muscle shortening (i.e. downstroke) normalized as percent of the wingbeat cycle averaged for all recorded wingbeats subsequent to the first. Error bars represent s.e.m. of the mean times of onset and offset.

Figure 8. (A) *In vivo* mean and maximum pectoralis mass specific power output scaled negatively with pectoralis mass, but less negatively than (B) the scaling of wingbeat frequency. Contrary to predictions of the power-limiting hypothesis (C) pectoralis muscle-mass specific work increased with pectoralis mass. All values are based on all recorded wingbeats subsequent to the first downstroke pooled across individuals within species. Error bars represent s.e.m.

Figure 9. (A) Peak pectoralis stress scaled negatively while (B) average stress scaled positively with body mass. Consequentially, work loops became less triangular and more rectangular with body mass, leading to (C) positive scaling of shape factor, which is the ratio of observed work to possible work given the total muscle strain and peak stress.

Figure 10. (A) Total shortening strain increased with body mass. (B) This positive scaling of total strain occurred as equal parts fractional lengthening and shortening. (C) Strain rate (muscle lengths s^{-1}) scaled negatively.

Table 1. Morphometrics of four species of corvids. Pectoralis mass and fascicle length for each individual were calculated as the average between left and right sides. All values presented as species mean ± s.e.m.

	Gray Jay	Black-billed Magpie	American Crow	Common Raven
n (individuals)	1	2	3	1
Body mass (kg)	0.0689	.1724 ± .0214	.3876 ± .0315	0.8949
Pectoralis mass (kg)	0.0045	.0110 ± .0010	.0276 ± .0021	0.0656
Fascicle length (mm)	30.5	36.7 ± 0.7	44.5 ± 4.0	56.8

Table 2. In vivo measurements and power calculations. All values mean ± s.e.m. (maximum) for all wingbeats excluding the first, pooled within species.

	Gray Jay	Black-billed Magpie	American Crow	Common Raven
Wingbeat frequency (Hz)	11.6 ± .0 (12.5)	9.0 ± .1 (10.3)	6.4 ± .1 (7.1)	5.6 ± .2 (5.8)
Mean F (N)	13.6 ± 0.4 (18.4)	30.1 ± 0.6 (41.0)	49.3 ± 1.2 (60.7)	125.1 ± 1.2 (127.4)
Peak force (N)	21.8 ± .5 (30.7)	40.0 ± .9 (50.2)	60.3 ± 3.0 (86.4)	149.8 ± 1.2 (151.9)
Mean stress (kPa)	97.7 ± 3.1 (132.3)	104.3 ± 1.4 (135.3)	69.2 ± 6.5 (113.6)	114.7 ± 1.1 (116.9)
Peak stress (kPa)	156.8 ± 3.7 (220.2)	138.5 ± 2.3 (165.7)	98.0 ± 7.7 (157.7)	137.4 ± 1.1 (139.2)
Frac. Lengthing	.21 ± .00 (.26)	.15 ± .01 (.22)	.23 ± .01 (.29)	.27 ± .01 (.28)
Frac. shortening	-.12 ± .00 (-.16)	-.20 ± .01 (-.26)	-.14 ± .01 (-.26)	-.17 ± .00 (-.18)
Shortening length (mm)	10.0 ± .1 (11.0)	12.9 ± .2 (14.3)	16.5 ± .8 (22.6)	25.2 ± .2 (25.6)
Shortening Velocity (L s^{-1})	6.1 ± .0 (6.7)	5.0 ± .1 (5.9)	3.7 ± .1 (4.7)	3.4 ± .0 (3.5)
Shortening Duty (% cycle)	.623 ± .005 (.647)	.624 ± .005 (.670)	.627 ± .011 (.684)	.718 ± .012 (.733)
Power (W)	1.58 ± .05 (2.12)	3.46 ± .08 (4.26)	5.18 ± .28 (7.78)	17.56 ± .48 (18.34)
Work (J)	.14 ± .00 (.18)	.39 ± .01 (.48)	.82 ± .05 (1.30)	3.15 ± .02 (3.18)
M_b specific Power (W kg^{-1})	350.1 ± 10.8 (470.8)	307.6 ± 6.4 (355.3)	185.1 ± 9.3 (289.3)	267.7 ± 7.3 (279.6)
M_b specific Work (J kg^{-1})	30.1 ± .9 (40.7)	34.4 ± .7 (40.1)	29.3 ± 1.6 (44.9)	48.0 ± .3 (48.5)

Figure 1

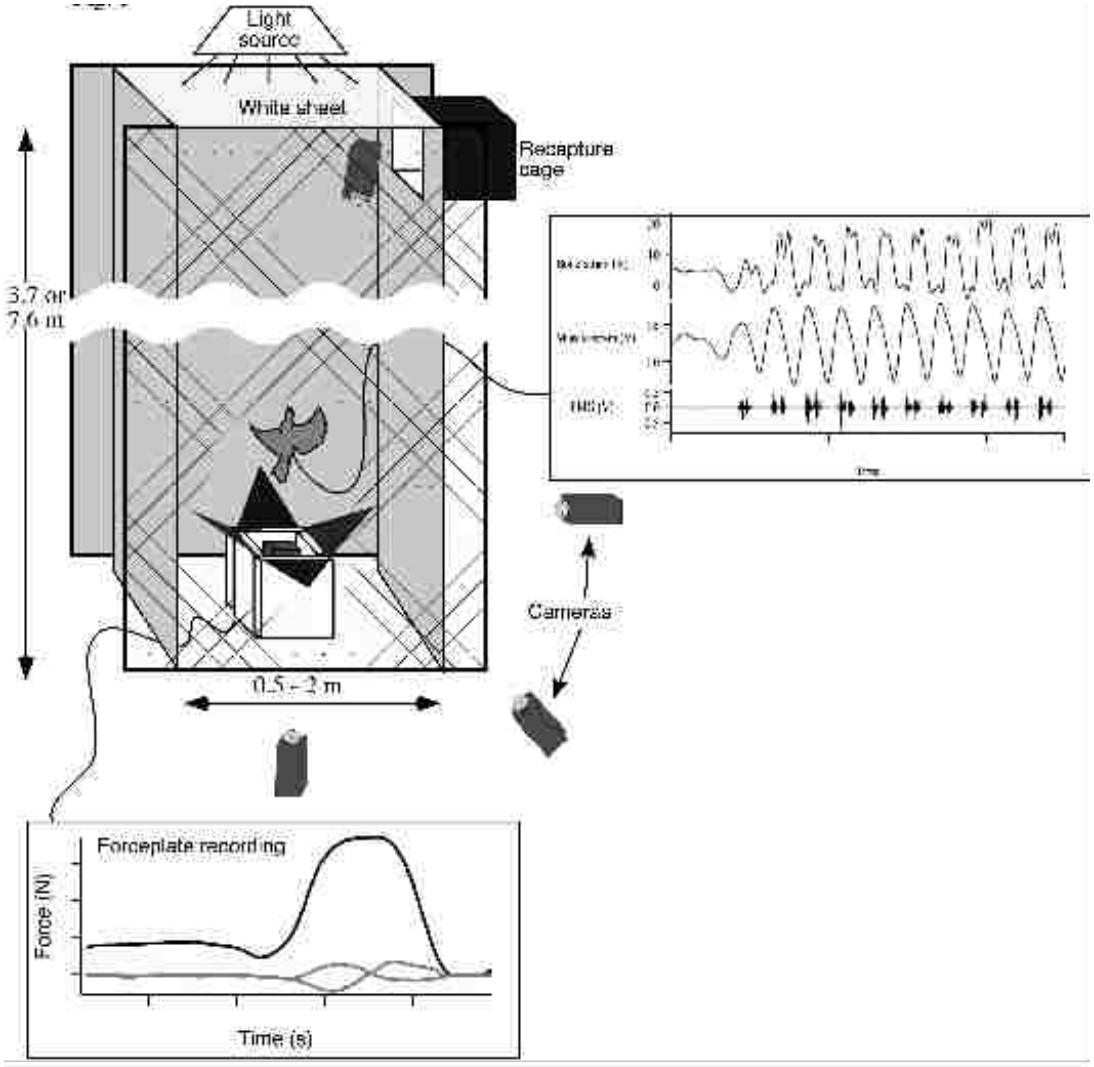
Light source
White sheet
Recapture cage
3.7 or 7.6 m
Cameras
0.5 - 2 m
Forceplate recording
Force (N)
Time (s)

Figure 2

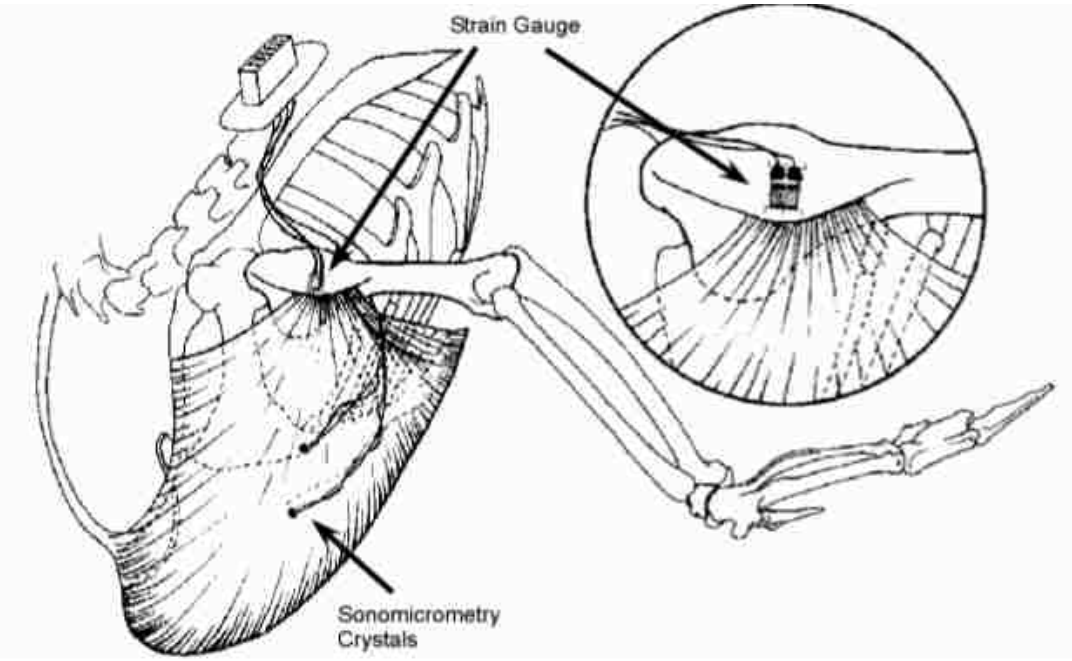

Figure 3

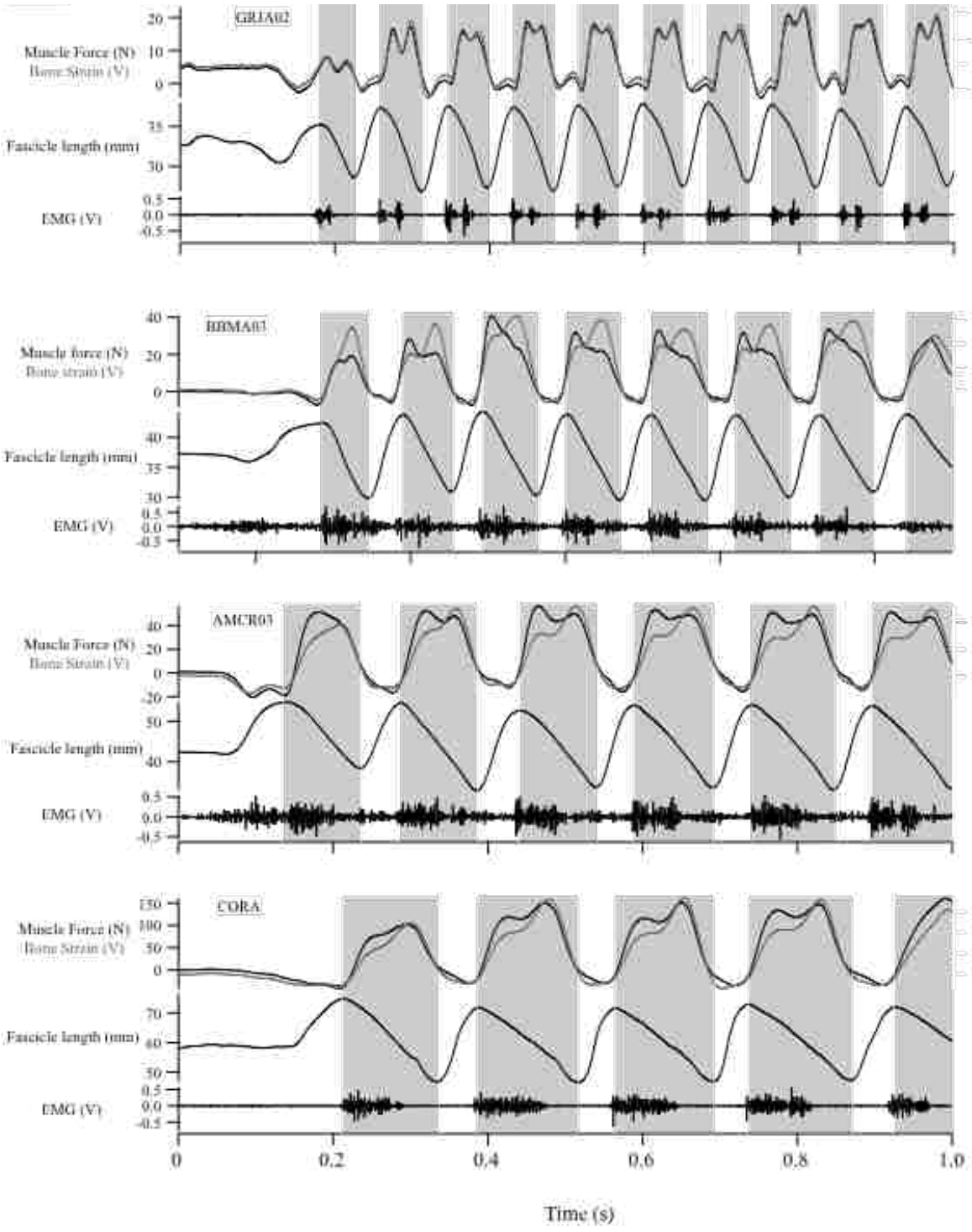
GRIA02
BBMA03
AMCR03
CORA
Muscle Force (N)
Bone Strain (V)
Fascicle length (mm)
EMG (V)
Time (s)

Figure 4

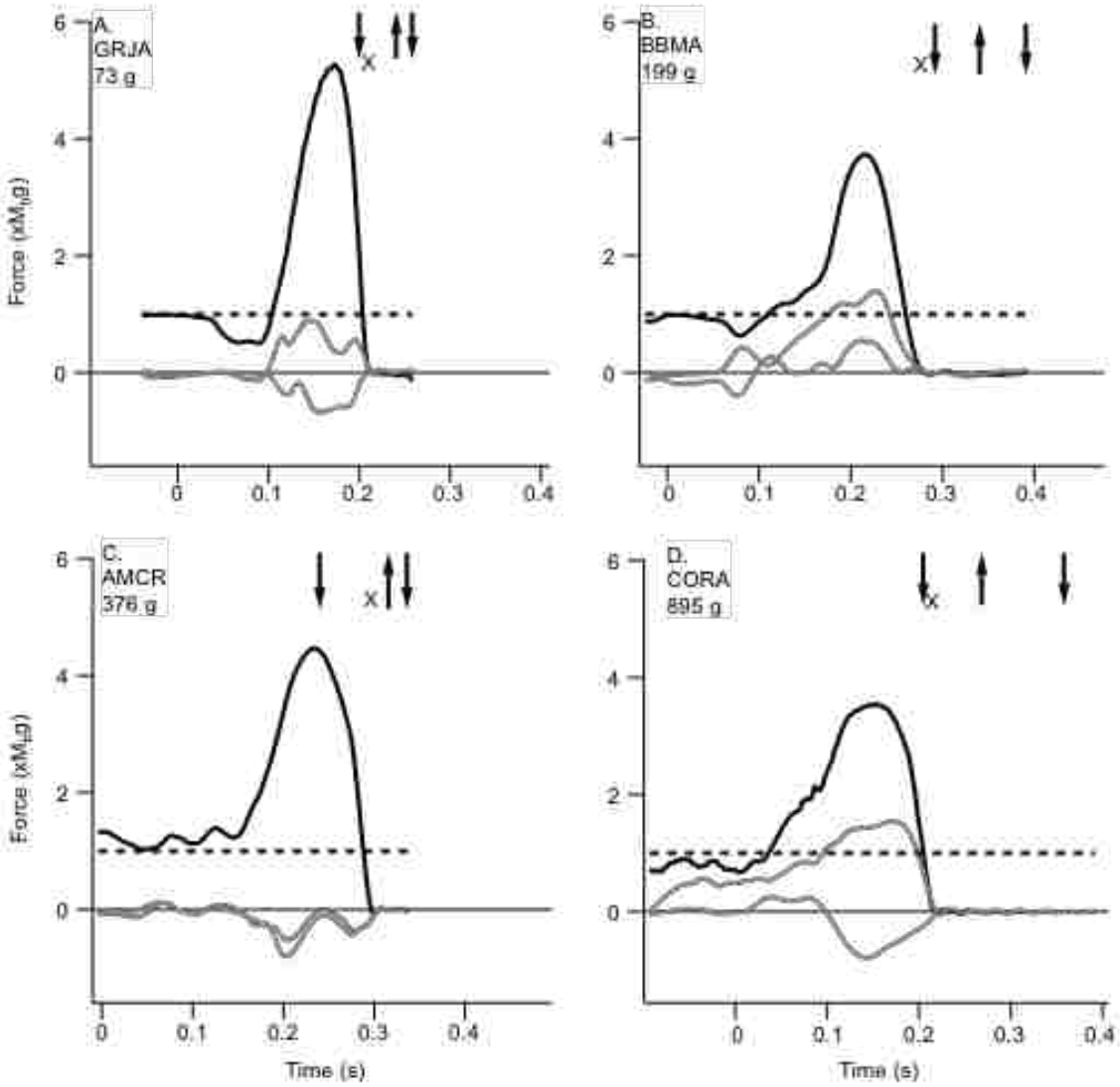
A.
GRJA
73 g
B.
BBMA
199 g
C.
AMCR
376 g
D.
CORA
895 g
Force (xM$_b$g)
Time (s)
0
0.1
0.2
0.3
0.4
2
4
6

Figure 5

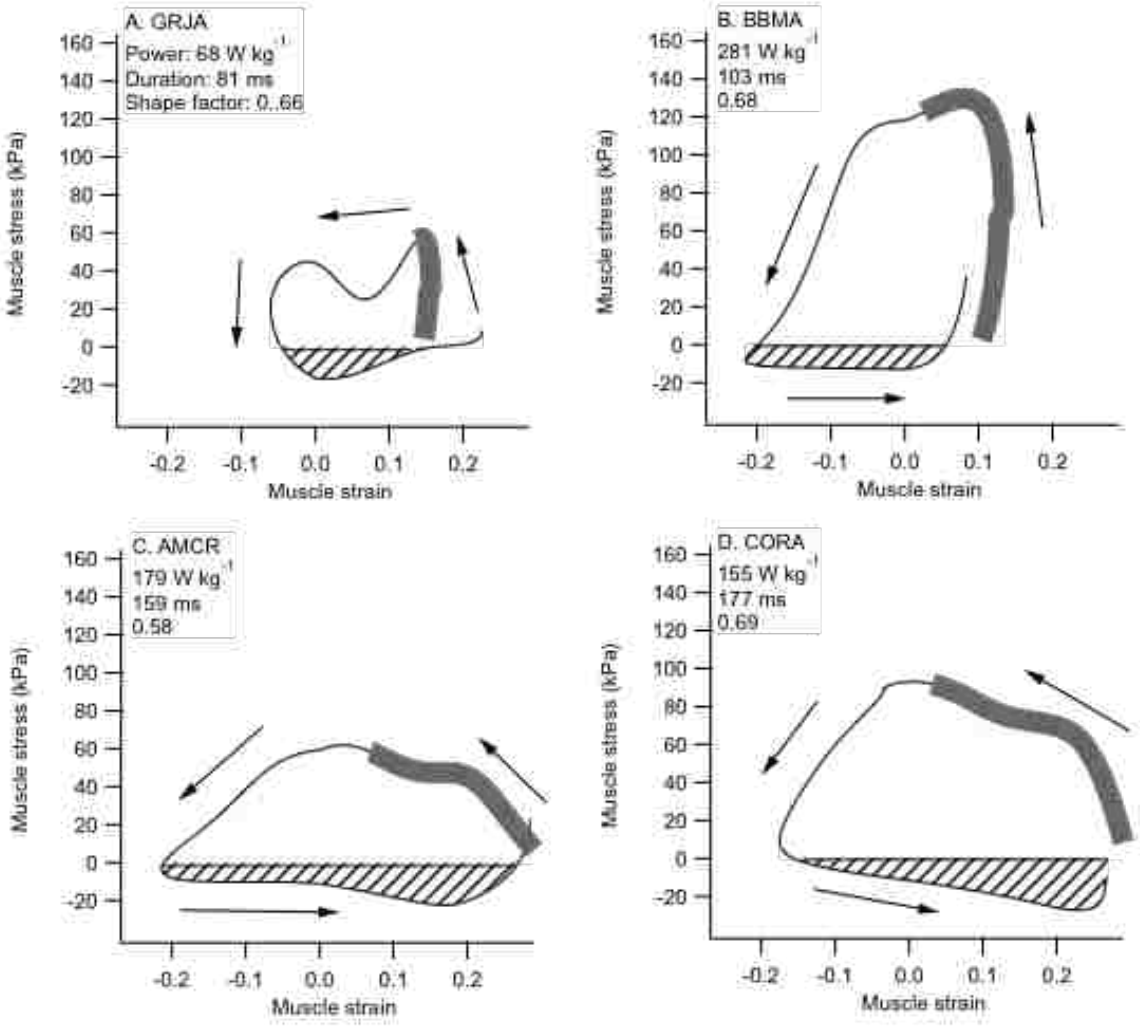
A. GRJA
Power: 68 W kg-1
Duration: 81 ms
Shape factor: 0..66
B. BBMA
281 W kg-1
103 ms
0.68
C. AMCR
179 W kg-1
159 ms
0.58
D. CORA
155 W kg-1
177 ms
0.69
Muscle stress (kPa)
Muscle strain

Figure 6

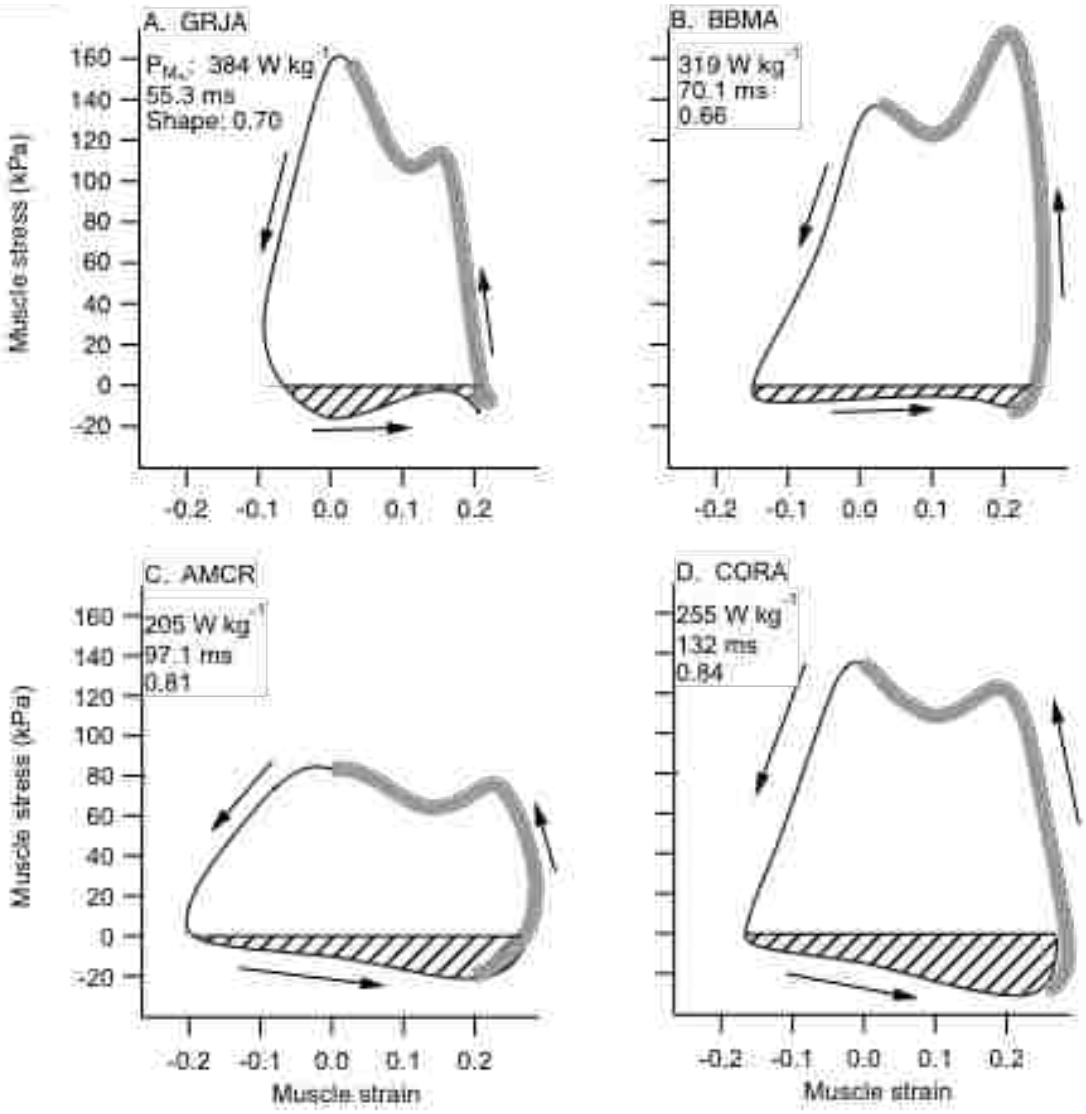
A. GRJA
$P_{M_{max}}$: 384 W kg^{-1}
55.3 ms
Shape: 0.70
B. BBMA
319 W kg^{-1}
70.1 ms
0.66
C. AMCR
205 W kg^{-1}
97.1 ms
0.81
D. CORA
255 W kg^{-1}
132 ms
0.84
Muscle stress (kPa)
Muscle strain
160
140
120
100
80
60
40
20
0
-20
-0.2
-0.1
0.0
0.1
0.2

Figure 7

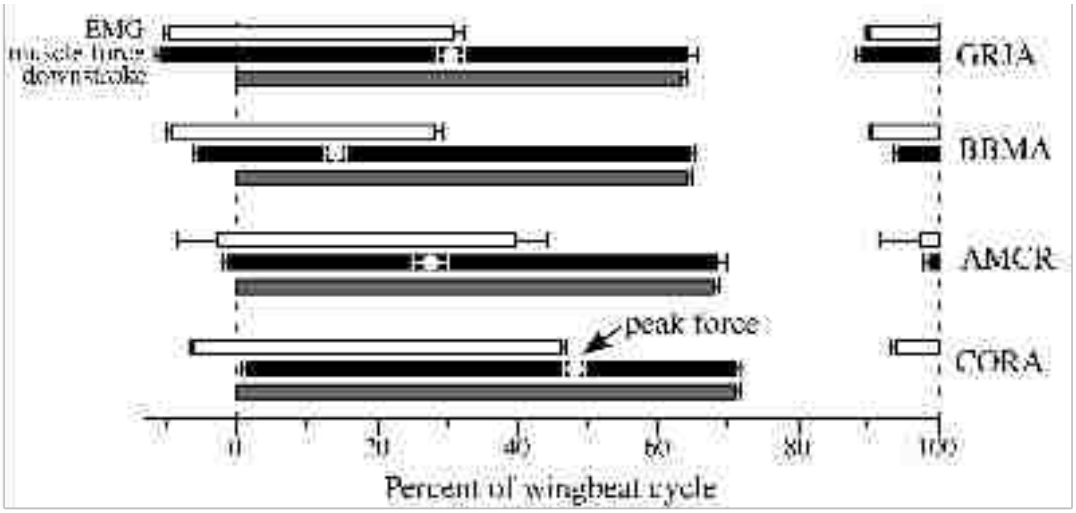
EMG
muscle force
downstroke
peak force
GRIA
BBMA
AMCR
CORA
0
20
40
60
80
100
Percent of wingbeat cycle

Figure 8

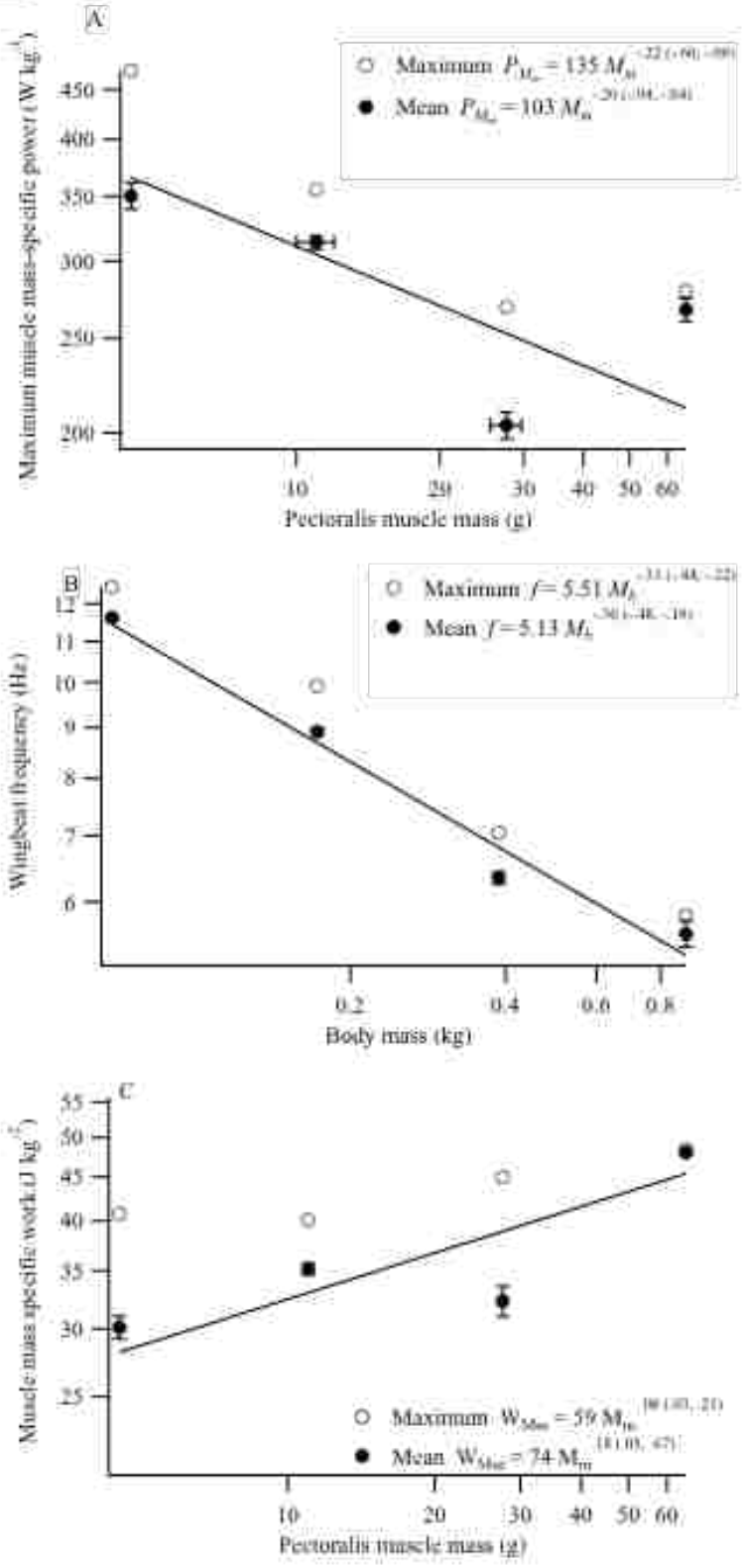
A
Maximum $P_{M_m} = 135\,M_m^{-.22\,(-.94,\,-.09)}$
Mean $P_{M_m} = 103\,M_m^{-.20\,(-.04,\,-.04)}$
Maximum mass-specific power (W kg^{-1})
450
400
350
300
250
200
10
20
30
40
50
60
Pectoralis muscle mass (g)
B
Maximum $f = 5.51\,M_b^{-.33\,(-.44,\,-.22)}$
Mean $f = 5.13\,M_b^{-.30\,(-.42,\,-.18)}$
Wingbeat frequency (Hz)
12
11
10
9
8
7
6
0.2
0.4
0.6
0.8
Body mass (kg)
C
Muscle mass specific work (J kg^{-1})
55
50
45
40
35
30
25
Maximum $W_{Mm} = 59\,M_m^{.09\,(.03,\,.21)}$
Mean $W_{Mm} = 74\,M_m^{.11\,(.03,\,.47)}$
10
20
30
40
50
60
Pectoralis muscle mass (g)

Figure 9

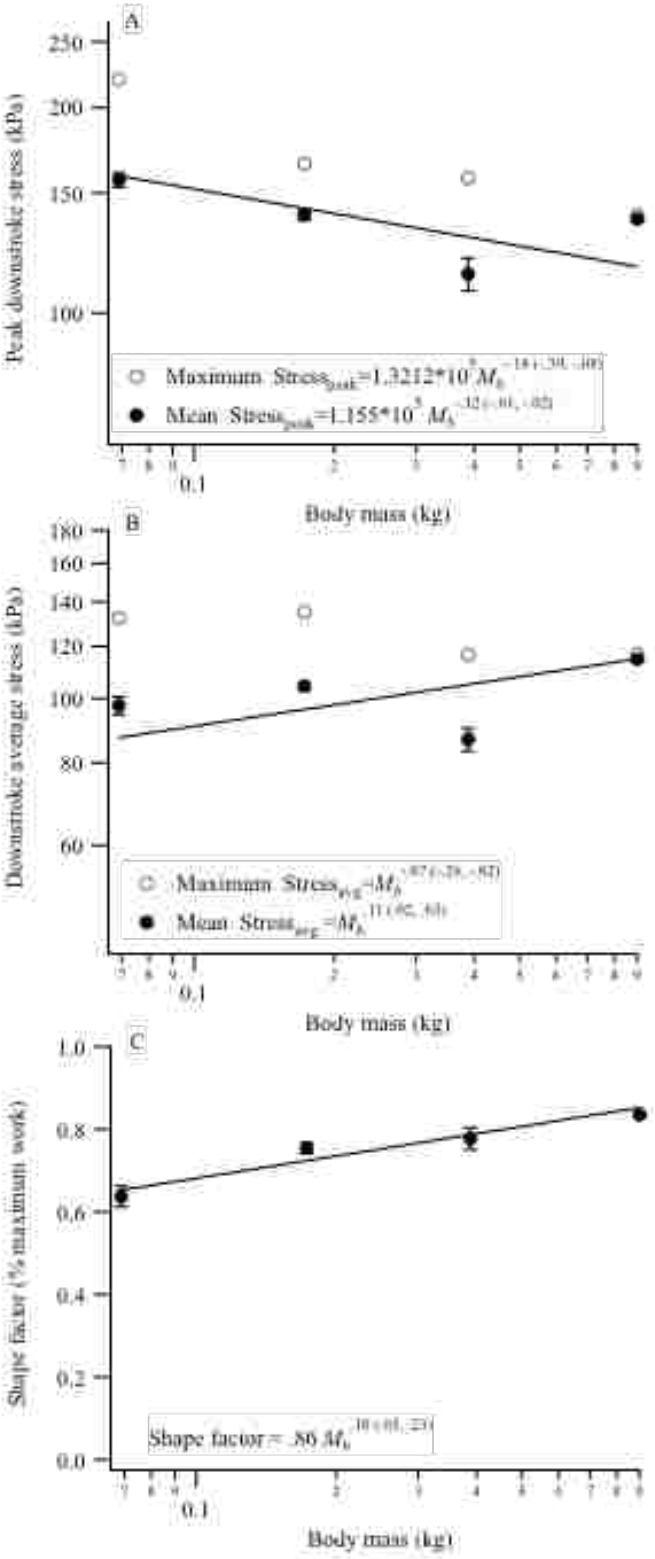
A
Peak downstroke stress (kPa)
250
200
150
100
Maximum Stress
Mean Stress
0.1
Body mass (kg)
B
Downstroke average stress (kPa)
180
160
140
120
100
80
60
Maximum Stress
Mean Stress
0.1
Body mass (kg)
C
Shape factor (% maximum work)
1.0
0.8
0.6
0.4
0.2
0.0
Shape factor =
0.1
Body mass (kg)

Figure 10

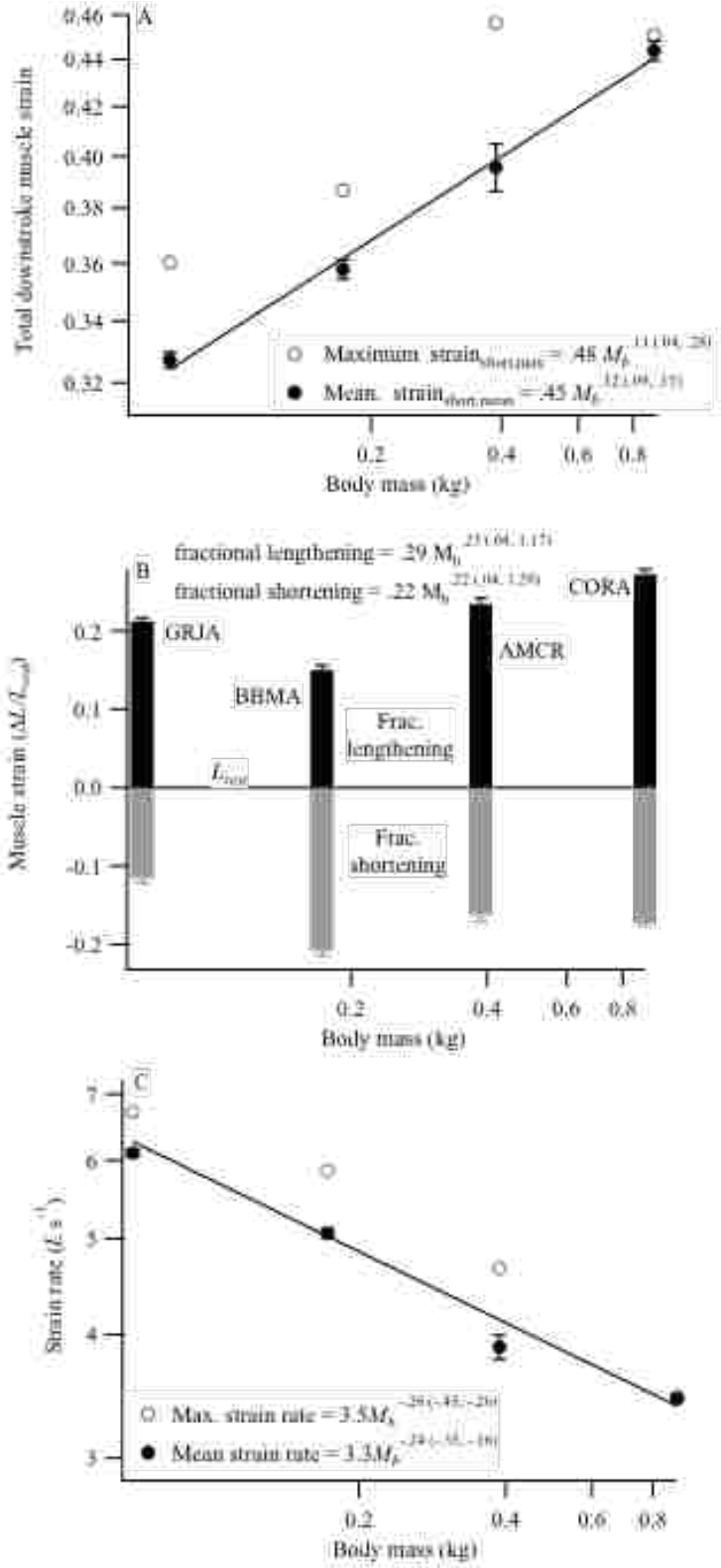
A
Total downstroke muscle strain
0.46
0.44
0.42
0.40
0.38
0.36
0.34
0.32
Maximum strain
Mean. strain
0.2
0.4
0.6
0.8
Body mass (kg)
B
fractional lengthening = .29 M
fractional shortening = .22 M
GRJA
BBMA
AMCR
CORA
Frac. lengthening
Frac. shortening
Muscle strain (ΔL/L
0.2
0.1
0.0
-0.1
-0.2
0.2
0.4
0.6
0.8
Body mass (kg)
C
Strain rate (L s
7
6
5
4
3
Max. strain rate = 3.5M
Mean strain rate = 3.3M
0.2
0.4
0.6
0.8
Body mass (kg)

Appendix I: Species morphological based measurements. Mean ± s.e.m. (maximum)

Species	n (beats)	S_{disc} (cm^2)	S_{wing} (cm^2)	Aspect Ratio	L_{wing} (cm)	S_{tail} (cm^2)
Gray Jay	7	600 ± 38 (814)	337 ± 7	1.65 ± 0.03	16.6 ± .1	84 ± 9
Black-billed magpie	7	1280 ± 152 (1850)	484 ± 33	2.07 ± 0.08	22.0 ± 1.0	158 ± 21
America Crow	3	3200 ± 94 (3340)	1010 ± 10	2.61 ± 0.09	35.9 ± .7	134 ± 10
Common Raven	2	5880 ± 241 (6130)	2050 ± 35	2.54 ± 0.07	50.8 ± .2	389 ± 2
Warbling vireo	11	147 ± 6 (185)	58 ± 2	2.32 ± 0.08	8.2 ± .1	15 ± 1
Cassin's vireo	15	191 ± 4 (222)	76 ± 2	2.29 ± 0.04	9.3 ± .1	18 ± 1
Red-eyed vireo	4	275 ± 28 (330)	92 ± 3	2.32 ± 0.13	10.2 ± .1	7 ± 0
Black-capped chickadee	22	110 ± 5 (156)	64 ± 3	1.63 ± 0.07	7.0 ± .1	14 ± 2
Cliff swallow	9	453 ± 32 (668)	97 ± 4	3.70 ± 0.12	13.3 ± .3	10 ± 1
Pygmy nuthatch	7	169 ± 11 (201)	57 ± 4	2.50 ± 0.26	8.0 ± .2	7 ± 0
Red-breasted nuthatch	6	164 ± 5 (178)	64 ± 2	2.24 ± 0.05	8.4 ± .1	8 ± 0
European starling	4	612 ± 9 (635)	164 ± 9	2.93 ± 0.12	15.4 ± .3	17 ± 1
Gray catbird	5	287 ± 22 (332)	101 ± 5	2.44 ± 0.07	10.9 ± .3	40 ± 2
Western bluebird	7	403 ± 9 (438)	113 ± 4	2.81 ± 0.09	12.5 ± .1	16 ± 2
Swainson's thrush	3	327 ± 6 (332)	136 ± 6	2.25 ± 0.05	12.3 ± .1	16 ± 2
American robin	5	665 ± 67 (834)	227 ± 17	2.30 ± 0.12	15.9 ± .3	55 ± 10
Ruby-crowned kinglet	13	116 ± 4 (151)	50 ± 2	2.07 ± 0.08	7.1 ± .2	12 ± 1
House sparrow	6	234 ± 7 (259)	93 ± 2	2.10 ± 0.03	9.8 ± .1	12 ± 1
American goldfinch	5	193 ± 4 (201)	60 ± 1	2.58 ± 0.02	8.7 ± .1	12 ± 1
House finch	3	291 ± 1 (293)	97 ± 2	2.48 ± 0.05	10.8 ± .2	10 ± 1
White-crowned sparrow	4	241 ± 4 (248)	89 ± 1	2.17 ± 0.04	9.7 ± .1	17 ± 1
Vesper sparrow	4	299 ± 14 (319)	98 ± 4	2.44 ± 0.10	10.8 ± .3	15 ± 2
Spotted towhee	5	287 ± 9 (315)	109 ± 5	2.06 ± 0.06	10.4 ± .2	20 ± 2
Song sparrow	5	201 ± 5 (215)	80 ± 3	2.10 ± 0.11	9.0 ± .1	13 ± 1
Chipping sparrow	4	214 ± 13 (236)	84 ± 2	2.07 ± 0.05	9.3 ± .1	18 ± 3
Dark-eyed junco	9	209 ± 9 (254)	83 ± 4	2.24 ± 0.12	9.4 ± .2	24 ± 3
Red-winged blackbird	2	604 ± 37 (641)	234 ± 1	2.37 ± 0.06	16.6 ± .3	29 ± 1
Western meadowlark	3	700 ± 14 (721)	252 ± 5	2.28 ± 0.09	16.9 ± .2	39 ± 2
MacGillivray's warbler	9	146 ± 4 (174)	54 ± 2	2.45 ± 0.09	8.0 ± .1	15 ± 1
Orange-crowned warbler	6	137 ± 4 (153)	51 ± 1	2.26 ± 0.06	7.6 ± .1	7 ± 1
Yellow-rumped warbler	5	206 ± 6 (222)	72 ± 5	2.65 ± 0.15	9.6 ± .1	13 ± 1
Yellow warbler	13	133 ± 4 (153)	44 ± 1	2.59 ± 0.07	7.5 ± .1	8 ± 0

Appendix II. Force plate measurements.

Species	Impulse (N s)	Peak GRF (N)	Jump duration (s)
Gray Jay	.19	2.98	.11
Black-billed magpie	.53	6.78	.17
America Crow	1.03	11.40	.20
Common Raven	2.96	26.60	.18
Warbling vireo	.03	.53	.12
Cassin's vireo	.02	.70	.06
Red-eyed vireo	.04	.84	.15
Black-capped chickadee	.02	.52	.10
Cliff swallow	.02	.61	.10
Pygmy nuthatch	.02	.44	.06
Red-breasted nuthatch	.03	.54	.13
European starling	.19	2.70	.11
Gray catbird	.07	.83	.12
Western bluebird	.06	1.12	.10
Swainson's thrush	.09	1.59	.11
American robin	.17	2.89	.09
Ruby-crowned kinglet	.01	.28	.11
House sparrow	.06	1.46	.06
American goldfinch	.02	.25	.12
House finch	.07	1.63	.08
White-crowned sparrow	.06	1.58	.07
Vesper sparrow	.08	1.39	.09
Spotted towhee	.09	2.42	.07
Song sparrow	.06	1.25	.09
Chipping sparrow	.02	.48	.08
Dark-eyed junco	.05	1.04	.07
Red-winged blackbird	.18	3.87	.09
Western meadowlark	.30	5.13	.09
MacGillivray's warbler	.03	.54	.13
Orange-crowned warbler	.02	.44	.11
Yellow-rumped warbler	.02	.47	.09
Yellow warbler	.02	.48	.07

Appendix III. Kinematic measurements. Mean ± s.e.m. (maximum)

Species	Travel angle (deg.)	Wing angular vel. (° s^{-1})	Global SPA (°)	Vertebral SPA (°)	Wing angle of attack	Stroke amplitude (°)	Body angle (°)	Body velocity (m s^{-1})	Tail angle of attack (°)	Tail spread (°)
Gray Jay	79 ± 2	3300 ± 106 (3600)	152 ± 2	132 ± 2	29 ± 1 (31)	136 ± 6 (166)	30 ± 3	2.35 ± 0.12 (2.86)	23 ± 3 (35)	74 ± 8 (96)
Black-billed magpie	58 ± 2	2980 ± 77 (3230)	143 ± 5	123 ± 6	38 ± 4 (62)	126 ± 4 (142)	25 ± 2	2.21 ± 0.19 (2.75)	29 ± 6 (59)	46 ± 4 (58)
America Crow	74 ± 4	1920 ± 69 (2050)	125 ± 16	115 ± 10	51 ± 21 (92)	103 ± 11 (116)	17 ± 18	2.20 ± 0.88 (3.81)	16 ± 2 (18)	43 ± 2 (47)
Common Raven	52 ± 5	1660 ± 44 (1700)	114 ± 0	112 ± 10	52 ± 12 (78)	118 ± 8 (126)	51 ± 6	1.90 ± 0.03 (1.93)	39 ± 3 (42)	76 ± 0 (76)
Warbling vireo	55 ± 7	6720 ± 119 (7390)	147 ± 3	124 ± 3	35 ± 2 (44)	140 ± 4 (157)	36 ± 3	2.22 ± 0.08 (2.54)	28 ± 3 (42)	54 ± 4 (72)
Cassin's vireo	60 ± 2	7320 ± 86 (7730)	142 ± 3	123 ± 3	39 ± 3 (72)	137 ± 9 (186)	37 ± 4	2.13 ± 0.13 (2.89)	31 ± 2 (49)	43 ± 2 (60)
Red-eyed vireo	82 ± 1	6500 ± 330 (7200)	142 ± 3	123 ± 4	38 ± 0 (39)	143 ± 5 (159)	39 ± 3	2.05 ± 0.05 (2.17)	25 ± 7 (37)	19 ± 1 (22)
Black-capped chickadee	72 ± 2	7030 ± 201 (8520)	140 ± 4	120 ± 3	41 ± 2 (70)	130 ± 8 (182)	27 ± 5	1.96 ± 0.17 (3.15)	26 ± 3 (71)	34 ± 4 (72)
Cliff swallow	43 ± 4	4610 ± 123 (5440)	140 ± 12	108 ± 11	44 ± 3 (67)	119 ± 4 (134)	46 ± 4	2.37 ± 0.19 (3.15)	34 ± 6 (64)	48 ± 2 (54)
Pygmy nuthatch	66 ± 5	6830 ± 339 (7550)	138 ± 5	130 ± 3	42 ± 4 (59)	149 ± 10 (204)	21 ± 9	1.31 ± 0.17 (1.97)	15 ± 3 (28)	43 ± 2 (51)
Red-breasted nuthatch	63 ± 3	6780 ± 272 (7690)	149 ± 3	115 ± 4	34 ± 1 (38)	136 ± 5 (154)	45 ± 4	1.92 ± 0.08 (2.15)	22 ± 6 (46)	53 ± 3 (65)
European starling	77 ± 2	5000 ± 95 (5120)	149 ± 3	129 ± 5	33 ± 4 (43)	154 ± 7 (167)	46 ± 6	2.72 ± 0.34 (3.39)	32 ± 1 (34)	41 ± 3 (47)
Gray catbird	52 ± 3	4900 ± 140 (5370)	142 ± 6	121 ± 4	36 ± 1 (40)	145 ± 9 (176)	34 ± 4	2.32 ± 0.07 (2.56)	9 ± 17 (41)	62 ± 2 (67)
Western bluebird	49 ± 3	4980 ± 115 (5490)	146 ± 4	121 ± 2	37 ± 3 (55)	139 ± 2 (146)	42 ± 5	2.54 ± 0.21 (3.09)	21 ± 3 (37)	40 ± 5 (52)
Swainson's thrush	70 ± 3	5850 ± 157 (6140)	129 ± 5	117 ± 2	34 ± 3 (38)	114 ± 8 (128)	15 ± 4	2.33 ± 0.11 (2.49)	13 ± 2 (15)	28 ± 5 (37)
American robin	68 ± 6	4770 ± 334 (5920)	156 ± 5	132 ± 4	39 ± 3 (45)	134 ± 6 (156)	30 ± 7	2.09 ± 0.33 (3.40)	37 ± 3 (44)	51 ± 9 (87)
Ruby-crowned kinglet	65 ± 2	6720 ± 193 (7910)	146 ± 3	112 ± 3	36 ± 2 (48)	139 ± 5 (178)	50 ± 2	2.39 ± 0.10 (3.22)	30 ± 4 (50)	52 ± 5 (79)
House sparrow	79 ± 1	7820 ± 123 (8260)	130 ± 12	106 ± 8	46 ± 5 (65)	114 ± 19 (146)	27 ± 12	1.74 ± 0.34 (2.79)	16 ± 2 (21)	25 ± 2 (36)
American goldfinch	30 ± 7	6400 ± 148 (6820)	162 ± 2	135 ± 1	30 ± 1 (32)	133 ± 2 (138)	36 ± 3	2.68 ± 0.19 (3.18)	30 ± 6 (41)	43 ± 2 (48)
House finch	68 ± 5	6940 ± 492 (7930)	144 ± 3	117 ± 6	37 ± 2 (44)	140 ± 5 (161)	37 ± 4	2.02 ± 0.15 (2.49)	27 ± 8 (41)	21 ± 3 (26)
White-crowned sparrow	79 ± 1	6660 ± 123 (6960)	144 ± 4	120 ± 4	35 ± 4 (47)	145 ± 9 (160)	32 ± 7	2.10 ± 0.18 (2.53)	8 ± 1 (11)	26 ± 1 (28)
Vesper sparrow	69 ± 4	6991 ± 271 (7490)	149 ± 5	124 ± 6	39 ± 2 (43)	147 ± 5 (158)	31 ± 5	2.31 ± 0.42 (3.08)	10 ± 3 (15)	40 ± 40 (54)
Spotted towhee	79 ± 2	5130 ± 131 (5590)	130 ± 7	110 ± 1	38 ± 4 (47)	122 ± 9 (147)	30 ± 12	2.05 ± 0.64 (3.61)	23 ± 3 (31)	18 ± 2 (24)
Song sparrow	83 ± 0	6300 ± 70 (6550)	149 ± 5	118 ± 2	34 ± 2 (40)	136 ± 5 (151)	38 ± 3	2.60 ± 0.11 (2.99)	19 ± 3 (30)	27 ± 2 (35)
Chipping sparrow	67 ± 4	7270 ± 408 (8120)	150 ± 2	129 ± 4	39 ± 3 (47)	147 ± 12 (176)	30 ± 4	2.17 ± 0.05 (2.30)	18 ± 2 (23)	39 ± 6 (50)
Dark-eyed junco	74 ± 1	6740 ± 314 (8850)	155 ± 2	124 ± 3	36 ± 2 (45)	136 ± 4 (154)	49 ± 3	2.37 ± 0.13 (3.11)	17 ± 2 (24)	46 ± 6 (79)
Red-winged blackbird	67 ± 2	5480 ± 110 (5590)	142 ± 3	109 ± 3	38 ± 5 (43)	121 ± 6 (127)	36 ± 4	2.19 ± 0.06 (2.24)	18 ± 0 (18)	31 ± 2 (32)
Western meadowlark	75 ± 5	4810 ± 95 (4990)	149 ± 3	120 ± 6	31 ± 2 (33)	130 ± 4 (134)	46 ± 2	2.18 ± 0.19 (2.44)	27 ± 4 (34)	52 ± 1 (55)
MacGillivray's warbler	63 ± 2	6670 ± 197 (7420)	150 ± 4	119 ± 3	35 ± 1 (41)	146 ± 6 (169)	41 ± 4	2.19 ± 0.10 (2.63)	10 ± 1 (15)	40 ± 2 (48)
Orange-crowned warbler	64 ± 4	6880 ± 247 (7520)	148 ± 5	125 ± 6	39 ± 4 (55)	124 ± 5 (139)	37 ± 6	1.74 ± 0.26 (2.81)	16 ± 3 (30)	27 ± 3 (32)
Yellow-rumped warbler	75 ± 3	5530 ± 433 (6490)	144 ± 3	123 ± 2	38 ± 2 (44)	129 ± 3 (140)	43 ± 7	1.92 ± 0.05 (2.08)	23 ± 2 (29)	44 ± 3 (53)
Yellow warbler	51 ± 4	6110 ± 149 (7060)	147 ± 5	114 ± 3	41 ± 2 (52)	144 ± 4 (164)	41 ± 5	1.66 ± 0.06 (2.03)	26 ± 6 (64)	42 ± 2 (65)

Appendix IV. Power components. Mean ± s.e.m. (maximum)

Species	Duty factor	f (Hz)	$P_{cl,Mb}$ (W kg^{-1})	$P_{ind,Mb}$ (W kg-1)	$P_{pro,Mb}$ (W kg-1)	$P_{tot,Mb}$ (W kg-1)	Induced velocity (m s^{-1})
Gray Jay	.46 ± .03	11.5 ± .3 (12.6)	24.1 ± 2.2 (31.8)	25 ± 1 (30)	0.2 ± 0.1 (0.8)	56 ± 49 (56)	2.1 ± 0.1 (2.6)
Black-billed magpie	.49 ± .02	9.2 ± .1 (9.5)	20.9 ± 2.2 (29.5)	20 ± 3 (32)	0.3 ± 0.1 (0.6)	51 ± 41 (51)	1.7 ± 0.3 (2.7)
America Crow	.52 ± .02	6.6 ± .1 (6.9)	19.5 ± 2.5 (23.9)	7 ± 0 (7)	0.3 ± 0.0 (0.4)	30 ± 27 (30)	0.6 ± 0.0 (0.6)
Common Raven	.51 ± .02	6.1 ± .4 (6.5)	18.9 ± 3.0 (21.9)	3 ± 0 (3)	0.9 ± 0.1 (1.0)	26 ± 23 (26)	0.3 ± 0.0 (0.3)
Warbling vireo	.44 ± .02	22.3 ± .6 (26.6)	25.4 ± 2.1 (33.4)	71 ± 6 (113)	0.4 ± 0.1 (0.7)	130 ± 97 (130)	6.1 ± 0.6 (9.8)
Cassin's vireo	.41 ± .01	23.0 ± .3 (24.9)	31.7 ± 3.5 (58.4)	51 ± 2 (78)	0.6 ± 0.1 (0.9)	100 ± 83 (100)	4.3 ± 0.2 (6.7)
Red-eyed vireo	.39 ± .01	20.3 ± .8 (21.7)	31.5 ± 4.2 (43.4)	43 ± 2 (50)	0.4 ± 0.1 (0.5)	86 ± 75 (86)	3.7 ± 0.2 (4.2)
Black-capped chickadee	.45 ± .01	23.7 ± .6 (27.3)	32.1 ± 2.7 (65.1)	70 ± 3 (88)	0.4 ± 0.1 (0.9)	119 ± 102 (119)	5.9 ± 0.2 (7.6)
Cliff swallow	.45 ± .02	13.4 ± .3 (14.2)	13.6 ± 1.0 (20.1)	42 ± 5 (79)	0.2 ± 0.0 (0.4)	90 ± 56 (90)	3.6 ± 0.4 (6.8)
Pygmy nuthatch	.53 ± .02	23.3 ± .9 (25.8)	29.4 ± 4.2 (46.2)	60 ± 6 (89)	0.3 ± 0.1 (0.5)	107 ± 90 (107)	5.1 ± 0.5 (7.6)
Red-breasted nuthatch	.45 ± .01	22.2 ± .6 (24.4)	27.2 ± 2.3 (35.4)	54 ± 2 (61)	0.5 ± 0.1 (0.9)	89 ± 82 (89)	4.6 ± 0.2 (5.2)
European starling	.47 ± .00	15.0 ± .4 (16.1)	23.4 ± 4.4 (30.4)	25 ± 1 (26)	0.2 ± 0.0 (0.2)	55 ± 49 (55)	2.2 ± 0.0 (2.2)
Gray catbird	.49 ± .02	16.8 ± .2 (17.3)	23.8 ± 2.4 (32.7)	43 ± 3 (53)	0.2 ± 0.0 (0.3)	74 ± 67 (74)	3.7 ± 0.2 (4.5)
Western bluebird	.52 ± .01	16.8 ± .5 (19.1)	24.6 ± 1.6 (32.7)	35 ± 1 (38)	0.3 ± 0.0 (0.5)	65 ± 60 (65)	2.9 ± 0.1 (3.3)
Swainson's thrush	.36 ± .01	16.4 ± .1 (16.6)	26.9 ± 4.1 (32.9)	34 ± 3 (39)	0.1 ± 0.0 (0.2)	68 ± 61 (68)	2.9 ± 0.2 (3.4)
American robin	.47 ± .08	13.7 ± .5 (15.0)	26.1 ± 2.7 (35.7)	24 ± 1 (26)	0.2 ± 0.1 (0.3)	62 ± 50 (62)	2.1 ± 0.1 (2.2)
Ruby-crowned kinglet	.46 ± .01	21.9 ± .4 (24.3)	19.4 ± 1.9 (28.8)	71 ± 2 (81)	0.3 ± 0.0 (0.4)	103 ± 91 (103)	6.1 ± 0.1 (7.0)
House sparrow	.47 ± .01	25.3 ± .8 (27.4)	44.2 ± 5.5 (66.6)	40 ± 1 (41)	0.4 ± 0.1 (0.6)	108 ± 84 (108)	3.4 ± 0.1 (3.5)
American goldfinch	.48 ± .01	20.2 ± .5 (21.4)	18.0 ± 1.5 (22.0)	97 ± 31 (217)	0.3 ± 0.1 (0.6)	231 ± 116 (231)	9.5 ± 3.7 (24.2)
House finch	.45 ± .03	26.4 ± 1.9 (36.5)	23.5 ± 3.6 (33.3)	72 ± 16 (128)	0.4 ± 0.1 (1.0)	158 ± 96 (158)	6.2 ± 1.4 (11.3)
White-crowned sparrow	.53 ± .01	22.4 ± .4 (23.2)	26.2 ± 3.9 (35.1)	44 ± 1 (46)	0.2 ± 0.0 (0.2)	81 ± 70 (81)	3.7 ± 0.1 (3.9)
Vesper sparrow	.48 ± .01	22.1 ± .5 (22.9)	57.6 ± 16.4 (106.9	35 ± 2 (42)	0.4 ± 0.0 (0.5)	138 ± 93 (138)	3.0 ± 0.2 (3.5)
Spotted towhee	.50 ± .01	16.3 ± .2 (17.0)	17.0 ± 2.0 (21.5)	43 ± 2 (49)	0.1 ± 0.0 (0.1)	69 ± 60 (69)	3.6 ± 0.2 (4.1)
Song sparrow	.50 ± .01	21.2 ± .4 (22.1)	28.9 ± 2.2 (35.1)	52 ± 1 (54)	0.2 ± 0.0 (0.2)	89 ± 81 (89)	4.4 ± 0.1 (4.6)
Chipping sparrow	.45 ± .02	22.3 ± 2.1 (27.7)	37.3 ± 5.4 (52.9)	49 ± 4 (59)	0.4 ± 0.1 (0.5)	104 ± 87 (104)	4.2 ± 0.3 (5.1)
Dark-eyed junco	.47 ± .01	22.3 ± .3 (24.1)	34.4 ± 3.5 (52.9)	50 ± 2 (64)	0.3 ± 0.1 (0.7)	109 ± 85 (109)	4.3 ± 0.2 (5.4)
Red-winged blackbird	.37 ± .00	15.1 ± .1 (15.2)	37.1 ± 1.3 (38.3)	22 ± 0 (22)	0.9 ± 0.1 (1.0)	61 ± 60 (61)	1.8 ± 0.0 (1.9)
Western meadowlark	.47 ± .02	15.3 ± .4 (16.0)	30.8 ± 3.6 (34.5)	19 ± 0 (20)	0.5 ± 0.1 (0.6)	54 ± 50 (54)	1.6 ± 0.0 (1.7)
MacGillivray's warbler	.44 ± .01	21.4 ± .5 (23.8)	22.5 ± 2.5 (37.6)	63 ± 3 (83)	0.3 ± 0.1 (0.7)	96 ± 86 (96)	5.4 ± 0.2 (7.1)
Orange-crowned warbler	.47 ± .01	22.6 ± .4 (23.6)	32.7 ± 3.6 (45.1)	63 ± 2 (68)	0.2 ± 0.0 (0.3)	102 ± 96 (102)	5.4 ± 0.2 (5.8)
Yellow-rumped warbler	.44 ± .02	18.0 ± .4 (19.6)	32.7 ± 4.5 (51.1)	48 ± 2 (58)	0.3 ± 0.1 (0.7)	95 ± 81 (95)	4.0 ± 0.2 (5.0)
Yellow warbler	.50 ± .01	21.7 ± .4 (24.4)	15.3 ± 1.6 (29.0)	72 ± 2 (86)	0.2 ± 0.0 (0.3)	97 ± 87 (97)	6.1 ± 0.2 (7.4)

$P_{PE, Mb}$ (W kg-1)	$P_{KE, Mb}$ (W kg-1)	C_L	C_D	$S_{disc, FR}$ (cm^2)	δ (radians)	F_R (N)
22.7 ± 1.6 (28.1)	1.35 ± 1.92 (6.91)	0.11 ± 0.02 (0.17)	0.43 ± 0.07 (0.72)	507 ± 33	0.86 ± 0.02	0.72 ± 0.01 (0.74)
17.5 ± 1.0 (20.5)	3.48 ± 1.64 (8.96)	0.40 ± 0.10 (0.67)	0.33 ± 0.04 (0.57)	904 ± 169	0.83 ± 0.02	1.95 ± 0.09 (2.21)
23.1 ± 2.1 (27.2)	-3.61 ± 1.20 (-1.67)	0.17 ± 0.03 (0.22)	0.37 ± 0.02 (0.41)	2724 ± 63	0.86 ± 0.02	3.69 ± 0.25 (3.94)
20.8 ± 0.4 (21.2)	-1.95 ± 3.39 (1.45)	0.09 ± 0.01 (0.11)	0.38 ± 0.06 (0.44)	5625 ± 63	0.83 ± 0.01	8.78 ± 0.00 (8.78)
16.4 ± 1.5 (23.4)	9.05 ± 1.82 (20.19)	0.12 ± 0.02 (0.23)	0.24 ± 0.03 (0.50)	111 ± 13	0.83 ± 0.01	0.10 ± 0.00 (0.10)
20.5 ± 1.5 (32.0)	11.18 ± 2.54 (26.39)	0.07 ± 0.01 (0.19)	0.20 ± 0.01 (0.24)	172 ± 9	0.81 ± 0.00	0.15 ± 0.00 (0.16)
20.6 ± 1.8 (24.8)	10.89 ± 2.60 (18.59)	0.06 ± 0.02 (0.09)	0.19 ± 0.01 (0.20)	219 ± 13	0.80 ± 0.00	0.16 ± 0.00 (0.16)
22.9 ± 1.3 (34.7)	9.16 ± 1.93 (34.17)	0.15 ± 0.02 (0.41)	0.35 ± 0.03 (0.82)	99 ± 6	0.83 ± 0.01	0.11 ± 0.00 (0.11)
10.2 ± 0.7 (13.5)	3.39 ± 1.06 (8.87)	0.15 ± 0.03 (0.36)	0.20 ± 0.02 (0.23)	304 ± 32	0.85 ± 0.01	0.20 ± 0.00 (0.20)
18.0 ± 2.5 (26.2)	11.34 ± 2.36 (20.09)	0.18 ± 0.08 (0.63)	0.21 ± 0.01 (0.24)	141 ± 17	0.82 ± 0.01	0.10 ± 0.00 (0.10)
19.9 ± 1.7 (25.2)	7.34 ± 2.32 (10.76)	0.06 ± 0.01 (0.09)	0.22 ± 0.02 (0.32)	151 ± 7	0.83 ± 0.01	0.10 ± 0.00 (0.10)
22.5 ± 0.5 (23.6)	0.85 ± 4.74 (7.35)	0.13 ± 0.02 (0.16)	0.28 ± 0.02 (0.32)	482 ± 13	0.89 ± 0.02	0.74 ± 0.00 (0.74)
16.4 ± 1.4 (20.8)	7.41 ± 1.50 (11.91)	0.14 ± 0.01 (0.18)	0.39 ± 0.07 (0.65)	235 ± 18	0.85 ± 0.02	0.29 ± 0.00 (0.29)
17.2 ± 1.4 (21.5)	7.40 ± 1.11 (11.44)	0.09 ± 0.02 (0.14)	0.20 ± 0.00 (0.23)	323 ± 13	0.85 ± 0.01	0.27 ± 0.00 (0.27)
21.6 ± 0.9 (23.2)	5.27 ± 3.93 (9.65)	0.10 ± 0.03 (0.14)	0.24 ± 0.00 (0.25)	317 ± 32	0.81 ± 0.01	0.29 ± 0.00 (0.29)
21.6 ± 1.0 (23.5)	4.42 ± 2.52 (12.23)	0.10 ± 0.02 (0.14)	0.24 ± 0.02 (0.28)	517 ± 21	0.88 ± 0.05	0.79 ± 0.02 (0.83)
14.8 ± 1.0 (19.9)	4.64 ± 1.51 (12.49)	0.11 ± 0.01 (0.22)	0.24 ± 0.03 (0.56)	100 ± 4	0.83 ± 0.01	0.05 ± 0.00 (0.06)
28.2 ± 1.3 (32.3)	15.96 ± 4.72 (34.27)	0.08 ± 0.01 (0.11)	0.28 ± 0.01 (0.33)	218 ± 8	0.85 ± 0.01	0.28 ± 0.00 (0.28)
10.2 ± 2.8 (18.3)	7.83 ± 1.89 (12.88)	0.23 ± 0.03 (0.33)	0.17 ± 0.04 (0.28)	99 ± 29	0.83 ± 0.01	0.12 ± 0.01 (0.13)
17.7 ± 1.1 (22.5)	5.81 ± 3.61 (17.97)	0.14 ± 0.07 (0.36)	0.23 ± 0.06 (0.51)	170 ± 44	0.81 ± 0.02	0.22 ± 0.00 (0.22)
23.9 ± 0.5 (24.5)	2.28 ± 4.27 (12.65)	0.28 ± 0.02 (0.31)	0.51 ± 0.01 (0.54)	202 ± 8	0.85 ± 0.00	0.27 ± 0.00 (0.27)
31.0 ± 2.6 (37.3)	26.68 ± 14.42 (69.60)	0.07 ± 0.00 (0.08)	0.16 ± 0.01 (0.17)	253 ± 16	0.86 ± 0.01	0.23 ± 0.00 (0.23)
19.8 ± 0.4 (20.7)	-2.83 ± 2.21 (2.01)	0.23 ± 0.04 (0.33)	0.39 ± 0.03 (0.47)	230 ± 19	0.87 ± 0.02	0.35 ± 0.00 (0.35)
22.4 ± 1.1 (25.4)	6.44 ± 1.72 (9.88)	0.20 ± 0.03 (0.27)	0.36 ± 0.02 (0.44)	160 ± 8	0.88 ± 0.02	0.20 ± 0.00 (0.20)
23.1 ± 2.9 (28.8)	14.25 ± 5.90 (31.55)	0.07 ± 0.02 (0.12)	0.15 ± 0.00 (0.16)	172 ± 16	0.82 ± 0.02	0.12 ± 0.00 (0.12)
23.1 ± 1.1 (27.9)	11.32 ± 3.43 (30.50)	0.13 ± 0.04 (0.41)	0.26 ± 0.04 (0.47)	170 ± 12	0.86 ± 0.01	0.20 ± 0.01 (0.21)
26.8 ± 1.6 (28.4)	10.24 ± 0.37 (10.61)	0.06 ± 0.00 (0.07)	0.23 ± 0.01 (0.24)	533 ± 6	0.83 ± 0.00	0.75 ± 0.00 (0.75)
28.6 ± 1.1 (30.4)	2.19 ± 2.63 (5.71)	0.09 ± 0.03 (0.13)	0.23 ± 0.01 (0.25)	621 ± 10	0.86 ± 0.02	0.98 ± 0.00 (0.98)
20.1 ± 1.0 (25.6)	2.49 ± 1.86 (13.60)	0.18 ± 0.04 (0.51)	0.40 ± 0.10 (1.30)	117 ± 6	0.84 ± 0.01	0.10 ± 0.00 (0.10)
20.8 ± 2.1 (27.5)	11.89 ± 2.08 (19.74)	0.10 ± 0.02 (0.13)	0.32 ± 0.02 (0.38)	116 ± 5	0.83 ± 0.01	0.08 ± 0.00 (0.09)
19.8 ± 1.4 (25.0)	12.87 ± 3.21 (26.04)	0.05 ± 0.02 (0.13)	0.19 ± 0.01 (0.25)	193 ± 14	0.85 ± 0.01	0.10 ± 0.00 (0.10)
13.5 ± 1.1 (18.6)	1.80 ± 1.08 (10.43)	0.14 ± 0.02 (0.34)	0.31 ± 0.02 (0.46)	102 ± 5	0.83 ± 0.01	0.09 ± 0.00 (0.09)

Appendix V: Surgical Methods and Signal Processing and Analysis

All implanted gauges were soldered to a plug made of two miniature connectors (GF-6 Microtech Inc., Boothwyn, USA) glued together using self-catalyzing cyanoacrylate adhesive, and embedded in an epoxy platform. The gauges on each plug consisted of two single-element strain gauges (FLA-1-11, Tokyo Sokki Kenkyujo, Ltd, Japan, 0.5-2 mm), one pair of sonomicrometry crystals (1 or 2 mm, 38 or 36 AUG, Sonometrics Corp. Canada), an indwelling EMG electrode (California Fine Wire Co., pair of twisted 100 μm diameter 99.9% silver wire, 1 mm inter-tip distance with 0.5 mm insulation removed), and a ground wire (3 cm 28 gauge insulated copper).

Birds were anesthetized using inhaled isofluorane (HME109, Highland medical Equipment, CA, 5% to induce, 2-3% to maintain). Feathers were removed at each incision site (the midline between scapulae, over each deltopectoral crest (DPC), and over the left pectoralis). A small (1-2 cm) incision was made in the skin at each location immediately prior to implantation at that site. Throughout the procedure all incision areas were kept moist with sterile saline, and sutured (4-0 monofilament) closed immediately after implantation at that site. Sonomicrometry crystals and EMG electrode were passed from the dorsal incision subcutaneously to the incision over the left pectoralis (Fig. 2). Ultra fine-tipped forceps were used to make two small holes in the superficial fascia and to separate the fascicles of the pectoralis, along a single long fascicle in the area of the central tendon, approximately 1.5 cm apart. Each sonomicrometry crystal was inserted 0.5 cm deep into each opening and oriented to provide the best signals. Each opening was closed and the crystal secured by suturing (0-6 polypropylene monofilament, Surgilene; Davis & Geck, Division of American

Cyanamid Co., Danbury, CT) the fascia across the hole and around the emerging wire. Each wire was also attached to the fascia with suture, leaving slack to prevent wingbeat movements from pulling the crystals out of the muscle. Immediately caudal to the sonomicrometry crystals the EMG electrode was inserted 0.5 cm deep in the muscle using a 24 gauge hypodermic needle. The wire was sutured to the fascia with slack as with the sonomicrometry leads.

The strain gauges were implanted bilaterally on the delto-pectoral crest (DPC) of the humerus (Fig. 2). Through a small incision dorsal to the DPC, scissors were used to separate the heads of the deltoideus muscle and to bluntly dissect subcutaneously to the midline incision; creating a tunnel through which a strain gauge and lead were passed. The implant site was cleared of muscle fibers, periosteum, and fatty deposits using a bone scraper, scalpel blade, and solvent (xylene or methyl-ethyl-ketone). The gauge was attached with self-catalyzing cyanoacrylate, oriented perpendicular to the long-axis of the humerus, and positioned mid-distally on the DPC at the cranial edge.

The bare end of the ground wire was sutured (0-3 silk) to the intervertebral ligament at the cranial end of the synsacrum. The cranial and caudal ends of the epoxy base of the back-plug were sutured (0-0 silk) to the intervertebral ligaments cranial to the ground wire. The skin was pulled over the epoxy base, leaving the plug exposed, sutured closed, and covered with elastic surgical tape. Post-surgical birds recovered in small heated cages supplied with food and water for 12-24 hours prior to flight tests.

Acquisition and signal processing

The back plug was attached to two shielded cables with six leads each (Cooner Wire, CA, 4 m total length, 17 g m^{-1} with a matching male microconnector, GM-6). The sonomicrometry signals were sent to a Tritron System 6 sonomicrometry amplifier (Triton Technology Inc., San Diego, CA), strain signals to a Measurements Group Vishay 2120A strain-gauge signal conditioner (Raleigh, NC), and the EMG signals to a Grass CP511 EMG amplifier (West Warwick, USA, gain 1000x, 100-3000 Hz bandpass filter). Each amplifier's output signal was recorded at 2 kHz in Axoscope (v 10.1, Molecular Devices, Sunnyvale, CA) *via* an Axon instruments Digitata 1322 16-bit A/D converter (Union City, CA).

Signal processing and analysis follows Hedrick et al (2003) and Tobalske and Biewener (2008). Briefly, EMG signals were filtered with a 250 Hz Butterworth high-pass filter to removed low frequency movement artifacts and rectified. EMG activity was defined as continuous peaks greater than two times mean baseline noise in the rectified signal.

Sonomicrometry and strain gauge signals were filtered with a 50 Hz digital Butterworth low-pass filter. Sonomicrometry signals were corrected to represent the average fascicle length. The measured distance between crystals was increased by 2.7% to account for the difference between the velocity of sound in muscle (1540 m s^{-1}; Goldman & Hueter 1956) and the velocity of sound assumed by the Triton amplifier (1500 m s^{-1}). This distance was then increased by 0.16 mm or 0.74 mm to account for the faster velocity of sound through the epoxy lens on the sonomicrometry electrode (1 mm and 2 mm crystals, respectively, Biewener et al. 1998a; Biewener et al. 1998b; Daley & Biewener 2003). Finally, a 5 ms phase delay and a frequency-dependent amplitude

attenuation (caused by the 100 Hz linear phase filter of the Triton amplifier) were corrected following the methods of Tobalske and Dial (2000). Resting length (L_{rest}) was recorded for each flight immediately prior to opening the enclosure while the bird was perched on the force plate with wings folded. Muscle strain (ε), was calculated as ΔL L_{rest}^{-1}, where ΔL is the difference between instantaneous fascicle length and L_{rest}.

Acquisition and signal processing

The back plug was attached to two shielded cables with six leads each (Cooner Wire, CA, 4 m total length, 17 g m^{-1} with a matching male microconnector, GM-6). The sonomicrometry signals were sent to a Tritron System 6 sonomicrometry amplifier (Triton Technology Inc., San Diego, CA), strain signals to a Measurements Group Vishay 2120A strain-gauge signal conditioner (Raleigh, NC), and the EMG signals to a Grass CP511 EMG amplifier (West Warwick, USA, gain 1000x, 100-3000 Hz bandpass filter). Each amplifier's output signal was recorded at 2 kHz in Axoscope (v 10.1, Molecular Devices, Sunnyvale, CA) *via* an Axon instruments Digitata 1322 16-bit A/D converter (Union City, CA).

Signal processing and analysis follows Hedrick et al (2003) and Tobalske and Biewener (2008). Briefly, EMG signals were filtered with a 250 Hz Butterworth high-pass filter to removed low frequency movement artifacts and rectified. EMG activity was defined as continuous peaks greater than two times mean baseline noise in the rectified signal.

Sonomicrometry and strain gauge signals were filtered with a 50 Hz digital Butterworth low-pass filter. Sonomicrometry signals were corrected to represent the

average fascicle length. The measured distance between crystals was increased by 2.7% to account for the difference between the velocity of sound in muscle (1540 m s^{-1}; Goldman & Hueter 1956) and the velocity of sound assumed by the Triton amplifier (1500 m s^{-1}). This distance was then increased by 0.16 mm or 0.74 mm to account for the faster velocity of sound through the epoxy lens on the sonomicrometry electrode (1 mm and 2 mm crystals, respectively, Biewener et al. 1998a; Biewener et al. 1998b; Daley & Biewener 2003). Finally, a 5 ms phase delay and a frequency-dependent amplitude attenuation (caused by the 100 Hz linear phase filter of the Triton amplifier) were corrected following the methods of Tobalske and Dial (2000). Resting length (L_{rest}) was recorded for each flight immediately prior to opening the enclosure while the bird was perched on the force plate with wings folded. Muscle strain (ε), was calculated as ΔL L_{rest}^{-1}, where ΔL is the difference between instantaneous fascicle length and L_{rest}.